©Copyright 2024
Ryan A. Lanzetta

A defective approach to the conformal bootstrap

Ryan A. Lanzetta

A dissertation
submitted in partial fulfillment of the
requirements for the degree of

Doctor of Philosophy

University of Washington

2024

Reading Committee:
Lukasz Fidkowski, Chair
Mark Rudner
Natalie Paquette

Program Authorized to Offer Degree:
Physics

University of Washington

Abstract

A defective approach to the conformal bootstrap

Ryan A. Lanzetta

Chair of the Supervisory Committee:
Associate Professor Lukasz Fidkowski
Department of Physics

Defects are an inherent part of statistical and condensed matter systems in the real world. At criticality, the problem of describing the interplay of defect and bulk degrees of freedom requires the application of state-of-the-art techniques in quantum field theory. When the bulk is described by a conformal field theory, the problem becomes especially rich due to the structure of consistency conditions following from conformal invariance. In this thesis, we develop a new set of numerical conformal bootstrap tools to constrain aspects of CFTs in the presence of defects of various kinds, and in various spacetime dimensions. We first devise a general technique for studying the consequences of 't Hooft anomalies in two dimensional conformal field theories, which we use to quantify the general result that anomalies guarantee low-energy, charged degrees of freedom. The approach combines the constraints of modular invariance and crossing symmetry of symmetry defect operators. We then demonstrate a new way to study endable line defects in CFTs in any dimension in a way that rigorously incorporates aspects of the bulk CFT data. We study the particular case of the pinning field defect of the $3d$ Ising CFT, deriving rigorous bounds on a number of quantities that characterize it.

TABLE OF CONTENTS

LIST OF FIGURES

ACKNOWLEDGMENTS

I feel extremely indebted to a number of people and institutions. I look back on many key moments in my life that have landed me here at the end of my PhD, brought about by various people, which I will allude to but will certainly not do justice to in most instances.

First, I thank the teachers in my high school. When I wanted to get myself on track the resources and wherewithal were present within my school to give me avenues for success and stimulation. Many are not served so well by public schools as I was. I especially thank my computer science and mathematics teachers Mrs. Fisher, Mrs. Bramanti, and Mr. Robinson for various opportunities and inspiration that they gave me. I also must shout out Mrs. Vachris for telling me on my last day of high school that she thinks I will have an interesting life. I hope I am living up to this expectation—I took it as a challenge.

I thank my PhD advisor, Lukasz Fidkowski, for collaboration, always being available to talk, trusting me to develop my own research style, and for his advocacy. Most advisors in condensed matter theory would not have had the breadth of knowledge, or boldness to have a student work on such a far-afield subject, to suggest I work on conformal bootstrap, which I think turned out to be a fantastic research direction for me. While having so much freedom was at times challenging, I cherish now my independence, which I hope sets me up for a long career in physics. I also thank Max Metlitski for being like a second advisor and for patience, encouragement, guidance, and collaboration.

I thank Stefan Gromoll for taking me under his wing at various points in time and setting a tremendous example for how to be a human being with a zest for many aspects of life, and inviting me over for many delicious meals when I was a (not-so) starving college student.

I am grateful for the time I spent at the City College of New York. I thank my friends

Kevin Becker, Lanie Leung, Abigail Murphy, and Joseph Shaker for many fun times. I thank especially my advisor Alexios Polychronakos and professors V.P. Nair and Sebastian Franco for helping me realize I wanted to become a theoretical physicist.

I thank my friends from UW Michael Clancy, Jeffrey Commons, Tahiyat Rahman, and Teresa Lo for their support and many fun and, in some cases, dangerous experiences (if you know you know). I especially thank Teresa for (re?)-introducing me to the Cocteau Twins.

I am grateful for the friends I've made "on the road," both at conferences and during the time I spent at UCSB. I thank my friends Arkya Chatterjee, Shang Liu, Nayan Myerson-Jain, Sal Pace, Akshat Pandey, Ryan Thorngren, and Carolyn Zhang for laughs, adventures, intense physics discussions, and most of all for listening to me rant like a crazy person about tori and cones.

I thank all my family for their support. I thank Nana and Aunt Jo for always being ready to help me and giving me so many great childhood memories. I thank my Mom for encouraging me to be whatever I want to be and showing me how to treat others. I thank my Dad for inspiring me to do physics and for many fun adventures. I thank Robin Root for being a good listener and encouraging my interest in writing. I thank Ciara for being a silly goose and being a wonderful and caring sister. I also thank Ann and Russ Glaser for giving me a sense of family here in Washington.

Finally I thank Elise for love, for being a partner in the truest sense, and for putting up with the craziness of the physics lifestyle. I can't wait to see what more adventures are in store.

Chapter 1

INTRODUCTION

Most of the matter that we encounter in everyday life is built out of protons, neutrons, and electrons. Grouping a small number of these particles together in slightly different ways gives rise to different types of atoms, which then form the chemical elements. The simplicity of these ingredients belies the vast complexity of materials we are familiar with from everyday life. The really remarkable thing is that the diversity of substances present around us is a result of subtle differences in how these basic building blocks are arranged at a microscopic scale. Understanding the relationship between the microscopic and macroscopic descriptions of matter, or understanding what possible phases of matter—i.e. an equivalence class of potentially different materials subject to different external parameters with a similar, robust set of macroscopic properties—a given material can realize, are questions of basic scientific importance, and have been a fruitful source of inspiration of theoretical and practical progress.

From the time of Plato, there were suspicions that nature can be described within this basic framework, in which simple building blocks conspire in large numbers to form complicated macroscopic structures. As the saying goes, *more is different* [8]. As our experimental and mathematical tools have improved, we learned how to describe the true structure of matter in substantially more detail. In the past century, new language was developed and a number of deep organizing principles emerged in theoretical physics, which preceded an explosion of progress in our understanding of materials present in nature and our ability to imagine artificial ones, bound only by the rules of quantum mechanics. The new language is *quantum field theory*, and the new organizing principles are *symmetry* and the *renormalization group*.

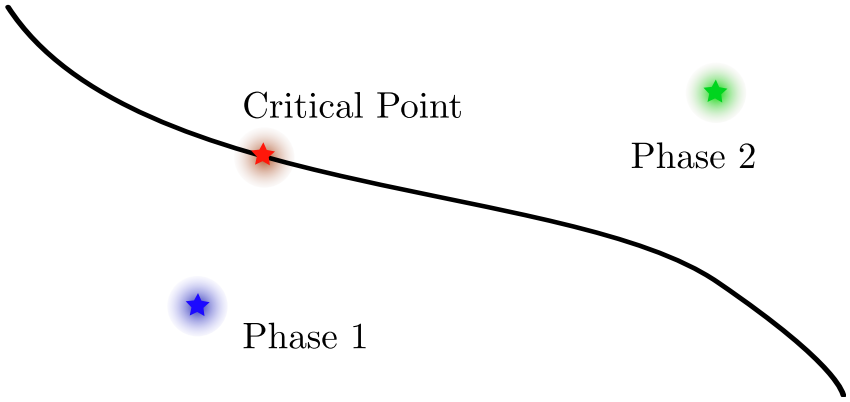

Figure 1.1: A cartoon of two phases of matter separated by a critical point. The space that the different phases, and the critical line separating them, occupy can represent different choices of external or internal parameters that leave the macroscopic properties intact.

We will see these tools and concepts appear throughout this thesis.

One of the more difficult problems that appears in the study of phases of matter is the characterization of phase transitions between different phases. For conventional phases of matter, such as classical magnetic systems like the Ising and $O(N)$ models, there is often a clear local quantity that characterizes the different phases that the system can realize called the order parameter. It turns out that an effective way to model such systems is often in terms of a continuum Lagrangian theory that models the long-wavelength fluctuations of this order parameter.

The power of symmetry, field theory, and renormalization is illustrated by the example of the lattice Ising model. Suppose we wish to describe the long-distance properties of a classical Ising system in D dimensions defined by the lattice energy functional

$$\mathcal{H} = \sum_{\langle ij \rangle} s_i s_j \tag{1.1}$$

where i, j label the lattice sites in the D-dimensional lattice and $s_i = 1, -1$ are Ising spins, which also correspond to the order parameter. In studying this model, one would like to characterize correlation functions $\langle s_{i_1} ... s_{i_n} \rangle$. It is possible to motivate the claim that, at long distances, this kind of model and its correlation functions are well-described in terms of the

continuum action

$$S = \int \left[\frac{1}{2} \partial_\mu \phi \partial^\mu \phi + \frac{m^2}{2} \phi^2 + \frac{\lambda}{4!} \phi^4 + ... \right] d^D x \tag{1.2}$$

Assuming m^2, λ are not too large relative to the kinetic term, we can say that the Lagrangian described above is (perturbatively) a *relevant* perturbation of the action describing a free scalar ϕ. The theory of this free field is *scale-invariant*, meaning the action is invariant under a transformation $x \to \alpha x$ for some $\alpha > 0$ if we also demand

$$\phi(\alpha x) = \alpha^{-\Delta} \phi(x) \qquad \Delta_{\phi^n} = n \frac{D-2}{2}. \tag{1.3}$$

This defines the notion of a *scaling dimension* Δ for the various terms appearing in 1.2, which follow in this case from simple dimensional analysis and requiring that S be dimensionless in our chosen units. Naively, non-zero values of the couplings m^2, λ explicitly violate the scale-invariance of the theory. It turns out, however, that upon carefully tuning these values it is possible to access the properties of a different, interacting field theory that is also scale-invariant. In one's favorite renormalization scheme, this is achieved by studying the theory in the presence of an explicit energy scale[1]—abstractly denoted by a parameter μ. Depending on the value of μ, i.e. which scale we probe, the theory may behave differently with different effective choices of the couplings i.e. m^2, λ may explicitly depend on μ. When we tune the couplings such that they are *invariant* under a change in scale, the theory is again scale-invariant, which is quantified using the so-called β-functions

$$\beta_{g_i} = \frac{\partial g_i}{\partial \log \mu}$$

where g_i represent arbitrary couplings. The β-functions can be computed perturbatively to give successive approximations to the true values of the couplings leading to a fixed-point and can also be used to solve the *flow* of the couplings, giving an explicit demonstration of the renormalization group flow, or how the effective couplings change at different scales.

[1] We have not tethered ourselves to a particular renormalization scheme in this discussion, i.e. whether to use an ultraviolet cutoff or to use dimensional regularization, etc., for simplicity. We can think of μ as representing an arbitrary choice amongst these possibilities.

The new theory will also possess a new set of fields with a completely different set of scaling dimensions than our original theory.

It turns out that the theories discussed so far are examples of *conformal field theories* (CFTs), i.e. theories that are invariant under conformal transformations and Weyl rescalings. Conformal transformations are those which preserve angles such as scale transformations, which we already introduced, rotations, translations, and special conformal transformations which are more exotic. While the perturbative techniques alluded to so far certainly allow one to gain a hands-on feel of the systems being studied, theories with such a large space-time symmetry give way to a much more efficient and effective description that completely circumvents the need for a Lagrangian, at least in principle.

A significant amount of progress is possible in the study of CFTs by focusing entirely on symmetry. In a CFT, we again have a set of local fields $\mathcal{O}_i$ that can be thought of as representing some local quantities of the system in question. They also possess a scaling dimension and transform under a scale transformation in an analogous fashion to (1.3) with an *a-priori* arbitrary positive value of Δ. Correlation functions of these operators are highly constrained by conformal symmetry. In general dimensions, two and three point functions of so-called *primary* operators are completely fixed by conformal invariance

$$\langle \mathcal{O}_i(x)\mathcal{O}_j(y)\rangle = \frac{1}{|x-y|^{2\Delta}} \tag{1.4}$$

$$\langle \mathcal{O}_i(x)\mathcal{O}_j(y)\mathcal{O}_k(z)\rangle = \frac{\lambda_{ijk}}{|x-y|^{\Delta_i+\Delta_j-\Delta_k}|x-z|^{\Delta_i+\Delta_k-\Delta_j}|y-z|^{\Delta_j+\Delta_k-\Delta_i}} \tag{1.5}$$

A further property of the primary operators is that they possess an operator product expansion (OPE), which defines a kind of operator algebra amongst the primary operators

$$\mathcal{O}_i(x) \times \mathcal{O}_j(y) = \sum_k \lambda_{ijk} C^D_{ijk}(x, y, \partial_y)\mathcal{O}_k(y) \tag{1.6}$$

which can be understood as being valid inside any correlation function. Here, C^D_{ijk} is a certain differential operator that is fully determined by conformal symmetry. This structure means that all higher-point functions are completely fixed once the content of the OPEs of all primary operators are fixed.

The rough structure of CFTs outlined so far gives just enough of a hint to see how an approach that is significantly different from the standard perturbative approach used in quantum field theory could be applicable in the study of conformal field theory. This begins our discussion of *bootstrap*. It turns out that not all choices of Δ_i, λ_{ijk}—which are sometimes referred to as the CFT data—are admissible, in the sense that they could lead to a violation of simple algebraic consistency conditions such as the associativity of the OPE

$$\mathcal{O}_i \times (\mathcal{O}_j \times \mathcal{O}_k) = (\mathcal{O}_i \times \mathcal{O}_j) \times \mathcal{O}_k. \tag{1.7}$$

This constraint may also be formulated as a relation between different four-point functions and in that context is called *crossing symmetry*. This is a highly non-trivial constraint, which is highly non-linear in the inputs and involves in general an infinite number of primary operators. Nonetheless, the framework outlined so far means that we may understand CFTs as points in the solution space, parametrized by the data of the scaling dimensions and OPE coefficients, of the crossing symmetry constraints, which is a fairly extreme departure from the usual situation encountered in perturbative approaches to QFT. The idea of using consistency conditions, rather than trying to solve specific models, to study a given physical system of interest is at the heart of the bootstrap philosophy. In perhaps the greatest achievement of this perspective, it led to the complete classification of unitary CFTs with central charge $c < 1$, known as the minimal models [13]. The euphoria of this achievement rather quickly wore off as it was realized that results of a similar magnitude would be hard to come by. About a decade and a half ago, thirty-odd years after the construction of the minimal models, it was realized that slightly moving the goalposts, and asking simpler questions about the admissibility of different choices of the CFT data, could yield powerful physical results through how various pieces of physics are encoded in the low-lying CFT data [124]. Instead of trying to solve the consistency conditions, the idea changed to asking if it is possible to *rule out* choices of CFT data with only some simple assumptions. The introduction of numerical optimization techniques, in particular semidefinite programming, gave rise to the modern numerical bootstrap program [119, 131].

So far, we have mainly discussed local operators in CFT. Equally important, however, are extended objects such as line defects, which also may be modeled using CFT tools. Extended objects are equally intrinsic to a given CFT and are important observables to understand, since they can describe the long-distance limit of various interesting objects such as impurities. In general, a defect will break the symmetries of the clean bulk. For a flat, P-dimensional defect, conformal symmetry is broken from $SO(D+1,1)$ to (at least) $SO(P+1,1)$ for when the defect qualifies as a conformal defect. This breaking leads to a completely new set of localized observables that live on the defect, with completely distinct scaling dimensions from those in the bulk. Defects also encode other information about a given CFT such as its global symmetries. Defects that are *topological*—i.e. those whose locus of support can be moved freely without affecting correlation functions, so long as no operator insertions are crossed—each correspond, in a generalized sense, to symmetries of the theory. Inserting background flux of these topological defects allows one to probe global aspects of the theory such as its 't Hooft anomalies.

In the rest of this thesis, it will be our goal to explore two questions relating to defects in conformal field theories from a bootstrap point of view: one will be a problem of learning about properties of a class of bulk CFTs from properties of defects they possess, and in the second problem we will do the reverse and try to learn about a particular defect given a particular bulk CFT. In the first problem, contained in chapter 2, we will explore universal constraints on bulk CFTs that have a certain kind of 't Hooft anomaly. Anomalies are an important property of a system, since they are preserved under RG flow and imply a degree of non-triviality for systems which possess them. We will see how the presence of a certain anomaly leads to universal, quantitative predictions for the CFT data such as guaranteeing an upper bound on the scaling dimension of charged operators. In the second problem, we will use bootstrap techniques to study the simplest non-trivial conformal line defect in an interacting CFT in $D > 2$: the pinning field defect of the $3d$ Ising CFT.

Chapter 2

BOOTSTRAPPING LIEB-SCHULTZ-MATTIS ANOMALIES

This chapter is based on:
Ryan Lanzetta, Lukasz Fidkowski
Bootstrapping Lieb-Schultz-Mattis anomalies.
Phys. Rev. B 107, 205137, May 2023.

2.1 Introduction

2.1.1 Overview

Identifying the low energy spectrum of a given lattice Hamiltonian is an important goal of quantum many-body theory. In certain cases, depending on the symmetries of the model, the qualitative nature of its spectrum can be constrained, thus restricting the potential quantum field theory (QFT) descriptions. A famous and powerful result of this kind, known as the Lieb-Schultz-Mattis (LSM) theorem, is that half-odd-integer spin Heisenberg chains are gapless [96]. This is to be contrasted with the Haldane gap for the case of integer spin [81, 1]. Following these results, various generalizations in similar spirit have been made: in higher dimensions [112, 82], with more generic spatial symmetries [115, 155, 88, 63], including the magnetic translation group [35, 104, 158], and with higher form symmetries [92]. In this work, we will be concerned with an extension of the LSM theorem involving translations to general global symmetry groups, where it is expected that a translationally invariant local spin chain with an on-site global symmetry represented projectively at each site cannot be trivially gapped [33, 110, 109, 121]. This leaves gaplessness or spontaneous symmetry breaking (SSB) as the only possibilities in one spatial dimension.

The modern formulation of LSM-type theorems is in terms of 't Hooft anomalies [71, 38, 42, 106, 47], which can be viewed as obstructions to gauging a global symmetry. For a lattice

model subject to the generalized translation LSM theorem with an internal symmetry G, what we will refer to as the *LSM anomaly* is a mixed anomaly between lattice translation symmetry and G. This anomaly arises due to the fact that inserting a defect of translation symmetry amounts to adding one site, which carries a projective representation of G. Thus, in the presence of such translation symmetry defects, it is not possible to gauge G. This 't Hooft anomaly must be matched by both the lattice and continuum QFT descriptions [86], making it a powerful non-perturbative tool to aid in identifying candidate low energy theories—typically a complicated task. More general anomalies in bosonic lattice models have been studied throughout the literature, see e.g. [34, 130, 152, 23].

Field theory descriptions of lattice models will generally possess a different set of symmetries, whose relation to the lattice symmetries is constrained by requiring the existence of a group homomorphism relation $\gamma : G_{\text{UV}} \to G_{\text{IR}}$ that specifies how the lattice symmetries are realized at low energy. The homomorphism γ must also be compatible with anomaly matching, in a sense that we will describe. In this work, we will consider $G_{\text{UV}} = \mathbb{Z}^{\text{trans}} \times \mathbb{Z}_N^2$ on an infinite lattice, which descsribes systems with translation symmetry and an internal $\mathbb{Z}_N^2$ symmetry. In the context of LSM, we assume that the lattice translation symmetry is realized as an *emanant* (in the sense of [36]) $\mathbb{Z}_N$ internal symmetry in the CFT description of the system, leading the CFTs we consider to have a minimal, internal symmetry group $G = \mathbb{Z}_N^3$. An emanant symmetry of a low-energy theory is one for which any operator that breaks it also breaks the microscopic symmetry from which it emanates. We note that $\mathbb{Z}_N$ is not the only possible such emanant symmetry, as we will discuss briefly later on, but we restrict our study to this case for simplicity and since it is realized in various relevant microscopic models and their field-theoretic descriptions [71, 4]. Note that for the remainder of the chapter we will refer to the particular continuum manifestations of these anomalies that we study as LSM anomalies, although in the continuum context they are anomalies of purely internal symmetries and do not have to arise out of lattice models with mixed anomalies between spatial and internal symmetries. Indeed, we will also discuss a scenario where the same $\mathbb{Z}_N^3$ mixed anomalies in the field theory description are emergent (that is, a microscopic

$\mathbb{Z}_N^2$ internal symmetry is assumed and the third $\mathbb{Z}_N$ is emergent and has a mixed anomaly with the microscopic symmetry), in the context multicritical points of symmetry protected topological (SPT) phases, where no LSM constraint is expected.

Within the realm of QFT, another set of non-perturbative techniques are those related to conformal field theory (CFT), among them being the numerical conformal bootstrap. Following recent work combining $\mathbb{Z}_N$ symmetries and anomalies with modular bootstrap [99, 100], in this work we will use conformal bootstrap to bound the space of CFTs that possess the aforementioned continuum versions of certain LSM anomalies arising in lattice models with global, internal symmetry $G_{\text{int}} = \mathbb{Z}_N^2$. Fully incorporating the signatures of these LSM anomalies into bootstrap is somewhat subtle; to do so, we introduce a new technique that augments modular bootstrap by incorporating additional numerical bounds that come from imposing crossing symmetry on four-point functions of certain symmetry defect operators. This approach allows us to obtain universal bounds on the local operator content of 1+1d CFTs in a way that is refined by LSM anomalies.

2.1.2 Background, Methods and Motivation

Lattice models with the kinds of symmetries and anomalies we have mentioned have received some recent attention, partially motivating this work. Under the assumption of a unique ground state, CFTs naturally describe gapless spin chains satisfying LSM constraints, since any scale-invariant, (1+1)d QFT is necessarily a CFT, under mild assumptions [160, 120, 25, 108]. Indeed, in some recent numerical simulation work it was observed that entire stable, gapless phases of translation-invariant spin chains, subject to LSM constraints with on-site $\mathbb{Z}_N \times \mathbb{Z}_N$ symmetries, are effectively described by theories within the conformal manifolds of $N-1$ compact bosons for $N = 2, 3$ [4]. It was argued in Ref. [4] that a similar compact boson description should be valid for arbitrary, odd N. Further, the authors of Ref. [4] suggest that the central charge $c = N - 1$ of the compact boson theories may be the minimum necessary to accommodate the LSM anomaly when the only microscopically-imposed symmetry is $\mathbb{Z}_N^3$, assuming that the $\mathbb{Z}_{\text{trans}}$ is realized as $\mathbb{Z}_N$ in the low energy global symmetry group G_{IR}. As

noted by Ref. [37], which also contains some discussion of the LSM anomalies studied in this work, if one imposes instead a larger $PSU(N)$ internal symmetry, which is apparently emergent in a subset of the models studied by Ref. [4], then this minimum central charge is indeed $c = N-1$ by the Sugawara construction [52]. However, as we will point out, there are trivial counterexamples to this bound when the minimum symmetry imposed at low energy is $\mathbb{Z}_N^3$ and N is a product of coprime integers. Nonetheless, with a suitable quantitative modification to the possible central charge bound in these cases, there persists the difficult problem of determining whether non-trivial counterexamples exist. Thus, one of the goals of this work will be to look for bootstrap signatures of potential theories with a lower central charge that could have the LSM anomalies.

One possible explanation for the lack of counterexamples to the suggested central charge bound is that the space of $(1{+}1)d$ CFTs with $c > 1$ remains largely uncharted territory. Unlike for $c < 1$, where all unitary theories are known [13, 68], most explicit constructions of compact, unitary CFTs with $c > 1$ are rational CFTs [107] (RCFTs) with enhanced symmetry or coupled free bosons. Resurrecting ideas used originally to exactly solve many of the known examples of $(1{+}1)d$ CFTs, in the past several years it was realized that instead of attempting full solutions of specific CFTs, a still powerful and more tractable goal is to attempt to rule out, using numerical optimization techniques such as linear or semidefinite programming, certain regions in the space of all possible CFTs [124, 60, 118]—this represents the modern, numerical conformal bootstrap program. This is possible due to unitarity and other more stringent mathematical consistency requirements inherent to CFTs. In general dimensions, the main consistency requirement is the crossing symmetry of four-point functions. Within numerical bootstrap, one can attempt to show that certain assumptions about the spectrum of a CFT can lead to incompatibility with crossing symmetry. This approach, termed *correlator bootstrap*, has had much success, and in some cases has gone so far as to produce numerical solutions to certain theories, as has been done in the case of the $3d$ Ising CFT [60, 61, 132]. These advances have especially been made possible following the introduction of specialized semidefinite programming packages for conformal bootstrap

applications such as SDPB [131].

In the setting of (1+1)d CFTs, the possible constraints on the CFT data are more powerful than in $d > 2$ due to the correspondence between the local primary operator spectrum and the decomposition of the torus partition function into Virasoro characters, which is subject to modular invariance. Both analytically and numerically, it was shown that imposing modular invariance of the partition function gives generic bounds on the operator content of a unitary, compact, bosonic (1+1)d CFT, guaranteeing, for instance, an upper bound on the scaling dimension of the lightest primary field for any CFT [85, 44]. This should be contrasted with correlator bootstrap, where to obtain any bounds one must typically make an additional assumption that the theory possesses some fields with a particular scaling dimension [1]. This approach, termed *modular bootstrap*, has also been generalized to bosonic, (1+1)d CFTs with anomalous and non-anomalous $\mathbb{Z}_N$ global symmetries by imposing modular covariance of the torus partition function twisted by symmetry defects [99, 100], as we mentioned. Additional progress in a similar vein has been made for fermionic CFTs with non-anomalous and anomalous global symmetries [17, 80, 79], but in this work we will focus on bosonic theories.

The $\mathbb{Z}_N$ anomalies studied in previous modular bootstrap works are characterized by anomalous spin selection rules for so-called defect operators hosted at the end of topological defect lines (TDLs) implementing the $\mathbb{Z}_N$ symmetry [30]. These spin constraints lead to stronger unitarity bounds on the scaling dimensions for such operators. From these inputs emerges the general result that anomalous $\mathbb{Z}_N$ symmetries are necessarily accompanied by charged degrees of freedom at low energy. Further, the bounds on $\mathbb{Z}_N$-symmetric operators depend strongly on the anomaly. However, more complicated symmetry groups may

[1] Actually, in general dimensions $d + 1 > 2$ there are ways to put universal bounds on the local operator spectrum. Most generally, every unitary CFT possesses a conserved stress tensor, so it may be used as an external field in correlator bootstrap calculations and the content of its OPE with itself may be studied, leading to universal bounds on the lightest operator [55]. However, it is not possible to obtain universal bounds in this way that are refined by discrete, internal symmetries since the stress tensor does not interact non-trivially with such symmetries. For continuous internal symmetries, a similar approach may be used to obtain universal bounds by using the conserved currents of the symmetry [56].

have more complicated anomalies with more subtle signatures, ones that even do not include anomalous defect spin-selection rules. A $\mathbb{Z}_N^3$ symmetry with the aforementioned LSM anomaly is one case where this scenario can occur. As already alluded to, the main distinguishing signature of the LSM anomaly is that symmetry defect operators of one $\mathbb{Z}_N$ subgroup transform in a projective representation of the remaining $\mathbb{Z}_N^2$ subgroup. Crucially, when N is odd, this is essentially the only signature of the LSM anomaly; in these cases, there are no non-trivial defect spin selection rules, so modular bootstrap by itself is insensitive to the LSM anomaly and, thus, cannot give a bound on charged operators. On the other hand, our approach gives rather tight bounds on charged operators at low central charge and uncovers various intriguing kinks.

To incorporate the LSM anomalies into bootstrap, we augment modular bootstrap by incorporating certain bounds coming from correlator bootstrap. Our approach exploits the constraining power of both crossing symmetry of defect operators and modular covariance of the twisted partition function as follows. Suppose we are trying to rule out some gap in the spectrum of scaling dimensions of local operators for CFTs with a particular central charge. In the case of the $\mathbb{Z}_N$ modular bootstrap, the presence of an anomaly sets *universal* lower bounds on the scaling dimension of any $\mathbb{Z}_N$ symmetry defect operator; for the LSM anomaly, we derive a non-universal lower bound that depends on the assumed gap in the local operator spectrum and, in some cases, the central charge. The reason for this lower bound is that taking the operator product expansion (OPE) of light defect operators can produce light local operators; precisely how light the defect operators can be without necessarily producing a local operator whose scaling dimension violates the assumed gap in the local operator spectrum is quantified using correlator bootstrap. Additionally, in some cases the gaps in the spectrum of local and defect operators further lead to a lower bound on the central charge. This provides yet another route to improve our lower bound on the scaling dimension of the lightest defect operator, since the lower bound on the central charge must not be higher than the assumed central charge. On the other hand, for modular covariance of the twisted partition function to be obeyed, the lightest local operator and the lightest defect

operator typically cannot both be too heavy; in particular, if the gap in the spectrum of local operators is large—for instance, a gap that we are trying to rule out—there often exists an upper bound on the gap in the spectrum of defect operators. This reasoning applies even when the gap among local operators is assumed to exist only in the charged sector, or only in the neutral sector. Modular bootstrap thus has the potential to rule out the combined gaps in the local and defect operator spectra, where the latter gap is implied by the former, leading to a contradiction and allowing us to rule out the assumed gap in the local operator spectrum.

Our main results, shown in Figures 2.1 and 2.2, are upper bounds, as a function of central charge c, on the lightest local operators with various symmetry properties for CFTs saturating the $\mathbb{Z}_N^3$ LSM anomaly for $N = 2, 3, 4, 5, 6$. These bounds can be thought of as a refinement of the more qualitative LSM-type theorems, which only exclude a non-degenerate gapped ground state. Our results, by contrast, state that, for CFTs saturating the LSM anomalies, not only must there exist charged states with energies $\mathcal{O}(1/L)$ (in a ring geometry with periodic boundary conditions with L the circumference and under the assumption of a unique ground state), but there is also a precise upper bound $\sim \Delta(c)/L$ on the energy of such states when the lattice model is described at low energy by a CFT with central charge c. There are various additional microscopic realizations of lattice models that can be described by the kinds of CFTs we put bounds on. These include certain multicritcal points of (1+1)d symmetry protected topological (SPT) phases and edge theories of certain (2+1)d SPT phases.

2.1.3 Organization

The structure of the remainder of this chapter is as follows. In section II we will present our universal bootstrap bounds on the local operator spectrum of (1+1)d CFTs with the $\mathbb{Z}_N^3$ LSM anomalies for various N, and further discuss the implications of our bounds to the theory of multicritical points of SPT phase transitions. In section III we will provide technical background regarding symmetries and anomalies in (1+1)d CFT, including details

about the TDL formalism and how the LSM anomalies manifest within it. Then in section IV we will explain aspects of our numerical bootstrap approach and additionally present some of the other numerical bounds (Figures 2.9 and 2.10) that went into our final calculations. Finally, in section V we will make closing remarks and discuss potential future avenues for research. We provide additionally an appendix with details about our modular bootstrap calculations.

2.2 Main Results

Here we present our main results, which include universal numerical bootstrap bounds on the local primary operator spectrum of unitary, compact (1+1)d CFTs with a $\mathbb{Z}_N^3$ symmetry and LSM anomaly. We further discuss an application of our numerical bounds to the theory of phase transitions between symmetry protected topological (SPT) phases. The precise details of the LSM anomaly and its implications on the structure of the theories that saturate it will be discussed later. We do not study theories with $c < 1$ since it is known that the unitary models cannot possess the kinds of symmetries, let alone anomalies, that we study in this work [128].

We obtain three types of numerical bounds, each of which will be an upper bound on the scaling dimension of the lightest scalar primary field transforming in some representation of $\mathbb{Z}_N^3$. The three possibilities we consider for the representations of operators are the trivial representation, any non-trivial representation, or any representation. The first two cases then are upper bounds on the scaling dimension of the lightest symmetric or charged scalar local primary, respectively, and the last case represents an upper bound on the lightest local, scalar operator. We only present bounds on the lightest $\mathbb{Z}_N^3$-symmetric operator for $N = 2, 3$, since for larger N the bounds converge very slowly, and the improvements introduced in this work do not improve our ability to guarantee relevant, symmetric, scalar operators.

Before discussing our bounds, we mention that examples of CFTs with the properties necessary for our bootstrap bounds to apply have been discussed, with emphasis on their LSM anomalies, in Ref. [4]. As mentioned, the main class of examples for theories with

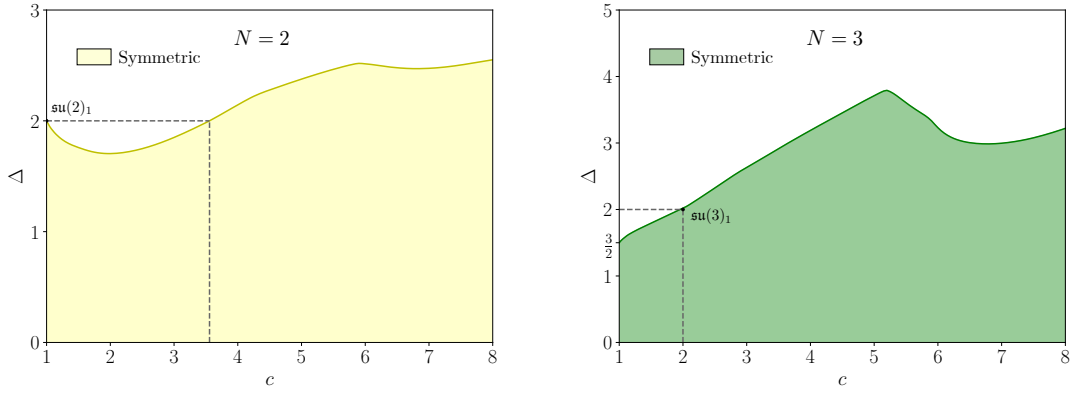

Figure 2.1: Upper bounds on the scaling dimension of the lightest $\mathbb{Z}_N^3$-symmetric scalar operator in a theory with the LSM anomaly, as a function of central charge, for $N = 2, 3$. The shaded region in each plot is thus the allowed region for the lightest symmetric, scalar operator. In obtaining these bounds, we did not make use of the additional improvements to standard modular bootstrap with global symmetry that we introduce in this work. The bounds were computed with $\Lambda^{\text{mod}} = 25$ and $S_{\text{max}}^{\text{mod}} = 50$ (see Section IV for implementation details).

the $\mathbb{Z}_N^3$ LSM anomalies may be found within the conformal manifolds of $N-1$ compact bosons with certain symmetry constraints. However, we also remark that it is possible to find examples of theories with these LSM anomalies with lower central charge than what is suggested in Ref. [4]. When $N = \prod_i n_i$ with n_i all coprime integers, CFTs with the $N = \prod_i n_i$ LSM anomaly can be constructed by taking the tensor product of theories with the LSM anomaly corresponding to each n_i. The reason for this is that in this situation $\mathbb{Z}_N = \bigoplus_i \mathbb{Z}_{n_i}$. It can be checked straightforwardly that projective representations of $\mathbb{Z}_N^2$ can be decomposed into tensor products of the projective representations of $\mathbb{Z}_{n_i}^2$ and further that the other properties implied by the LSM anomaly corresponding to N, such as the spin selection rules of defect operators (see section III and Table 2.1), are the same. Using, for instance, the WZW models $\mathfrak{su}(n_i)_1$, we can thus construct theories with the $N = \prod_i n_i$ LSM anomaly that have central charge $c = \sum_i (n_i - 1) < N - 1$.

2.2.1 Universal bounds on lightest $\mathbb{Z}_N^3$-symmetric scalar

Here we discuss our bounds on the lightest $\mathbb{Z}_N^3$-symmetric scalar operator for $N = 2, 3$, which are shown in Figure 2.1. Bounds on symmetric, scalar operators are interesting primarily to determine whether theories whose central charge is within a certain range *cannot* describe stable gapless phases where the microscopically-imposed symmetry is $\mathbb{Z}_N^3$. In the presence of such a symmetry-preserving relevant operator, an RG flow may be triggered to a nearby phase with the same symmetry, but due to the anomaly this flow will generally lead either to a phase where the symmetry is spontaneously broken, or perhaps the flow will end at a non-trivial CFT fixed point. In either case, the initial CFT is thus unstable. The calculations performed in this section involve only the standard modular bootstrap setup with global symmetries and $\mathbb{Z}_N$ anomalies of Refs. [99, 100], with slight modification to include the larger symmetry group. It turns out that our improvements to this setup, which we use in the remainder of our calculations, do not lead to an enlargement of the range of values of central charge where a relevant symmetric scalar is guaranteed. This trend continues for larger N, where our methods do not lead to any non-trivial range of values of the central charge for which a relevant, $\mathbb{Z}_N^3$-symmetric operator is guaranteed.

$N = 2$

For $N = 2$, modular bootstrap is somewhat sensitive to the LSM anomaly since it sees that one of the $\mathbb{Z}_2$ TDLs is anomalous (see i.e. Table 2.1). Our bound leads to a range of values of central charge such that any theory in the range with the $N = 2$ LSM anomaly must contain a relevant, $\mathbb{Z}_2^3$-symmetric scalar operator. The range is approximately

$$1 < c < 3.5565$$

Our bound is saturated at $c = 1$ by $\mathfrak{su}(2)_1$, whose lightest operator symmetric under $\mathbb{Z}_2^3$ is exactly marginal with $\Delta = 2$.

$N = 3$

In this case, we see that any CFT with a non-anomalous $\mathbb{Z}_3^3$ symmetry (or, equivalently for the calculations presented here, a $\mathbb{Z}_3^3$ symmetry with the LSM anomaly) must have a relevant symmetric scalar if its central charge is $c < 2$. The WZW model $\mathfrak{su}(3)_1$ nearly saturates our bound at $c = 2$, whose lightest operator $\mathbb{Z}_3^3$-symmetric is exactly marginal. In Ref. [100], it was shown also that when $c < 2$ a $\mathbb{Z}_3$-symmetric, relevant, scalar operator must be present. The analogous bounds for $\mathbb{Z}_3^3$ cannot be stronger than this bound, since imposing more symmetry can only make it harder for a given operator to remain symmetric, so it is interesting that our $\mathbb{Z}_3^3$ bound is still powerful enough to guarantee relevant operators in this range of central charge.

2.2.2 Universal bounds on lightest $\mathbb{Z}_N^3$-charged scalar

We now discuss our bounds on the lightest $\mathbb{Z}_N^3$ charged operator, which are shown in Figure 2.2. We define a $\mathbb{Z}_N^3$-charged operator as a local operator transforming in any non-trivial representation of $\mathbb{Z}_N^3$. For odd, prime N, this choice loses no generality since all non-trivial representations are equivalent in the sense that they are related by outer automorphisms, i.e. a relabeling of the group elements. This relabeling is allowed since each $\mathbb{Z}_N$ TDL for a given N has the same spin-selection rule (see section III and Appendix A). For even N, there are different classes of representations, so in principle more refined bounds could be obtained by bounding the lightest operator in each class separately but, for simplicity, we will not present such bounds.

$N = 2$

Our $N = 2$ bound does not contain many features. The known theories with minimal central charge and the $N = 2$ LSM anomaly are the $c = 1$ compact boson theories on the circle branch. The theory that maximizes the gap in the $\mathbb{Z}_2^3$-charged operator spectrum is the WZW model $\mathfrak{su}(2)_1$, whose lightest charged, scalar operator has scaling dimension $\Delta = \frac{1}{2}$.

$N = 3$

Our bound on the lightest charged operator for $N = 3$ has various interesting features. First of all, the bound approaches $\Delta = 0$ as $c \to 1$, which is in agreement with the analytical analysis of $c = 1$ theories that no such theory can have the LSM anomaly for $N = 3$. This is quite striking in modular bootstrap calculations, which typically are not quite so strong, and is a feature shared by our bounds for other choices of $N > 2$. The most obvious feature is that the $\mathfrak{su}(3)_1$ WZW CFT, which is the principal example of a WZW CFT with the $N = 3$ LSM anomaly, sits at a prominent kink of our upper bound. The $\mathfrak{su}(3)_1$ theory has $c = 2$ and its lightest charged scalar has scaling dimension $\Delta = \frac{2}{3}$.

We stress that in this case, since N is odd, modular bootstrap alone does not give a bound at all on the lightest charged operator since all $\mathbb{Z}_3$ subgroups, in this case, have no $\mathbb{Z}_3$ anomaly.

$N = 4$

This bound displays a few kink-like features at low values of the central charge that we cannot, at present, explain. The $c = 3$ compact boson theories are the only theories we know of with the $N = 4$ LSM anomaly, among which is the WZW model $\mathfrak{su}(4)_1$. It is expected that $\mathfrak{su}(4)_1$ maximizes the scalar gap among the toroidal compactification CFTs at $c = 3$ [3, 10] (Maximizing the scalar gap in the moduli space of such theories at generic integral c is a difficult problem. See additionally Ref. [16] for interesting work related to this.). However, the question of which CFT absolutely maximizes the scalar gap at $c = 3$ remains an interesting puzzle; the universal upper bound on the scalar gap calculated in Ref. [44] is not saturated by $\mathfrak{su}(4)_1$ at $c = 3$. Consequently, we do not know whether there is any $c = 3$ theory that saturates our even larger upper bound on the lightest $\mathbb{Z}_4^3$ charged operator for theories with the $N = 4$ LSM anomaly.

$N = 5$

This bound is similar to the bound for $N = 3$ since again modular bootstrap alone gives no bound. Below $c = 4$, which is the minimal central charge we know of where theories with the $N = 5$ LSM anomaly are known to exist, we see two features that resemble kinks. The first occurs at $c \approx 2$ and is somewhat soft. Our upper bound at $c = 2$ is approximately equal to $\Delta = 0.462$. At this time we are not aware of any evidence to suggest that this corresponds to an actual theory, so it will be interesting to study this feature in future work. The second kink is more sharply defined and is somewhat more intriguing. The location of this kink, according to our plot in Figure 2.2 which was computed with derivative orders $\Lambda^{\text{mod}} = \Lambda^{\text{cor}} = 25$ (for an explanation of the parameters describing our computational setup, see section IV), is almost exactly at $c = \frac{14}{5}$, where our upper bound is equal to $\Delta = 0.8006$. This puts the WZW model $(\mathfrak{g}_2)_1$ essentially right at the location of this kink. However, as we discuss in the next subsection, we were able to rule out $(\mathfrak{g}_2)_1$ from having the $N = 5$ LSM anomaly with a more intensive calculation, so the origin of this kink remains a mystery.

At $c = 4$, the WZW CFT $\mathfrak{su}(5)_1$ is well within the allowed region, but as was the case with $N = 4$ we are not sure of a systematic way to maximize the scalar gap among the $c = 4$ compact boson theories, subject to the appropriate symmetry requirements, let alone among all CFTs, to see whether ultimately our bound is saturated by an actual CFT. Using the formalism developed in Refs. [57, 10] seems like a promising approach, but we leave this interesting exercise to future work.

$N = 6$

This bound resembles closely our bound for $N = 4$, where we see some unexplained features at relatively low central charge. This is the first case where N is a product of coprime integers, so we can realize theories with the $N = 6$ LSM anomaly by taking the tensor product of any $N = 2$ theory with a $N = 3$ theory. Thus, using our currently known examples, we can produce theories with central charge equal to either $c = 3$ or $c = 5$ by taking

the corresponding number of compact bosons and imposing the appropriate symmetries. Examples of WZW models (or tensor products thereof) in this category include $\mathfrak{su}(2)_1 \otimes \mathfrak{su}(3)_1$ and $\mathfrak{su}(6)_1$. Our analysis here is limited again by the issues we mentioned for $N = 4, 5$, and the WZW models we mentioned are even farther from achieving saturation with our bounds.

2.2.3 Universal bounds on lightest local scalar

As we are especially interested in finding numerical evidence for CFTs with the $\mathbb{Z}_N^3$ LSM anomaly with $c < N-1$ for odd N, to which the suggested lower bound in Ref. [4] applies, we additionally obtain bounds on the lightest local operator transforming in any representation of $\mathbb{Z}_N^3$. This is the strongest gap assumption we can make, while still being universal, and thus gives, numerically, the strongest bounds. We thus expect any features corresponding to actual theories to have the most clarity within these bounds. To obtain these bounds, we incorporate the correlator bootstrap lower bounds on central charge from Figure 2.10 in addition to the bounds on scaling dimension from Figure 2.9. This leads to a notable improvement of our bounds at relatively low central charge; we note that the stronger gap assumption within modular bootstrap alone did not lead to a significant difference in the resulting bounds.

$N = 3$

As expected, the theory $\mathfrak{su}(3)_1$ continues to lie at the $c = 2$ kink of this bound, which is sharpened further by the stronger assumptions placed on the operator content. Interestingly, at $c \approx 1.7$ it appears that another feature emerges. However, this feature does not take a sharper shape upon using more derivatives in the linear functional within modular bootstrap, as our bounds are very close to saturation in this range of central charge. The question of whether or not this feature is due to an actual CFT is left open. Above $c = 2$, our bound converges to the bound on the lightest scalar operator in any CFT obtained in Ref. [44].

$N = 5$

The feature present at $c \approx 2$ in the bound on the lightest charged scalar did not survive the stronger assumptions used to obtain this bound. Thus, if that feature is due to an operator in an actual CFT with the $N = 5$ LSM anomaly, this operator would have to be symmetric under the $\mathbb{Z}_5^3$ symmetry that carries the anomaly.

Similarly to the $N = 3$ case, the stronger assumptions used to obtain this bound sharpen the kink near $c = 2.8$ and, for the size of the functional used in making the $N = 5$ plot of Figure 2.2, the theory $(\mathfrak{g}_2)_1$ is not yet ruled out. However, we also did a calculation where we improved some of our parameters to $\Lambda^{\text{mod}} = 41$ and $S^{\text{mod}}_{\text{max}} = 80$. Our bound at $\Lambda^{\text{mod}} = 25$ is very close to saturation in this range of central charge, but nonetheless we obtained an upper bound of $\Delta = 0.79990$ at $c = 2.8$, thus ruling out $(\mathfrak{g}_2)_1$. Studying this kink further is an interesting task we leave to future work. Even though we have not yet exactly pinned down the location of the kink, it seems a strong possibility that, in this case, we have uncovered evidence for a non-trivial example of some theory with the $N = 5$ LSM anomaly that has $c < 4$.

2.2.4 Application to multicritical points of (1+1)d symmetry protected topological phases

Symmetry protected topological (SPT) phases are a special class of gapped Hamiltonians with a global symmetry G. When placed on a manifold without boundary, SPT phases possess a unique, G-symmetric ground state that cannot be connected to a trivial product state by applying a finite depth local unitary circuit (FDLUC), where the local unitaries in the circuit individually preserve the global symmetry [32]. In one spatial dimension, SPT phases protected by a symmetry group G are classified by the group cohomology group $H^2(G, U(1))$. The group cohomology group encodes the algebraic structure of the phases under stacking, which is determined by its group multiplication [31]. Further, the class $[\alpha] \in H^2(G, U(1))$ labelling each phase determines the projective representation carried at each boundary endpoint when a Hamiltonian in a non-trivial SPT phase is placed on a lattice

with a boundary.

An interesting area of study is that of the nature of second-order phase transitions between SPTs [143, 141, 146, 142]. It has been argued by Bultinck [24] that for any SPT phase $[\alpha]$ satisfying the property that two copies of it is in the trivial SPT phase, i.e. $[\alpha]^2 = [1]$, any critical point describing a second-order phase transition between $[1]$ and $[\alpha]$ will have an emergent $\mathbb{Z}_2$ symmetry having a mixed anomaly with the internal symmetry G of the neighboring SPT phases. The mixed anomaly is given by a type-III cocycle $\omega \in H^1(\mathbb{Z}_2, H^2(G, U(1))) \subset H^3(\mathbb{Z}_2 \times G, U(1))$, which has the interpretation, in CFT language, that a defect operator of the emergent $\mathbb{Z}_2$ symmetry carries a projective representation of G.

We can roughly sketch the argument for the emergent symmetry and anomaly as follows. A key feature of an SPT Hamiltonian is that there is a FDLUC $\mathcal{U}$ building its ground state from a trivial product state. Importantly, a FDLUC preserves the correlation length.

Now, consider a one-parameter path of Hamiltonians that passes through a critical point separating the phases $[1]$ and $[\alpha]$ where $[\alpha]^2 = [1]$. We assume that this critical point is a CFT, and we restrict the path of Hamiltonians to lie in the vicinity of the critical point such that the low energy spectrum everywhere along the path is reproduced by a Hamiltonian of the form

$$H(\delta) = H_{\text{CFT}} + \delta\Phi \tag{2.1}$$

where Φ is a perturbation by a relevant operator in the CFT. We expect this scenario since, generically, the perturbation Φ will open a gap and SPT phases are gapped. Without loss of generality, we assume that $H(\delta)$ is in the trivial phase when $\delta < 0$ and in the non-trivial phase when $\delta > 0$. Next, note that given any Hamiltonian in the trivial SPT phase H_0, there exists a G-symmetric FDLUC $\mathcal{U}$ for which $H_\alpha \equiv \mathcal{U} H_0 \mathcal{U}^\dagger$ is in the non-trivial SPT phase and, additionally, has an identical correlation length. It is argued that $\mathcal{U}$ becomes a symmetry at the critical point. At a minimum, we can conclude that $\mathcal{U}$ is a $\mathbb{Z}_2$ symmetry, but in some cases it is possible to argue for an even larger emergent symmetry at similar critical points [137, 136]. Thus $\mathcal{U}$ (really, the restriction of $\mathcal{U}$ to the low energy Hilbert space) must precisely

be the unitary that changes the sign of the perturbation i.e. $\mathcal{U}\Phi\mathcal{U}^\dagger = -\Phi$. Further, by the properties of SPT states, we would expect that upon truncating $\mathcal{U}$ to an interval, $\mathcal{U}$ would no longer commute with the global symmetry; instead, the parts of $\mathcal{U}$ deep in the bulk would commute, but the boundary would host a projective representation of G [62]. This should be reflected in the CFT through the 't Hooft anomaly of the full $\mathbb{Z}_2 \times G$ symmetry, which is captured by a 3-cocycle $\omega \in H^1(\mathbb{Z}_2, H^2(G, U(1))) \subset H^3(\mathbb{Z}_2 \times G, U(1))$. In total, at the critical point $\mathcal{U}$ is an internal symmetry having a mixed anomaly with G, and there exists a relevant operator charged under $\mathcal{U}$ which drives the transition.

We may now produce a simple generalization of this result to the case of a multicritical point between SPT phases generated by a phase $[\alpha]$ such that $[\alpha]^N = [1]$. Such a family of phases is given, for example, by SPT phases protected by $G = \mathbb{Z}_N \times Z_N$ for which $H^2(G, U(1)) = \mathbb{Z}_N$, which is relevant to this work.

In this setting, we may now consider an $(N-1)$-parameter family of Hamiltonians

$$H(\delta_1, ..., \delta_{N-1}) = H_{\text{CFT}} + \sum_i \delta_i \Phi_i \tag{2.2}$$

and essentially repeat the argument above with minimal modification. The main difference between the previous case and this case is that the FDLUC $\mathcal{U}$ will cyclically permute the N different phases leading to a $\mathbb{Z}_N$ action among the fields that perturb the CFT into the different SPT phases, i.e. $\mathcal{U}\Phi_i\mathcal{U}^\dagger = \sum_j U_{ij}\Phi_j$ with $U^N = I$. We have presented an illustration of such a hypothetical critical point in Figure 2.3 for the case $N = 3$.

The transition to the neighboring SPT phases for such a multicritical point would be driven by relevant perturbations that are charged under the emergent $\mathbb{Z}_N$ but preserve the microscopic $\mathbb{Z}_N \times \mathbb{Z}_N$. An interesting class of theories to consider are ones where there are no relevant operators that are symmetric under the full $\mathbb{Z}_N^3$ symmetry. This is the generic case that is expected without additional fine-tuning. For $N = 3$, we see that such critical points, which do not contain $\mathbb{Z}_3^3$-symmetric relevant operators, must have $c \geq 2$ using Figure 2.1. On the contrary, with a symmetry-preserving relevant perturbation there could be neighboring phases where $\mathcal{U}$ is an exact lattice symmetry (but, generically, it will not necessarily be a

$\mathbb{Z}_N$ symmetry). Due to the anomaly, these phases cannot be trivially gapped and therefore must be SSB or gapless.

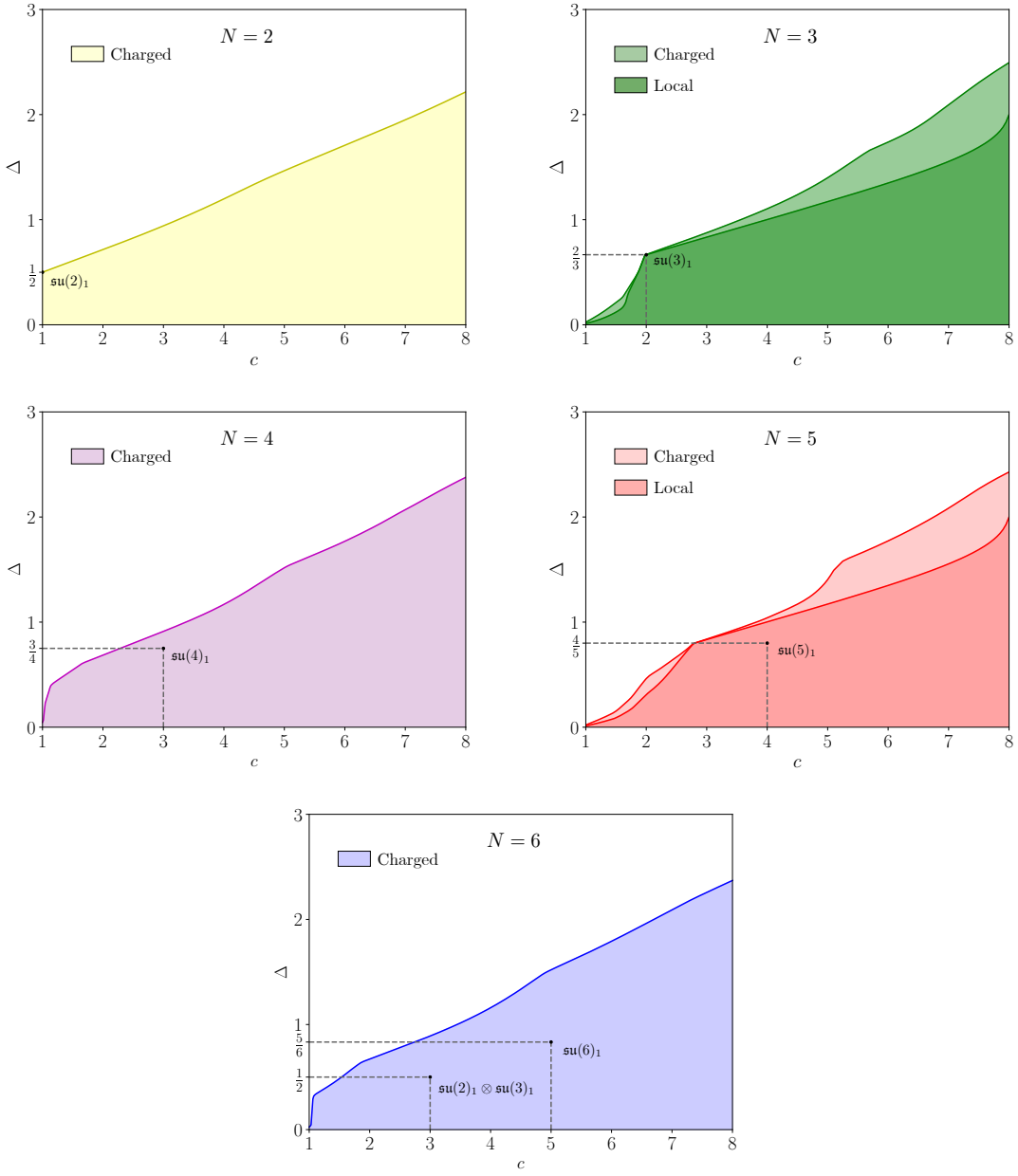

Figure 2.2: Two kinds of universal upper bounds on the scaling dimension of local operators. For $N = 2, ..., 6$, we find an upper bound on the scaling dimension of the lightest charged, scalar operator, where a charged operator is any operator transforming in a non-trivial representation of $\mathbb{Z}_N^3$. For $N = 3, 5$, we additionally obtain a stronger bound on the lightest local operator, irrespective of its symmetry properties. The shaded regions represent the allowed regions for the scaling dimensions of such operators in each of the aforementioned cases. The bounds shown here make full use of our improvements to modular bootstrap with global symmetries and anomalies and were computed with $\Lambda^{\text{mod}} = 25$ and $S_{\text{max}}^{\text{mod}} = 50$ (see Section IV for implementation details).

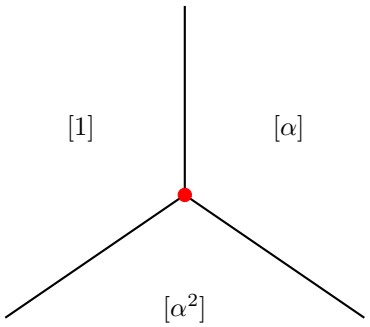

Figure 2.3: A hypothetical phase diagram where all N of the $\mathbb{Z}_N \times \mathbb{Z}_N$ SPT phases, where each phase is labeled by its respective class $[i] \in H^2(\mathbb{Z}_N \times \mathbb{Z}_N, U(1)) = \mathbb{Z}_N$, meet at a multicritical point (marked in red), illustrated in particular for the case $N = 3$. The dimension of such a phase diagram increases with N. We expect the multicritical point to possess a mixed anomaly of the kind studied in this work, and our numerical bounds restrict the properties of CFTs that can describe such multicritical points.

2.3 LSM anomalies on the lattice and in the continuum

The microscopic assumptions leading to the generalized LSM theorem manifest in a CFT as a particular set of properties possessed by so-called topological defect lines (TDLs) that implement the symmetries. In this section we first describe the lattice symmetries and anomalies and their relation to those in the continuum field theory. Then, we discuss the continuum description of these symmetries and anomalies using the TDL formalism with emphasis on aspects that enter in bootstrap calculations.

2.3.1 Lattice symmetries and anomaly matching

Consider a local lattice system defined on a spatial ring with L sites and a tensor product Hilbert space $\mathcal{H} = \bigotimes_{i=1}^{L} \mathcal{H}_i$, where the Hilbert space at each site is finite-dimensional. We will consider nearest-neighbor Hamiltonians for such a system of the form

$$H = \sum_i H_{i,i+1} \tag{2.3}$$

where $H_{i,i+1}$ acts on at most the sites $i, i{+}1$. The assumption of a nearest-neighbor Hamiltonian is generic under the assumptions of spatial locality and finite on-site Hilbert space dimension, since we may group finitely many sites together for a non-nearest-neighbor Hamiltonian while preserving these assumptions to obtain nearest-neighbor interactions.

As already stated, we will be interested in considering Hamiltonians with symmetry $G_{\mathrm{UV}} = \mathbb{Z}^{\mathrm{trans}} \times \mathbb{Z}_N^2$. We will denote the operator generating unit translations for the system, in the presence of periodic boundary conditions, by T, i.e. for any operator $\mathcal{O}_i$ acting at a single site i we have $T\mathcal{O}_i T^\dagger = \mathcal{O}_{i+1}$. We will also assume that the internal $\mathbb{Z}_N^2$ is generated by unitary operators of the following form

$$X = \bigotimes_{i=1}^{L} X_i \qquad Z = \bigotimes_{i=1}^{L} Z_i$$
$$X^N = Z^N = 1 \qquad [X, Z] = 0$$

The key microscopic assumption leading to the LSM anomaly, together with translation symmetry, is that

$$X_i Z_i = e^{2\pi i p/N} Z_i X_i. \tag{2.4}$$

That is, when the symmetry generators are restricted to a single site they form a projective representation of $\mathbb{Z}_N^2$ characterized by $\alpha_p \in H^2(\mathbb{Z}_N^2, U(1))$ with

$$\alpha_p(g,h) = \exp\left(\frac{2\pi i}{N}\eta_p(g,h)\right) = \exp\left(\frac{2\pi i p}{N} g_1 h_2\right). \tag{2.5}$$

Note that the multiplication in the product $g_1 h_2$ should be viewed as multiplication of real numbers, not the group multiplication for $\mathbb{Z}_N$ elements. Of course, all of the aforementioned symmetry generators commute with the Hamiltonian, but in light of (2.4) the assumed $\mathbb{Z}^{\text{trans}} \times \mathbb{Z}_N^2$ group structure further requires $L = 0 \mod N$.

To diagnose the anomaly of the system, we may follow e.g. [138, 63, 159], identifying the anomaly of our $(1{+}1)d$ system as being related to a $(2{+}1)d$ SPT protected by an internal symmetry. The idea is to consider the degrees of freedom of our original $(1{+}1)d$ system as being built from a stack of $(1{+}1)d$ SPTs that terminate at each site of our lattice. The $(1{+}1)d$ SPT assigned to each lattice site is determined by the projective representation carried by each site, which is uniform in our case and given by (2.5).

LSM constraints for translation symmetry in $(1{+}1)d$, related to a $(1{+}1)d$ SPT class such as α_p as previously discussed, are associated with anomaly 3-cocycles of the form [159]

$$\Omega_{\text{UV}}(g,h,k) = \exp\left(i\tau(g)\alpha_p(h,k)\right) \tag{2.6}$$

where $\alpha_p \in H^2(\mathbb{Z}_N^2, \mathbb{Z}_N)$ and $\tau \in H^1(\mathbb{Z}, \mathbb{Z}) = \mathbb{Z}$. Note that τ may be pulled back to a $\mathbb{Z}$ gauge field whose holonomy around all of space measures the number of lattice sites [138].

At low energy, lattice models of this kind may be described by CFTs. CFTs with internal, discrete symmetry G have anomalies valued in $H^3(G, U(1))$ [32]. As stated, in this work we consider lattice models that flow to CFTs with minimal internal symmetry $G = \mathbb{Z}_N^3$, which comes from the $\mathbb{Z}$ lattice translation symmetry becoming an emanant $\mathbb{Z}_N$, whose anomaly is

given by

$$\omega_{\mathrm{IR}}(g,h,k) = \exp\left(\frac{2\pi i}{N} g_1 h_2 k_3\right). \tag{2.7}$$

We will refer to ω_{IR} as an "LSM anomaly" in the remainder of this work, even though as we emphasized previously its interpretation as an LSM anomaly only truly holds at the lattice level in reference to mixed anomalies between spatial and internal lattice symmetries.

The remaining task of this section is to show that the assumed symmetry and anomaly of the CFT is compatible with the anomaly matching constraint of the lattice model. To do this, we must specify a group homomorphism γ from the UV to the IR symmetry groups, and show that the pullback of the IR anomaly cocycle through γ reproduces the UV anomaly cocycle. Denoting an element $g \in G_{\mathrm{UV}}$ by $g = (g_1, g_2, g_3)$ we use the homomorphism $\gamma : \mathbb{Z}^{\mathrm{trans}} \times \mathbb{Z}_N^2 \to \mathbb{Z}_N^3$

$$\gamma((g_1, g_2, g_3)) = (g_1 \bmod N, g_2, g_3).$$

It is easily seen that $\Omega_{\mathrm{UV}} = \gamma^* \omega_{\mathrm{IR}}$ since Ω_{UV} is only sensitive to $g \in \mathbb{Z}^{\mathrm{trans}}$ mod N anyway, and γ is merely the map sending such g to its mod N value. Finally, γ is surjective onto the subgroup $\mathbb{Z}_N^3 \subset G_{\mathrm{IR}}$, so we conclude that the proposed symmetry and anomaly is able to match the symmetry and anomaly of the lattice.

We finally remark that there are other emanant symmetries that could match the anomaly of the lattice. In particular, any cyclic group of the form $\mathbb{Z}_{kN}$ with k a positive integer would suffice, consistent with the mod N periodicity of the translation-twisted boundary conditions. For simplicity, we will not explore these other possibilities further.

2.3.2 Topological defect lines

To describe discrete, possibly anomalous, 0-form symmetries in (1+1)d we will follow the TDL formalism as described in Ref. [30], which draws on various earlier works in both physics and mathematics (see [113, 114, 117, 69, 90, 70] and other references contained therein). In

this section, we will review the salient features of the TDL formalism for our work, but for a more detailed account see Ref. [30].

In modern language, symmetries are implemented by topological operators inserted along subdimensional manifolds of spacetime [73, 30]. Invertible 0-form symmetries in $(1{+}1)d$ are implemented via TDLs, which are associated with oriented, closed curves labeled by elements of a group G. The TDLs are topological, in the sense that their support may be moved freely inside correlation functions so long as the change does not sweep the TDL past a charged operator. An important feature of TDLs is that they commute with the stress tensor. Thus, two operators that are related to each other by action by a TDL (illustrated in Fig. 2.6) must have the same conformal dimensions. The mathematical structure underlying the TDL formalism is that of a fusion category [65, 30]. In this work we will focus on fusion categories $\mathcal{C} = \mathrm{Vec}_G^\omega$ [65], i.e. G-graded vector spaces twisted by a 3-cocycle $\omega \in H^3(G, U(1))$, which describe an anomalous group G symmetry with anomaly ω.

Suppose we have a CFT with an internal symmetry G. To each group element $g \in G$, we associate an extended, oriented topological line operator $\mathcal{L}_g$ which acts on the primary fields of the theory. Two TDLs $\mathcal{L}_g$ and $\mathcal{L}_h$ supported on topologically equivalent lines may be fused together to create the line $\mathcal{L}_{gh}$, so the fusion of TDLs obeys the group multiplication law of G. For a given TDL $\mathcal{L}$, we will denote its orientation reversal (which corresponds to the inverse line when $\mathcal{L}$ is invertible) by $\bar{\mathcal{L}}$. We will denote a unitary operator acting on the Hilbert space $\mathcal{H}$ of local operators, i.e. a TDL $\mathcal{L}_g$ supported on a time slice, by $\hat{\mathcal{L}}_g$, and we will denote the action of such operators on a field ϕ as $\hat{\mathcal{L}}_g \cdot \phi$. TDLs have more explicit constructions as well in terms of topological interfaces between a given CFT and itself, which may be studied via the folding trick [113, 123].

A given TDL $\mathcal{L}_g$ may terminate at a point, and at this point will live a *defect operator* [145, 114, 30]. Such an operator may be constructed through the operator state mapping, since quantizing the theory in a cylinder geometry with a boundary condition twisted by $\mathcal{L}_g$ is equivalent to the theory in radial quantization with a primary field at the origin attached to a TDL. The possible $\mathcal{L}_g$ defect operators, which we will refer to as ϕ^g, live in

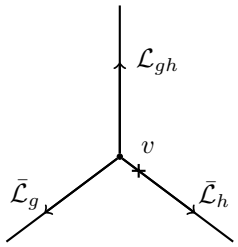

Figure 2.4: A 3-way junction with junction vector $v \in V_{\mathcal{L}_{gh},\bar{\mathcal{L}}_g,\bar{\mathcal{L}}_h}$. The convention for the junctions is that we label lines oriented pointing outwards from the junction.

the *defect Hilbert space* $\mathcal{H}_{\mathcal{L}_g}$ (sometimes we will refer to the defect Hilbert spaces as twisted sectors). More generally, multiple TDLs $\mathcal{L}_{g_1}, ..., \mathcal{L}_{g_n}$ may terminate at a n-way junction and correspondingly there will be a *junction Hilbert space* $\mathcal{H}_{\mathcal{L}_{g_1},...,\mathcal{L}_{g_n}}$, defined similarly. Due to the fusion properties of the lines, there is an isomorphism between $\mathcal{H}_{\mathcal{L}_{g_1,...,g_n}}$ and $\mathcal{H}_{\mathcal{L}_{g_1},...,\mathcal{L}_{g_n}}$. The junction Hilbert space may contain a state which is proportional to the vacuum of the bulk theory with conformal dimensions $(0, 0)$, which is unique for the CFTs we consider in this work. We denote the space of such states in $\mathcal{H}_{\mathcal{L}_{g_1},...,\mathcal{L}_{g_n}}$ by $V_{\mathcal{L}_{g_1},...,\mathcal{L}_{g_n}}$ and refer to it as the *junction vector space*. Since the TDLs we consider are all invertible, their fusion does not involve direct summation so each $V_{\mathcal{L}_{g_1},...,\mathcal{L}_{g_n}}$ is either one or zero dimensional depending on whether the TDLs forming the junction fuse to the trivial line or not. Thus, there is a single *junction vector* $v \in V_{\mathcal{L}_{g_1},...,\mathcal{L}_{g_n}}$ for each junction which keeps track of the overall phase associated with each junction, relative to the bulk vacuum state. In Figure 2.4 we illustrate a 3-way junction, where the "$\times$" keeps track of the cyclic ordering of the outward-pointing TDLs.

The effect of 't Hooft anomalies in this context is to extend the possible symmetry representations of defect operators to include fractionalized and/or projective representations. Specifically, we may construct unitary operators $\hat{\mathcal{L}}_h^g$ that implement the h symmetry in $\mathcal{H}_g$ for any $g, h \in G$. Note that $\hat{\mathcal{L}}_h^g$ depends also on a choice of junction vectors, but we will leave that dependence implicit. The TDL configuration defining this unitary is shown in Figure 2.6, which we call the lasso action. To determine aspects of the symmetry action in

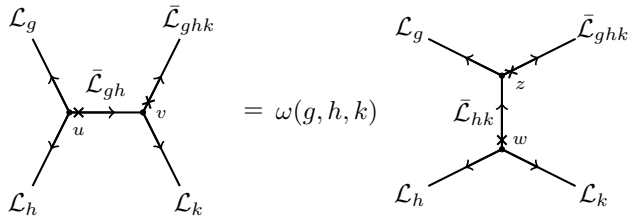

Figure 2.5: For any configuration of invertible TDLs involving external TDLs g, h, k and $(ghk)^{-1}$, there are two ways to resolve the configuration into one involving only 3-way junctions. The two decompositions differ by a 3-cocycle phase ω. We leave implicit the dependence of ω on the junction vectors appearing in the diagram.

the defect Hilbert spaces, one may perform a sequence of F-moves to compare $\hat{\mathcal{L}}_h^g \hat{\mathcal{L}}_k^g$ with $\hat{\mathcal{L}}_{hk}^g$, which will be equal up to a phase i.e.

$$\hat{\mathcal{L}}_h^g \hat{\mathcal{L}}_k^g = \chi^g(h,k) \hat{\mathcal{L}}_{hk}^g. \tag{2.8}$$

The phases $\chi^g(h,k)$ are related to the slant products of $[\omega]$, which are topological invariants of the twisted quantum double $\mathcal{Z}(\mathrm{Vec}_G^\omega)$ of Vec_G^ω [53, 151]. Using the TDL formalism, the slant product takes the form

$$\chi^g(h,k) = \frac{\omega(g,h,k)\omega(\bar{h},gh,k)\omega(h,k,\overline{hk})}{\omega(\bar{k},\bar{h},ghk)\omega(k,\bar{k},\bar{h})} \tag{2.9}$$

The derivation of (2.9) is shown in Fig. 2.7. For each junction vector $v \in V_{\mathcal{L}_g,\mathcal{L}_h,\mathcal{L}_{\overline{gh}}}$, performing a change of basis $v \to \beta(g,h)v$ for a $U(1)$ rotation by the 2-cochain $\beta(g,h)$ leads to a change in ω [30]

$$\omega(g,h,k) \to \omega(g,h,k)\frac{\beta(h,k)\beta(g,hk)}{\beta(g,h)\beta(gh,k)}. \tag{2.10}$$

One may easily verify that the following quantity [37]

$$\iota_g(h,k) = \frac{\chi^g(h,k)}{\chi^g(k,h)}$$

is an invariant of $[\omega]$ under an arbitrary change of basis in the junction vector spaces. When $\iota_g(h,k)$ is non-trivial the symmetry generators do not commute in the defect Hilbert space,

	Order of $g \in G$				
N	2	3	4	5	6
2	1 if $g = (1,1,1)$ 0 else				
3		0			
4	0		2 if g_i odd 0 else		
5				0	
6	1 if $g = (3,3,3)$ 0 else	0			3 if g_i odd 0 else

Table 2.1: The values k of $\mathbb{Z}_M$ anomalies appearing in (2.11) for elements of the groups $\mathbb{Z}_N^3$ for theories with the LSM anomaly, i.e. when the full cocycle is given by (2.14). The columns are organized by the order of the elements $g = (g_1, g_2, g_3) \in \mathbb{Z}_N^3$, and the rows each correspond to a different choice of N.

signifying a non-trivial projective representation since the symmetry generators commute when acting on the Hilbert space of local operators. The symmetry properties of defect operators under the full internal symmetry group of the theory can be thought of as topological invariants, which lead to a finer classification of CFTs enriched by symmetries. For recent explorations of this idea, see e.g. Ref. [147].

One class of 't Hooft anomalies that have been studied in recent modular bootstrap work involve a single $\mathbb{Z}_N$. These so-called type-I anomalies manifest as anomalous spin-selection rules in the defect Hilbert spaces, which can be directly used as input into the modular bootstrap [99, 100]. In contrast, we will be mostly interested in type-III anomalies [122, 140], of which the continuum LSM anomaly is a particular case, whose signatures are more subtle, involving defect operators in the defect Hilbert spaces of one $\mathbb{Z}_N$ subgroup transforming in a non-trivial projective representation of the remaining $\mathbb{Z}_N^2$ subgroup.

We will now summarize the consequences of each of these two classes of anomalies on the operator content of CFTs, each of which generally appears in the theories we consider.

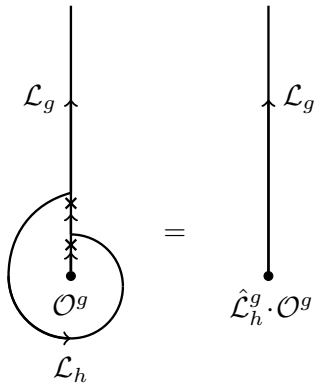

Figure 2.6: In each defect Hilbert space $\mathcal{H}_g$ the unitary $\hat{\mathcal{L}}_h^g$ implementing the action of an element $h \in G$ can be defined by wrapping an h-TDL counter-clockwise around a defect operator $\mathcal{O}^g$ inserted at the origin (in radial quantization) and collapsing the loop down to a point, as shown. This defines the action $\hat{\mathcal{L}}_h^g |\mathcal{O}^g\rangle$ on states in $\mathcal{H}_g$. We will take $U \cdot \mathcal{O} \equiv U\mathcal{O}U^\dagger$ to mean conjugation of $\mathcal{O}$ by the unitary U. One can also perform an F-move on this configuration to obtain a different convention for resolving the symmetry action, which would differ possibly from this one by a phase for invertible TDLs. Note that if g is the trivial line this reduces to the usual way that symmetry acts on local operators.

Type-I anomalies

In the case that G has a $\mathbb{Z}_M$ subgroup, the subgroup may have a $\mathbb{Z}_M$ or "type-I" anomaly [122]. In particular, the restriction of the full cocycle, which encodes the full anomaly of G, to this subgroup may be cohomologous to [122]

$$\omega(a,b,c) = \exp\left(2\pi i \frac{ka}{M^2}\left(b + c - [b+c]_M\right)\right) \tag{2.11}$$

where $a, b, c \in \mathbb{Z}_M$ and $[k] \in \mathbb{Z}_M = H^3(\mathbb{Z}_M, U(1))$ labels the anomaly. Note that $[a+b]_M \equiv a + b \mod M$. The main signature of a TDL $\mathcal{L}_g$ generating a $\mathbb{Z}_M$ symmetry with anomaly $[k]$ is that that the defect Hilbert space $\mathcal{H}_g$ will contain states whose spins are in [30]

$$s \in k/M^2 + \mathbb{Z}/M \tag{2.12}$$

Non-zero k thus corresponds to an anomalous spin selection rule for the defect operators. We will refer to a TDL generating a $\mathbb{Z}_M$ subgroup as non-anomalous if $k = 0$ and anomalous

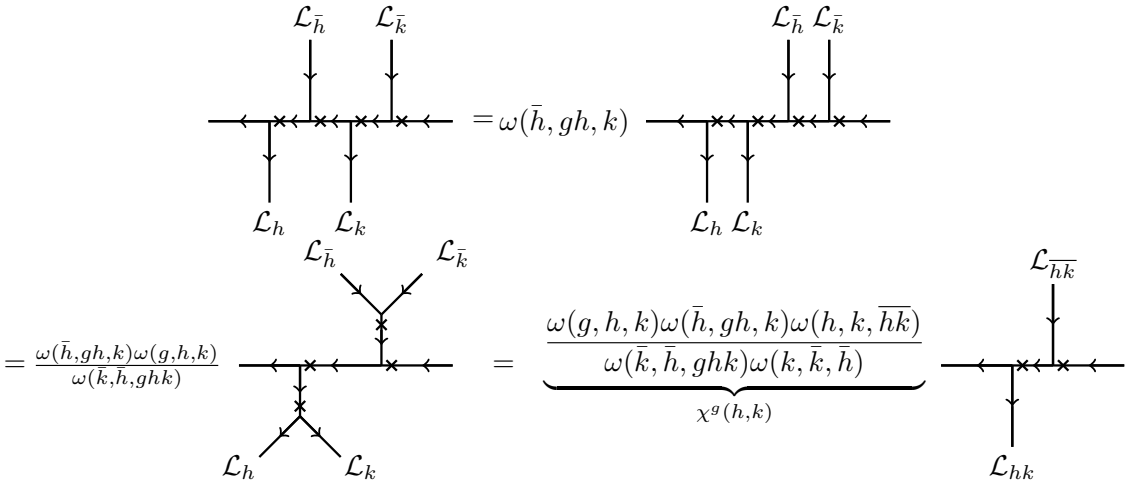

Figure 2.7: The graphical derivation of the slant product formula for $\chi^g(h,k)$. This diagram should be considered as part of a larger diagram in which the $\mathcal{L}_h$ and $\mathcal{L}_k$ TDLs are connected and each encircle a defect operator $\mathcal{O}^g$, as in the lasso diagram of Fig. 2.6. The final step in the derivation involves the phase factor associated with shrinking the bubble of the composite line $\mathcal{L}_{gh}$. This factor is determined by using the single bubble to create a second identical bubble using a sequence of F-moves, which allows the phase associated with a single bubble to be determined.

otherwise. The anomaly forces the minimum possible scaling dimension for a defect operator on such a TDL to be $\Delta = \min(\frac{|k|}{M^2}, \frac{|k-M|}{M^2})$ as opposed to $\Delta = 0$ for a non-anomalous TDL.

A $\mathbb{Z}_M$ anomaly can be detected by, for instance, studying the torus partition function of the theory twisted by symmetry defects and imposing covariance of the partition function under the modular S transformation, see e.g Refs. [99, 100]. To deduce the spin selection rule of a TDL $\mathcal{L}_g$, with g generating a $\mathbb{Z}_M$ subgroup, given any 3-cocycle ω, we can use the formula

$$e^{2\pi i M s} = \prod_{i=1}^{M-1} \omega(g^{-1}, g^i, g) \tag{2.13}$$

given in Ref. [127] and solve for the allowed values of s. The $\mathbb{Z}_M$ anomalies possessed by theories with the LSM anomalies that we study are listed in Table 2.1.

Type-III anomalies

The LSM anomalies (2.7) we consider, reproduced below for convenience with $p = 1$ and henceforth referred to as ω,

$$\omega(g, h, k) = \exp\left(\frac{2\pi i}{N} g_1 h_2 k_3\right) \tag{2.14}$$

are examples of "type-III" anomalies. The signature of this anomaly in CFT is that defect operators of one $\mathbb{Z}_N$ subgroup transform in a projective representation of the remaining $\mathbb{Z}_N \times \mathbb{Z}_N$ subgroup.

More specifically, let g_1, g_2, and g_3 be the generators of the three $\mathbb{Z}_N$ subgroups in $\mathbb{Z}_N^3$. Let us now consider a defect operator that lives at the end of a TDL $\mathcal{L}_{g_1}$. One can show using $\chi^{g_1}(g_2, g_3)$ that, in the presence of $\mathcal{L}_{g_1}$, the TDLs $\mathcal{L}_{g_2}$ and $\mathcal{L}_{g_3}$ no longer commute when the $\mathbb{Z}_N^3$ symmetry has the anomaly (2.14). For illustrative purposes, the unitaries $\hat{\mathcal{L}}_{g_2}^{g_1}$ and $\hat{\mathcal{L}}_{g_3}^{g_1}$ may be taken to satisfy

$$\hat{\mathcal{L}}_{g_2}^{g_1} \hat{\mathcal{L}}_{g_3}^{g_1} = e^{2\pi i/N} \hat{\mathcal{L}}_{g_3}^{g_1} \hat{\mathcal{L}}_{g_2}^{g_1} \tag{2.15}$$

(i.e. $\chi^{g_1}(g_2, g_3) = e^{2\pi i/N}$) meaning g_2, g_3 are realized projectively. Thus, the entire g_1 defect Hilbert space decomposes as a direct sum of such projective representations since the choice of defect operator is arbitrary.

A convenient basis for such $\mathbb{Z}_N \times \mathbb{Z}_N$ projective representations is the clock and shift basis. In this basis, g_2 is diagonalized so that states in $\mathcal{H}_{g_1}$ carry definite g_2 charge. Then, g_3 acts as a shift operator which increases g_2 charge by one modulo N. That is, we can choose primary fields $\phi_0^{g_1}, ..., \phi_{N-1}^{g_1}$ in $\mathcal{H}_{g_1}$, all with identical conformal dimensions, such that

$$\hat{\mathcal{L}}_{g_2}^{g_1} \cdot \phi_I^{g_1} = e^{2\pi i I/N} \phi_I^{g_1} \tag{2.16}$$

$$\hat{\mathcal{L}}_{g_3}^{g_1} \cdot \phi_I^{g_1} = \phi_{[I+1]_N}^{g_1}. \tag{2.17}$$

From this, we see that given a single primary field in $\mathcal{H}_{g_1}$ we can infer the existence of $N - 1$ more fields of the same conformal dimensions. Additionally, since a unitary CFT has a well-defined Hermitian conjugate, when $g_1 \neq g_1^{-1}$ there also must exist N more fields

living in $\mathcal{H}_{g_1^{-1}}$. Thus, we see that a feature of theories with the $\mathbb{Z}_N^3$ LSM anomaly is that the degeneracy of Virasoro defect primary fields with fixed conformal dimensions is a multiple of N when the defect corresponds to an order N element of G.

2.3.3 Gauging non-anomalous TDLs

A CFT with $G = \mathbb{Z}_N^3$ and the LSM anomaly described above contains various non-anomalous TDLs which, consequently, may be gauged (in CFT terminology, orbifolded). For the parts of our calculations involving correlation functions of defect operators, it will be somewhat simpler to view things from the point of view of the gauged theory since, from this perspective, many of the technicalities one needs to be aware of when working with defect operators can be avoided [2].

Let $H = \mathbb{Z}_N$ be such a non-anomalous $\mathbb{Z}_N$ subgroup. Given some CFT $\mathcal{T}_{\text{LSM}}$ with the LSM anomaly, when we gauge H we end up with a new theory $\tilde{\mathcal{T}}_{\text{LSM}} = \mathcal{T}_{\text{LSM}}/H$, which generally will have a different spectrum of local operators. The gauging procedure amounts to first throwing away all local operators that are charged under H, leaving only the H-invariant operators. This theory, keeping just symmetric local operators, will generically not be modular-invariant, so in addition to the H-invariant local operators we must also bring down H-invariant defect operators from the H-twisted sectors [144, 145, 135, 20]. Due to the spin-charge relation for defect operators [99, 100], this amounts to adding all integer spin defect operators from the H-twisted sectors. Since $H^2(\mathbb{Z}_N, U(1))$ is trivial, we do not additionally need to specify a discrete torsion class as another ingredient to this gauging procedure [144, 145].

When a set of TDLs is gauged, the gauged theory will, in general, possess a different set of TDLs from the ungauged theory. We may conclude various facts about the TDLs of $\tilde{\mathcal{T}}_{\text{LSM}}$ with the help of some results contained, for instance, in Ref. [20] and also Ref. [139]. The key thing to note is that local operators must transform in *linear* representations, but, at

[2] We thank Sahand Seifnashri and especially Shu-Heng Shao for helpful conversations and suggestions related to the content in this section.

first sight, the defect operators coming from $\mathcal{T}_{\text{LSM}}$, which are promoted to local operators of $\tilde{\mathcal{T}}_{\text{LSM}}$, transform in projective representations of the $G/H = \mathbb{Z}_N^2$ symmetry. Thus, to restore a linear representation of this symmetry in $\tilde{\mathcal{T}}_{\text{LSM}}$, the projective phases $\chi^g(h,k)$ for $g \in H$, $h,k \in G/H$ are promoted into central elements of the symmetry group $\tilde{G}$ of $\tilde{\mathcal{T}}_{\text{LSM}}$, so we can identify $\tilde{G}$ as a central extension of G/H by H with presentation

$$\langle a,b,c | a^N, b^N, c^N, aba^{-1}b^{-1}c^{-1}, aca^{-1}c^{-1}, bcb^{-1}c^{-1} \rangle. \tag{2.18}$$

In $\tilde{\mathcal{T}}_{\text{LSM}}$, the operators transforming in one-dimensional irreducible representations (irreps) of $\tilde{G}$ were local operators in $\mathcal{T}_{\text{LSM}}$, and operators transforming in higher dimensional irreps were defect operators of $\mathcal{T}_{\text{LSM}}$.

When N is prime, the groups with presentation given by (2.18) are known as Heisenberg groups $\text{He}(3,\mathbb{Z}_N)$. When $N=2$, we can also identify $\text{He}(3,\mathbb{Z}_2) \cong D_8$ where D_8 is the square dihedral group. This particular case of gauging was studied in a rather different context in Ref. [72]. When N is not prime, the representation theory of the groups that we might still call $\text{He}(3,\mathbb{Z}_N)$ differs from the prime case. In mathematics literature such groups have a different naming convention, but we will still refer to groups with presentation (2.18) as $\text{He}(3,N)$.

We imported information about the representation theory of the groups $\text{He}(3,N)$ with the help of `GAP` [75]. For each N we consider, the information about the corresponding group is contained in the `SmallGroups` library. The `SmallGroups` identification numbers for the groups are (8,3), (27,3), (64,18), (125,3), and (216,77) for $N = 2,...,6$. We will label representations of $\text{He}(3,N)$ by R_n where n is the index of the representation in `GAP`.

2.3.4 Comments on correlation functions of defect operators

The OPE is a mapping between two separated local fields ϕ_a, ϕ_b and linear combinations of local fields at a single point, schematically expressed as

$$\phi_a \times \phi_b \sim \sum_{\mathcal{O}} \lambda_{\phi_a\phi_b\bar{\mathcal{O}}}\mathcal{O}$$

where the (possibly complex) numbers $\lambda_{\phi_a\phi_b\bar{\mathcal{O}}}$ are called the OPE coefficients, and $\bar{\mathcal{O}}$ denotes the Hermitian conjugate of $\mathcal{O}$.

The OPE can also be taken between defect operators, but it has a slightly different interpretation, since in general the inputs and outputs of the defect OPE will live in different defect Hilbert spaces. Again schematically, if we take defect operators living at the ends of TDLs $\mathcal{L}_g$ and $\mathcal{L}_h$, their OPE can be written as follows

$$\phi_a^g \times \phi_b^h \sim \sum_{\mathcal{O}^{gh}} \lambda^v_{\phi_a^g \phi_b^h \bar{\mathcal{O}}^{\overline{gh}}} \mathcal{O}^{gh}$$

where we use the notation $\bar{g} \equiv g^{-1}$. It is important to note that OPE coefficients of defect operators depend, up to a phase, on a junction vector v. This is because in order to calculate the OPE coefficient, one constructs a four-point function containing three defect operators together with a junction vector connecting the TDLs of the defect operators in a configuration such as that of Figure 2.4, with defect operators added to ends of the TDLs. Further, since there are three different junction vectors for a given 3-way junction (when the TDLs forming the junction are all invertible), there is freedom to choose a junction vector when writing down OPE coefficients. Thus, there is a separate OPE coefficient for each junction vector, but all choices are related to each other in a fixed way via the cyclic permutation map between junction vector spaces [30], which results in an overall phase difference. Strictly speaking, the OPE coefficient for defect operators may also depend on the angle of the TDL leaving the defect operators, but since we deal only with scalar defect operators, which transform trivially under rotations, we do not encounter this complication.

In the most general setting, there are a few differences that must be accounted for when considering correlation functions of defect operators. First of all, the non-local nature of the defect operators leads, in some cases, certain correlation functions of defect operators to be multi-valued maps of the positions of the operators in the correlation function. This is because winding an operator charged under the TDL attached to a defect operator must involve acting on the charged operator with the TDL. Additionally, defect operators obey a modified version of crossing symmetry. A correlation function of four defect operators is

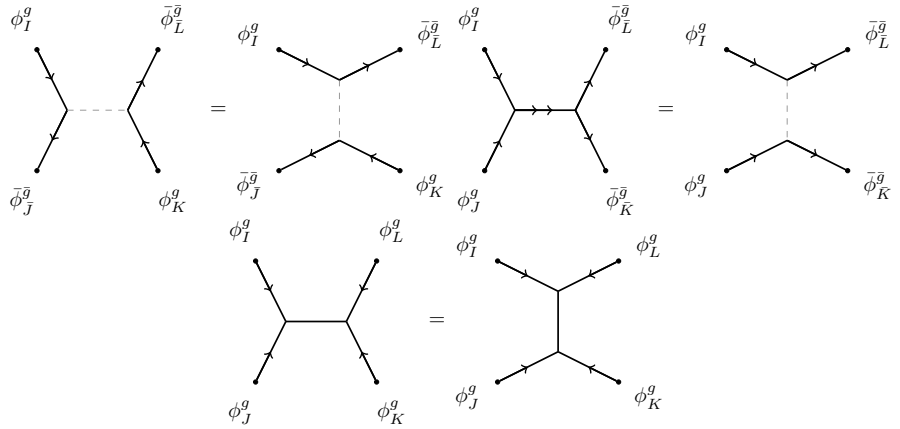

Figure 2.8: A pictorial representation of the four-point functions of defect operators that we impose crossing symmetry on in our bootstrap calculations. In these configurations, all the external TDLs are either $\mathcal{L}_g$ or $\bar{\mathcal{L}}_g$. The internal TDL marked by a double arrow represents $\mathcal{L}_{g^2}$, but when $\mathcal{L}_{g^2}$ squares to the trivial line, like when $N = 4$, we denote it by an orientation-less TDL such as in the bottom diagram. When $N = 2$ all diagrams are equivalent. For general $N > 2$, only the top and middle diagrams are consistent with the group multiplication except when $N = 4$ where the bottom diagram is consistent as well. Due to the gauging argument, we can neglect the dependence on the junction vectors since there is a canonical choice that removes the phase $\omega(g, h, k)$ in our cases, which involve only external defect operators hosted on a single $\mathbb{Z}_N$ TDL or its inverse. We could also even consider these to be correlation functions of local operators, but to emphasize the more generic scenario we stick to drawing defect operators.

really a six-point function of the defect operators along with two junction vectors, which can be represented graphically by attaching defect operators to the TDLs in the left-hand side of the graphical equation in Figure 2.5. Crossing symmetry is then modified since there may be a phase $\omega(g, h, k)$ accrued when relating the two OPE channels of the four external operators. Further, the intermediate operators will live in potentially different defect Hilbert spaces. For more discussion on correlation functions of defect operators, see also Ref. [29, 89].

Appealing to the gauging argument from the previous subsection, we will now argue that the version of crossing symmetry obeyed by the scalar defect operators we consider in this work is identical to certain local operators. Again, let $\mathcal{T}_{\text{LSM}}$ be defined as before and $H = \mathbb{Z}_N$ be a non-anomalous subgroup of $G = \mathbb{Z}_N^3$. Consider external defect operators $\phi_I^g, \bar{\phi}_{\bar{I}}^{\bar{g}}$,

for $I = 1..., N$, where we take g to generate H. Since scalar defect operators are neutral under H, upon gauging H they are promoted to local operators in $\tilde{\mathcal{T}}_{\text{LSM}}$ that, without loss of generality, can be taken to transform in representations $R_{N^2+1}, \bar{R}_{N^2+1}$ of $\text{He}(3, N)$, which are N-dimensional irreps. Since all operators appearing in OPEs of the defect operators $\phi_I^g, \bar{\phi}_{\bar{I}}^{\bar{g}}$ will also be neutral under H by $\mathbb{Z}_N$ charge conservation, gauging does not modify the values of the correlation functions that they generate. In particular, this means that it must be possible to set the extra phase that could appear in Figure (2.5) equal to 1 since we can exactly relate the value of the defect operator correlation function to a correlation function involving only local operators via gauging. Thus, for the purpose of bootstrap, the crossing equations we generate from viewing the external operators as defect operators in $\mathcal{T}_{\text{LSM}}$ or local operators in $\tilde{\mathcal{T}}_{\text{LSM}}$ will be identical. We should note, however, that if one wants to strictly think of everything in terms of defect operators, an analogous statement is that all the phases $\omega(\bar{g}, \bar{h}, \bar{k})$ can be set equal to 1 for the four-point functions we consider, which only involve TDLs corresponding to elements of H, by a careful choice of junction vectors, which is done partially in Appendix A of Ref. [30]. We note that, for these reasons, we may drop all dependence on junction vectors from the diagrams we draw and formulae we write down. This is reflected in the diagrams representing the four-point functions we consider, as in figure 2.8.

2.4 Numerical Bootstrap approach

The bounds presented in the main results section are obtained via a new approach that uses correlator bootstrap bounds as additional input to modular bootstrap, thereby augmenting the usual procedure to incorporate global symmetries into modular bootstrap. Here we outline the details of how our bounds are obtained.

2.4.1 Correlator bootstrap with defect operators

We first will show both how the local operator spectrum and central charge of unitary CFTs with a $G = \mathbb{Z}_N^3$ internal symmetry and LSM anomaly are constrained when there is an

additional assumption that the theory possesses certain light defect operators hosted on TDLs of the theory. To obtain central charge bounds, we additionally assume a non-generic gap, the value of which we scan over, to the scaling dimension of any local operator appearing in the OPEs of the defect operators.

To do correlator bootstrap, one must first derive the crossing symmetry constraints arising from all possible four-point functions involving the external operators under consideration. Deriving these constraints by hand is rather cumbersome. Since we know the bootstrap equations for the defect operators of interest are equivalent to those of local operators transforming in N-dimensional irreps of $\mathrm{He}(3, N)$, we use the `autoboot` package by Go and Tachikawa to generate the semidefinite constraints [78]. `autoboot` is a tool specially designed for producing the crossing symmetry constraints for fields transforming in arbitrary global symmetry representations[3]. Here we simply summarize the constraints we impose in an abstract form and list the spectrum assumptions used for semidefinite programming; the constraints themselves are generally too unwieldy to report here, but can be made available upon request or simply obtained via `autoboot`.

The output of `autoboot` is a set of vector-matrix-valued functions of the conformal cross-ratios $\mathbf{V}^{\Delta_D}_{R,\Delta,s}(x,\bar{x})$ (i.e. vectors whose components are matrices, with the matrix entries being functions of the conformal cross-ratios), each of which represents the crossing symmetry constraint due to external fields with scaling dimension Δ_D transforming in N-dimensional irreps of $\mathrm{He}(3, N)$ and internal fields transforming in a representation R with scaling dimension Δ and spin s. We take the functions $\mathbf{V}^{\Delta_D}_{R,\Delta,s}(x,\bar{x})$ to have components expressed in terms of the global conformal blocks for $(1{+}1)d$ CFTs, given by [111, 39]

$$g_{\Delta,s}(x,\bar{x}) = \frac{(-2)^{-s}}{1+\delta_{s,0}}(k_{\Delta+s}(x)k_{\Delta-s}(\bar{x}) + k_{\Delta-s}(x)k_{\Delta+s}(\bar{x})) \tag{2.19}$$

where

$$k_\beta(x) = x^{\beta/2}{}_2F_1\left(\frac{\beta}{2},\frac{\beta}{2},\beta,x\right). \tag{2.20}$$

[3]We thank Mocho Go and Yuji Tachikawa for their time in assisting us in setting up `autoboot` and finding a bug that prevented our correlator bootstrap calculations from working.

Each component of the vectors $\mathbf{V}^{\Delta_D}_{R,\Delta,s}(x,\bar{x})$ corresponds roughly to a distinct four-point function, although the actual implementation in `autoboot` combines different four-point functions using certain invariant tensors of the symmetry group. If we denote all distinct OPE coefficients, where the internal field is $\mathcal{O}_R$ and where we use I, J to label different choices of external fields, by $\lambda_{I\mathcal{O}_R}$ (i.e. I labels a pair of fields here), we can compactly express the crossing symmetry constraints as

$$\sum_{I,J}\sum_{R}\sum_{\mathcal{O}_R}\lambda_{I\mathcal{O}_R}\lambda_{J\mathcal{O}_R}[\mathbf{V}^{\Delta_D}_{R,\Delta_{\mathcal{O}_R},s_{\mathcal{O}_R}}]^{kIJ}=0 \tag{2.21}$$

for each k, indexing the different individual crossing symmetry constraints. Note that the OPE coefficients in (2.21) can be chosen to be real [78].

We now proceed with the usual bootstrap algorithm: we make some assumptions about the spectrum of operators of a given theory and see if our assumptions leads to a violation of (2.21) using semidefinite programming.

To do the semidefinite programming, we will use `SDPB` [131] to search for a (matrix-valued) linear functional acting on the space of vector-matrix-valued functions of $x, \bar{x}$ that obeys a number of semi-definiteness properties. For our purposes α may be expressed in a basis of derivatives of the cross ratios evaluated at the crossing-symmetric point $x, \bar{x} = \frac{1}{2}$

$$\alpha[\mathbf{V}(x,\bar{x})]=\sum_{k}\sum_{\substack{m,n=0\\ m+n\leq\Lambda^{\text{cor}}}}^{\Lambda^{\text{cor}}}a^{k}_{mn}\partial_x^m\partial_{\bar{x}}^n[\mathbf{V}(x,\bar{x})]^k\Big|_{x=\bar{x}=\frac{1}{2}} \tag{2.22}$$

where Λ^{cor} is the correlator bootstrap derivative order. The properties we need α to obey will depend on whether we are obtaining upper bounds on scaling dimensions or lower bounds on central charge. In the remaining part of this section we explain the constraints on the linear functional in each of these contexts.

Upper bounds on scaling dimension

In order to obtain upper bounds on the scaling dimension of local operators, we will assume that there exist some scalar defect operators $\phi^g_I, \bar{\phi}^{\bar{g}}_{\bar{I}}$ which have the lowest scaling dimension,

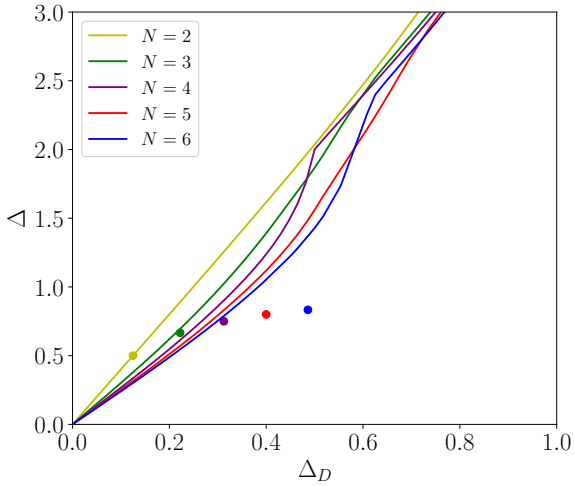

Figure 2.9: Upper bounds on the scaling dimension of the lightest $\mathbb{Z}_N^3$ charged, scalar operator appearing in the OPE of scalar defect operators with scaling dimension Δ_D living on a non-anomalous $\mathbb{Z}_N$ TDL in theories with the LSM anomaly for $N = 2, ..., 6$. The bound is not noticeably changed if the bound is calculated instead for the lightest local operator transforming in *any* representation of $\mathbb{Z}_N^3$. For each N we assign different colors. The matching colored dots indicate, for each N, points corresponding to the scaling dimension of the lightest $\mathbb{Z}_N^3$-charged local operator appearing in the OPE of the lightest scalar $\mathbb{Z}_N$ defect operator living on a non-anomalous $\mathbb{Z}_N$ TDL for $\mathfrak{su}(N)_1$. The $\mathfrak{su}(N)_1$ points for $N = 2, ..., 6$ are $(\frac{1}{8}, \frac{1}{2}), (\frac{2}{9}, \frac{2}{3}), (\frac{5}{16}, \frac{3}{4}), (\frac{2}{5}, \frac{4}{5})$, and $(\frac{35}{72}, \frac{5}{6})$. These bounds were computed with $\Lambda^{\text{cor}} = 25$ and $S^{\text{cor}}_{\text{max}} = 50$.

equal to Δ_D, among all defect operators in the defect Hilbert spaces corresponding to non-anomalous, order N TDLs. Recall that we label irreps of $\text{He}(3, N)$ as R_i according to their index in `GAP`. For the purposes of bootstrap, we may take these defect operators as transforming in the representation $R_{N^2+1}, \bar{R}_{N^2+1}$ of $\text{He}(3, N)$ when N is prime or, when $N = 4, 6$, transforming in R_{21}, R_{54} respectively—all such irreps are N dimensional. For brevity later, we will denote the set of all N-dimensional irreps by $[N]$. Taking OPEs of these defect operators may produce either local operators or defect operators. This can be

seen in the gauged language by observing first that

$$R_{N^2+1} \otimes \bar{R}_{N^2+1} = \bigoplus_{i=1}^{N^2} R_i$$

where on the right-hand side all direct summands are one-dimensional irreps. Note that this is the only possibility for $N = 2$ since in this case R_5 is a real representation. The one-dimensional irreps can be viewed as representations of $\mathbb{Z}_N^3$, and thus we see that the anomaly forces the OPE of the defect operators to contain $\mathbb{Z}_N^3$-charged operators. For $N > 2$ we also have

$$\begin{aligned}
&N \text{ prime:} && R_{N^2+1} \otimes R_{N^2+1} = N R_{N^2+2} \\
&N = 4: && R_{21} \otimes R_{21} = \bigoplus_{i=17}^{20} 2R_i \\
&N = 6: && R_{54} \otimes R_{54} = 3R_{47} \oplus 3R_{49} \oplus 3R_{51} \oplus 3R_{53}.
\end{aligned}$$

When N is prime, the above tensor products decompose into a direct sum of N copies of another N dimensional irrep, and when $N = 4, 6$ the decomposition is achieved by a combination of irreps of dimension $N/2$. These tensor product decompositions reflect, in the TDL language, that, for prime N, taking the OPE of identical defect operators living on a non-anomalous, order N TDL produces defect operators which also live on order N, non-anomalous TDLs. Thus, the scaling dimensions of such operators, when they are scalar, are bounded from below by Δ_D. For our cases $N = 4, 6$ this is not the case; instead two such defect operators create defect operators living on an order $N/2$ non-anomalous TDL, and we make no assumption about the spectrum of such operators beyond what is guaranteed by unitarity.

We now describe how to rule out various assumptions on the scaling dimension of the lightest operators appearing in the OPE of defect operators with the above listed properties. For all N we refer to an operator transforming in *any* non-trivial one-dimensional representation of $\mathrm{He}(3, N)$, which can be interpreted as an operator transforming in a non-trivial

representation of $\mathbb{Z}_N^3$, as a charged operator, and refer to an operator transforming in the trivial representation as a symmetric operator. We will denote the assumed minimum scaling dimensions of any scalar symmetric/charged local operator appearing in the OPE of the defect operators by $\Delta_0^{\min}, \Delta_Q^{\min}$ respectively. We will use $[0]$ and $[Q]$ to denote, respectively, the set of trivial and non-trivial one-dimensional irreps. We will refer to these minimum scaling dimensions $\Delta_0^{\min}, \Delta_Q^{\min}$ as the gaps. To attempt to rule out these gaps, we seek a linear functional α of the form (2.22), satisfying

$$\alpha[\mathbf{V}^{\Delta_D}_{R_1,0,0}] = 1$$

$$\alpha[\mathbf{V}^{\Delta_D}_{R_i,\Delta,s}] \succeq 0 \qquad \forall \Delta \geq \begin{cases} \Delta_0^{\min} & R_i \in [0], s = 0 \\ \Delta_Q^{\min} & R_i \in [Q], s = 0 \\ \Delta_D & R_i \in [N], s = 0, N \text{ odd} \\ |s| & \text{else} \end{cases}$$

where $M \succeq 0$ for a real, symmetric matrix M means that M is positive semidefinite. It is necessary to truncate the values of spin for which we impose the above constraints to only include $|s| \leq S_{\text{max}}^{\text{cor}}$, which we choose to be sufficiently large so that our bounds at fixed Λ^{cor} are stable to an increase in $S_{\text{max}}^{\text{cor}}$. Upon finding such a linear functional, we would conclude that the given assumptions are inconsistent with crossing symmetry of the defect operators. If $\Delta_0^{\min} = 0$, we would conclude that $\Delta_Q^{\min}$ is an upper bound on the lightest charged operator appearing in the OPE of the defect operators. If $\Delta_0^{\min} = \Delta_Q^{\min} = \Delta^{\min}$, we conclude that $\Delta^{\min}$ is an upper bound on the lightest operator of any charge.

Finally, we will denote by $\Delta_Q^*(N, \Delta_D)$ the optimal, to within some small numerical tolerance, upper bound on the scaling dimension of the lightest charged, local, scalar, operator which appears in the OPE of scalar defect operators transforming in the $R_{N^2+1}, \bar{R}_{N^2+1}$ representations of $\text{He}(3, N)$ with scaling dimension Δ_D. These bounds are shown in Figure 2.9. We note that we found the bounds to remain unchanged upon doing similar calculations with

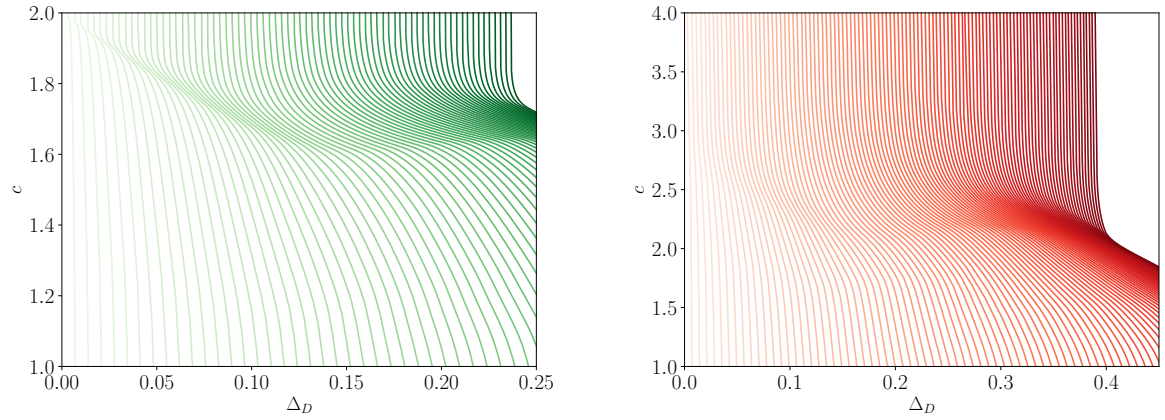

Figure 2.10: Lower bounds on central charge for $N = 3$ (left) and $N = 5$ (right) as a function of the scaling dimension of the lightest scalar defect operator living on an order N non-anomalous TDL in a theory with the LSM anomaly. Each solid curve represents a different value of the minimum scaling dimension for the lightest scalar, local operator appearing in the OPE of the external defect operators. For $N = 3$ we compute the curves for values where the gap to the minimum value of the scaling dimension for such operators is $\Delta = 0.01, ..., 0.75$ and, for $N = 5$, $\Delta = 0.01, ..., 1.05$, each with spacing 0.01 between successive values. The darkness of the curve indicates the value of the gap from low to high with increasing darkness. For $N = 3$, the computed values of the central charge lower bound are less than $c = 2$, and for $N = 5$ all computed values are less than $c = 4$, in agreement with known theories. To obtain these bounds we used $\Lambda^{\text{cor}} = 15$ with $S^{\text{cor}}_{\text{max}} = 30$.

$\Delta_0^{\text{min}} = \Delta_Q^{\text{min}}$, i.e. the resulting bound is on the lightest local operator. We do not present bounds on the lightest symmetric operator since our bounds could not guarantee that the OPE of defect operators must produce a relevant symmetric scalar for any choice of Δ_D, so we do not consider such bounds to be particularly interesting.

Lower bounds on central charge

For the central charge bounds, we will assume N is odd and prime since these are the cases for which we are most interested in refining our bounds.

Every unitary, (1+1)d CFT possesses conserved, spin-2, quasiprimary fields which are the holomoprhic and anti-holomorphic stress tensor fields $T(z), \bar{T}(\bar{z})$. With the appropriate

normalization [118], the OPE coefficient of a primary field ϕ with scaling dimension Δ, its conjugate, and the stress tensor is given in $1{+}1d$ by[4]

$$\lambda_{\phi\bar{\phi}T} = \frac{2\sqrt{\dim R}\Delta}{\sqrt{c}},$$

where R is the representation of the internal symmetry group that ϕ transforms in. In the following we will take $\dim R = N$, applicable to the cases that we consider.

To bound the central charge, we again consider some defect operators $\phi_I^g, \bar{\phi}_{\bar{I}}^{\bar{g}}$ whose scaling dimension is Δ_D. We then expand (2.21) as

$$\begin{aligned} 0 = [\mathbf{V}^{\Delta_D}_{R_1,0,0}]^k + \lambda^2_{\phi^g\bar{\phi}^{\bar{g}}T}[\mathbf{V}^{\Delta_D}_{R_1,2,2}]^k \\ + \sum_{I,J}\sum_{R}\sum_{\substack{\mathcal{O}_R\neq T,\bar{T}\\ \Delta_{\mathcal{O}_R}>0}} \lambda_{I\mathcal{O}_R}\lambda_{J\mathcal{O}_R}[\mathbf{V}^{\Delta_D}_{R,\Delta_{\mathcal{O}_R},s_{\mathcal{O}_R}}]^{kIJ} \end{aligned} \tag{2.23}$$

We now act on (2.23) with a linear functional of the form (2.22)

$$\alpha[\mathbf{V}^{\Delta_D}_{R_1,2,2}] = 1$$

$$\alpha[\mathbf{V}^{\Delta_D}_{R_i,\Delta,s}] \succeq 0 \qquad \forall \Delta \geq \begin{cases} \Delta^{\min} \text{ if } R_i \in [0]\cup[Q], s=0 \\ \Delta_D \text{ if } R_i \in [N],\ s=0 \\ |s| \text{ otherwise} \end{cases}.$$

Note that here we have assumed that the scaling dimension of any scalar, local operator appearing in the OPE of the external defect operators has scaling dimension at least $\Delta^{\min}$. It is necessary to impose some gap in the spectrum of symmetric, scalar operators in order to obtain any central charge bounds, since otherwise we would not be able to have $\alpha[\mathbf{V}^{\Delta_D}_{R_1,0,0}] < 0$. Acting with such a functional and rearranging terms allows us to conclude

$$\lambda^2_{\phi^g\bar{\phi}^{\bar{g}}T} = \frac{4N\Delta_D^2}{c} \leq -\alpha[\mathbf{V}^{\Delta_D}_{R_1,0,0}],$$

[4]Note that the extra factor of $\sqrt{\dim R}$ arises due to the definition in `autoboot` of the OPE coefficient $\lambda_{\phi\bar{\phi}I} = \sqrt{\dim R}$ for an operator ϕ transforming in the representation R of the internal symmetry.

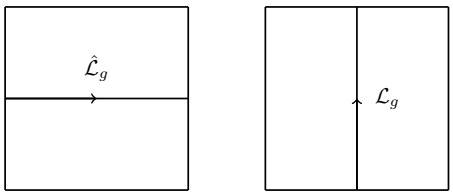

Figure 2.11: Each square represents a torus, since opposite edges are identified, where we quantize the theory on horizontal spatial slices. On left is the torus partition with a horizontal twist, corresponding to acting with symmetry accross one period of imaginary time evolution. On right is the torus partition function with a vertical twist, corresponding to the partition function of the theory subject to a $\mathcal{L}_g$-twisted boundary condition.

which means, assuming $-\alpha[\mathbf{V}^{\Delta_D}_{R_1,0,0}] > 0$ consistent with a gap $\Delta^{\min}$ not being ruled out,

$$c \geq \frac{4N\Delta_D^2}{-\alpha[\mathbf{V}^{\Delta_D}_{R_1,0,0}]}. \tag{2.24}$$

Thus, we want to minimize $-\alpha[\mathbf{V}^{\Delta_D}_{R_1,0,0}]$ consistent with the previously stated constraints to find the strongest lower bound on c, which is again done using `SDPB`. We will denote our lower bounds obtained in this way, which are presented in Figure 2.10, by $c^*(N, \Delta_D, \Delta^{\min})$. Central charge bounds in 1+1d CFT have been obtained in other works, e.g. in Ref. [149], so in order to verify the correctness of our setup, we reproduced some of the central charge bounds contained therein.

2.4.2 Modular bootstrap

Twisted partition functions

The partition function of a unitary, compact, (1+1)d CFT on a spacetime torus encodes the spectrum of scaling dimensions and spins of each primary field of the theory. When the theory has a global, internal symmetry G, we can assign additional quantum numbers accounting for the particular representations ρ of G that states in the Hilbert space of the theory transform in. The torus partition function (which will be denoted pictorially by an empty square with opposite edges identified, i.e. either diagram in Figure 2.11 with the

trivial TDL in place of $\mathcal{L}_g$) with modular parameters $\tau, \bar{\tau}$ takes the form (when $c > 1$)

$$Z(\tau, \bar{\tau}) = \mathrm{Tr}(q^{L_0 - \frac{c}{24}} \bar{q}^{\bar{L}_0 - \frac{c}{24}}) \tag{2.25}$$

$$= \sum_{h,\bar{h}} \sum_{\rho} n^{\rho}_{h,\bar{h}} \, \chi_{h,\bar{h}}(\tau, \bar{\tau}) \tag{2.26}$$

where $q = e^{2\pi i \tau}, \bar{q} = e^{-2\pi i \bar{\tau}}$, $\chi_{h,\bar{h}}(\tau, \bar{\tau}) = \chi_h(\tau)\bar{\chi}_{\bar{h}}(\bar{\tau})$, and χ_h are the Virasoro characters

$$\chi_0(\tau) = \frac{(1-q)}{\eta(\tau)} q^{-\frac{c-1}{24}} \qquad \chi_h(\tau) = \frac{1}{\eta(\tau)} q^{h - \frac{c-1}{24}}$$

where $\eta(\tau)$ is the Dedekind eta function. Note that to do modular bootstrap calculations, we use so-called reduced characters, defined by replacing $\chi_h(\tau) \to \tau^{1/4}\eta(q)\chi_h(\tau)$. Henceforth, when we write $\chi_h(\tau)$ etc. we will always be referring to these reduced Virasoro characters. In (2.26), $n^{\rho}_{h,\bar{h}}$ are positive integers equal to the dimension of the irreducible representation ρ times its multiplicity within each Verma module for conformal dimensions $h, \bar{h}$. The assumption of compactness ensures that there is a unique ground state and a discrete spectrum when the spatial extent of spacetime is finite. The partition function is constrained to be invariant under $SL(2, \mathbb{Z})$ modular transformations. Such transformations relate descriptions of the same tori with different values of the modular parameters and are generated by the modular S and T transformations

$$S : \tau \to -1/\tau \qquad T : \tau \to \tau + 1.$$

Imposing equivalence of the torus partition function under such transformations leads to the modular invariance constraints

$$Z(\tau, \bar{\tau}) = Z(-1/\tau, -1/\bar{\tau}) = Z(\tau + 1, \bar{\tau} + 1).$$

We can also use TDLs to construct other partition function-like objects that probe aspects of the G global symmetry, which we will call twisted partition functions. These are constructed by considering the theory on a spacetime torus in the presence of TDLs wrapped around the cycles of the torus. When a TDL corresponding to the group element g is wrapped around a spatial cycle, illustrated in the left diagram within Figure 2.11, this corresponds to

acting with $\hat{\mathcal{L}}_g$ across one period of imaginary time evolution. Specializing to $G = \mathbb{Z}_N^3$, let us denote the group elements of $\mathbb{Z}_N^3$ by three-component $\mathbb{Z}_N$-valued vectors i.e. $g = (i, j, k)$ for some $i, j, k \in \mathbb{Z}_N$. Similarly, let us denote representations of G, which are all one dimensional, in a similar way but, for differentiation, with square brackets $\rho = [i, j, k]$. Then, a state transforming in a representation ρ of G transforms under g as

$$\hat{\mathcal{L}}_g \left|\rho\right\rangle = e^{2\pi i \langle \rho, g\rangle / N} \left|\rho\right\rangle$$

where $\langle \rho, g\rangle = ii' + jj' + kk'$ for $g = (i, j, k)$, $\rho = [i', j', k']$. With this, we may express the torus paritition function with a horizontal twist as

$$\begin{aligned} Z^g(\tau, \bar{\tau}) &= \mathrm{Tr}_{\mathcal{H}} \left(\hat{\mathcal{L}}_g q^{L_0 - \frac{c}{24}} \bar{q}^{\bar{L}_0 \cdot - \frac{c}{24}} \right) \\ &= \sum_{h,\bar{h}} \sum_{\rho \in \mathrm{Rep}(G)} n^{\rho}_{h,\bar{h}} e^{2\pi i \langle \rho, g\rangle / N} \chi_h(\tau) \bar{\chi}_{\bar{h}}(\bar{\tau}). \end{aligned}$$

Likewise, if a g-TDL is wrapped around a cycle in the time direction, illustrated within Figure 2.11 on the right, then the resulting twisted partition function represents the partition function of the theory where the trace is taken over the defect Hilbert space $\mathcal{H}_g$

$$\begin{aligned} Z_g(\tau, \bar{\tau}) &= \mathrm{Tr}_{\mathcal{H}_g} (q^{L_0 - \frac{c}{24}} \bar{q}^{\bar{L}_0 - \frac{c}{24}}) \\ &= \sum_{h,\bar{h}} n^{g}_{h,\bar{h}} \chi_{h,\bar{h}}(\tau, \bar{\tau}). \end{aligned}$$

The coefficients of the above twisted partition function $n^g_{h,\bar{h}}$ are again positive integers representing the degeneracy of each defect operator with conformal dimensions $h, \bar{h}$. Of course, as we explained previously, the states in the defect Hilbert space may be dressed with (fractionalized) global symmetry quantum numbers as well, but this fact will not be important for our modular bootstrap calculations.

The twisted partition functions are also subject to modular transformation relations. Covariance under T leads to the spin selection rule (2.12) [99, 100, 30]. Since a modular S transformation swaps the two cycles of the torus it interchanges the space and time directions.

Thus, we see that

$$Z^g(-1/\tau,-1/\bar{\tau}) = Z_g(\tau,\bar{\tau}) \tag{2.27}$$

$$Z_g(-1/\tau,-1/\bar{\tau}) = Z^{\bar{g}}(\tau,\bar{\tau}). \tag{2.28}$$

The defect Hilbert space spectrum is thus completely determined by the local operators of the theory and their symmetry representations. Now, we can construct a $2|G|-1$ dimensional vector of twisted partition functions

$$\mathbf{Z}(\tau,\bar{\tau}) = \begin{pmatrix} Z(\tau,\bar{\tau}) \\ Z^g(\tau,\bar{\tau}) \\ \vdots \\ Z_g(\tau,\bar{\tau}) \\ \vdots \end{pmatrix}.$$

This allows us to compactly express the modular transformation relations amongst the twisted partition functions

$$\mathbf{Z}(-1/\tau,-1/\bar{\tau}) = P\mathbf{Z}(\tau,\bar{\tau}) \tag{2.29}$$

where P is a permutation matrix implementing the relations (2.27,2.28) between the components of $\mathbf{Z}$.

Borrowing terminology from Refs. [99],[100], $\mathbf{Z}$ is currently expressed in the *twist basis*, but in order to do bootstrap calculations to obtain bounds which depend on the symmetry representations it is necessary to write $\mathbf{Z}$ in the *charge basis*, in which positivity is manifest. This is done by performing a discrete Fourier transformation on the partition functions Z^g, leading to partition functions counting the contributions from states transforming in a single representation ρ

$$\begin{aligned} Z^\rho(\tau,\bar{\tau}) &= \frac{1}{|G|}\sum_{g\in G} e^{-2\pi i\langle\rho,g\rangle/N} Z^g(\tau,\bar{\tau}) \\ &= \sum_{h,\bar{h}} n^\rho_{h,\bar{h}} \chi_h(\tau)\bar{\chi}_{\bar{h}}(\bar{\tau}). \end{aligned}$$

We remind the reader again that the vertically twisted partition functions Z_g already have a decomposition into Virasoro characters with positive coefficients, so no additional change of basis is needed in those instances. Writing $\mathbf{Z}(\tau,\bar{\tau}) = C\tilde{\boldsymbol{Z}}(\tau,\bar{\tau})$, where $\tilde{\mathbf{Z}}$ is the twisted partition function in the charge basis and C is a matrix implementing the discrete Fourier transformation, we see that $\tilde{\boldsymbol{Z}}$ transforms under the modular S transformation as

$$\tilde{\mathbf{Z}}(-1/\tau,-1/\bar{\tau}) = F\tilde{\mathbf{Z}}(\tau,\bar{\tau})$$

where $F = C^{-1}PC$.

There is an additional step that we perform that greatly simplifies our calculations, which is a generalization of the procedure outlined in Ref. [100] for reducing the dimension of the vector of twisted partition functions $\tilde{\mathbf{Z}}$. Given some group G, each outer automorphism $\gamma \in \mathrm{Out}(G)$ will generate a reduced vector partition function where the components consist of summing over the twisted partition functions, in the twist basis, corresponding to TDLs which lie in equivalence classes under γ. The simplest non-trivial example of this is when $\gamma(g) = g^{-1}$, which pairs each TDL with its orientation reversal, which generates the reduction employed in Ref. [100]. In general, to lose no generality in the bootstrap calculations, one finds the largest subgroup of outer automorphisms, which we will denote $\Gamma \subseteq \mathrm{Out}(G)$, that does not mix TDLs with different $\mathbb{Z}_N$ anomalies and performs the reduction with the outer automorphisms in this subgroup. We will denote the equivalence classes of TDLs that are related to each other by group automorphisms in Γ by $[1],...,[n_\Gamma]$. That is, denoting elements of G by g_n, one finds a reduction matrix

$$r_{mn} = \begin{cases} 1 & g_n \in [m] \\ 0 & \text{else} \end{cases}. \tag{2.30}$$

The full reduction matrix, in the twist basis, is then given by taking two copies of r_{mn}, where each copy reduces the horizontally/vertically twisted partition functions (note that the copy for the vertically twisted partition functions excludes the redundant first row of r

representing the untwisted partition function)

$$R_{mn} = \begin{cases} r_{mn} & 1 \le m \le n_\Gamma, 1 \le n \le |G| \\ r_{(m-n_\Gamma+1)(n-|G|+1)} & \substack{n_\Gamma+1 \le m \le 2n_\Gamma-1 \\ |G|+1 \le n \le 2|G|-1} \\ 0 & \text{else} \end{cases} . \tag{2.31}$$

Finally, in the charge basis we write $\tilde{R} = RC$. Then, defining $\tilde{\mathbf{Z}}_{\text{red}} = \tilde{R}\tilde{\mathbf{Z}}$ we may write the simplified modular covariance equation

$$\tilde{\mathbf{Z}}_{\text{red}}(-1/\tau, -1/\bar{\tau}) = F_{\text{red}}\tilde{\mathbf{Z}}_{\text{red}}(\tau, \bar{\tau}) \tag{2.32}$$

where $F_{\text{red}} = \tilde{R}F\tilde{R}^T(\tilde{R}\tilde{R}^T)^{-1}$. We present F_{red} for the groups $\mathbb{Z}_N^3$ we consider in this work in Appendix A. Finally, we define the vectors

$$[\mathbf{M}^j_{h,\bar{h}}(\tau, \bar{\tau})]_i = \delta_{ij}\chi_{h,\bar{h}}(-1/\tau, -1/\bar{\tau}) - [F_{\text{red}}]_{ij}\chi_{h,\bar{h}}(\tau, \bar{\tau}). \tag{2.33}$$

Then the statement of modular covariance of the twisted partition function may be expressed as

$$\sum_{j,h,\bar{h}} n^j_{h,\bar{h}}\mathbf{M}^j_{h,\bar{h}}(\tau, \bar{\tau}) = 0. \tag{2.34}$$

Bounding the local operator spectrum

To put upper bounds on the scaling dimension of local operators, similarly to correlator bootstrap we aim to show via semidefinite programming that certain assumptions about the spectrum of local and defect operators in a CFT with some global symmetry and anomaly, encoded in the twisted partition functions, lead to a violation of (2.34). The new ingredients to the standard modular bootstrap program with global symmetries that we introduce are our bounds coming from correlator bootstrap, which allow the more subtle LSM anomaly to enter our final modular bootstrap calculations. We will explain how those bounds lead to non-trivial lower bounds on the scaling dimension of the lightest defect operators, under the assumption of gaps in the spectrum of local operators, and how this can be used to

generate universal upper bounds on the scaling dimension of the lightest local operators with various symmetry properties. Incorporating the bounds from correlator bootstrap gives strictly stronger bounds than modular bootstrap alone, and is essential for finding any bound at all on the lightest charged operator when N is odd.

We can make stronger assumptions about the defect operator spectrum due to our previously obtained bounds $\Delta^*(N, \Delta_D)$ and $c^*(N, \Delta_D, \Delta^{\min})$, for reasons we now explain.

As before, let $\Delta_0^{\min}$ and $\Delta_Q^{\min}$ denote the assumed lower bounds on the scaling dimension of any scalar, local operator that is, respectively, symmetric or charged under $\mathbb{Z}_N^3$. Next define

$$\begin{aligned}&\tilde{\Delta}_D^{\text{scal}}(\Delta_0^{\min}, \Delta_Q^{\min}) \\ &\qquad \equiv \min\{\Delta_D : \Delta^*(N, \Delta_D) \geq \max(\Delta_0^{\min}, \Delta_Q^{\min})\}.\end{aligned}$$

This represents the minimum scaling dimension of a defect operator living on a non-anomalous, order N TDL whose OPE does not necessarily contain local operators whose scaling dimensions violate the assumed gaps. Thus, $\tilde{\Delta}_D^{\text{scal}}(\Delta_0^{\min}, \Delta_Q^{\min})$ is a lower bound on the scaling dimension of any such defect operator. To incorporate the central charge lower bounds, when $\Delta_0^{\min} = \Delta_Q^{\min} = \Delta^{\min}$, we define

$$\tilde{\Delta}_D^{\text{cent}}(\Delta^{\min}, c) \equiv \min\{\Delta_D : c^*(N, \Delta_D, \Delta^{\min}) \leq c\}$$

which represents the minimum defect operator scaling dimension consistent with gaps $\Delta_0^{\min}, \Delta_Q^{\min}$ and central charge c. Note that, in practice, we can only compute the curves $c^*(N, \Delta_D, \Delta^{\min})$ for a finite list of values $\{\Delta^{(i)}\}$ for the gap in the local operator spectrum $\Delta^{\min}$. Consequently, we perform an interpolation between the central charge curves to achieve the corresponding curve for values of $\Delta^{\min}$ between some $\Delta^{(i)}$ and $\Delta^{(i+1)}$. Given functions $f_i(\Delta_D), f_{i+1}(\Delta_D)$

representing such neighboring curves, we use the interpolation $\tilde{f}_{i,i+1}(\Delta_D)$ given by

$$\begin{aligned}\tilde{f}_{i,i+1}(\Delta_D) &\equiv f_{i,i+1}^{-1}(\Delta_D) \\ f_{i,i+1}(c) &\equiv (1-x)f_i^{-1}(c) + xf_{i+1}^{-1}(c) \\ x &\equiv \frac{\Delta^{\min} - \Delta^{(i)}}{\Delta^{(i+1)} - \Delta^{(i)}}.\end{aligned}$$

This has the effect of smoothing out our bounds but introduces a small degree of non-rigorousness. Our focus in this work is primarily on showing the existence of a bound and its general, qualitative features, so consequently we do not attempt to quantify the error introduced in this way. However, we should certainly discuss this effect in relation to our claim that $(\mathfrak{g}_2)_1$ is outside the allowed region in our $N = 5$ bound on the lightest local scalar. We can safely rule out $c = \frac{14}{5}$ and $\Delta^{\min} = \frac{4}{5}$ since the curve $c^*(5, \Delta_D, \frac{4}{5})$ is computed exactly, up to discretization effects in Δ_D that should be very small as the curves are quite smooth.

At this point we see that there are two, independent lower bounds on the defect operator scaling dimension that are consistent with either the gaps $\Delta_0^{\min}, \Delta_Q^{\min}$ or the central charge c; a theory with a defect operator of a lower scaling dimension than the maximum of the two would thus be inconsistent. Finally we define

$$\Delta_D^{\min}(\Delta_0^{\min}, \Delta_Q^{\min}, c) \equiv \max\{\tilde{\Delta}_D^{\text{scal}}, \tilde{\Delta}_D^{\text{cent}}\}$$

and conclude that this is the lowest possible value of the defect operator scaling dimension consistent with the gaps $\Delta_0^{\min}, \Delta_Q^{\min}$ and c.

The final step is to do a standard modular bootstrap calculation to determine whether the gaps in the local operator spectrum and the gap in the defect operator spectrum are inconsistent with modular covariance of the twisted partition function. To do this, we seek a linear functional, which acts on vector-valued functions of the modular parameters, of the form

$$\alpha[\mathbf{M}(\tau,\bar{\tau})] = \sum_j \sum_{\substack{m,n=0 \\ m+n\leq\Lambda^{\text{mod}}}}^{\Lambda^{\text{mod}}} a_{mn}^j \partial_\tau^n \partial_{\bar{\tau}}^m \left[\mathbf{M}(\tau,\bar{\tau})\right]_j \Bigg|_{\tau=i,\bar{\tau}=-i} \tag{2.35}$$

where Λ^{mod} is the modular bootstrap derivative order. In our setup, we will allow primary operators of three different types to enter the spectrum of the theories we consider: the vacuum primary with $h = \bar{h} = 0$, degenerate primaries with either h or $\bar{h}$ being equal to 0, and non-degenerate primaries with $h, \bar{h} > 0$. For the case of degenerate primaries and the vacuum, the degenerate Virasoro character of weight 0 enters, while in the non-degenerate case only the non-degenerate characters enter. Further, we will assume that the spectrum of the theories we consider is parity invariant, meaning $n^j_{h,\bar{h}} = n^j_{\bar{h},h}$ without loss of generality, since the anomalies considered in this work are compatible with such an assumption [11, 99, 100]. We thus will define

$$\mathbf{M}^j_{\Delta,s}(\tau,\bar{\tau}) \equiv \mathbf{M}^j_{h,\bar{h}}(\tau,\bar{\tau}) + \mathbf{M}^j_{\bar{h},h}(\tau,\bar{\tau})$$

where $\Delta = h + \bar{h}, s = h - \bar{h}$ and we assume $s \geq 0$. Note that, in this notation, we can denote the contribution from degenerate Virasoro primaries (including that of the vacuum) by $\mathbf{M}^j_{s,s}(\tau,\bar{\tau})$ for $s > 0$. The linear functional (2.35) that we search for will be constrained to have the following properties

$$\begin{aligned}
&\alpha[\mathbf{M}^1_{0,0}] = 1 \\
&\alpha[\mathbf{M}^i_{\Delta,s}] \geq 0 \qquad \forall \Delta \geq \begin{cases} \Delta^{\text{min}}_0 & i = 1, s = 0 \\ \Delta^{\text{min}}_Q & 2 \leq i \leq n_\gamma, s = 0 \\ \Delta^{\text{min}}_D & i = 2n_\gamma - 1, s = 0 \\ |s| & \text{else, } s \leq S^{\text{mod}}_{\text{max}} \in S_i \end{cases} \\
&\alpha[\mathbf{M}^i_{s,s}] \geq 0 \qquad \forall s \leq S^{\text{mod}}_{\text{max}} \in S_i
\end{aligned}$$

where we use S_i to denote the spins allowed by the spin selection rule for the local operators, which are just any integer, and defect operators, given in Table 2.1, for the i^{th} composite sector. Note that $2n_\gamma - 1$ is the index denoting the composite defect sector corresponding to non-anomalous, order N TDLs. Further we denote our spin truncation parameter for our modular bootstrap calculations by $S^{\text{mod}}_{\text{max}}$.

Upon finding such a linear functional α, we conclude that the assumed gaps $\Delta_0^{\min}$ and $\Delta_Q^{\min}$ are inconsistent with both modular covariance of the twisted partition function and crossing symmetry of defect operators. When we successfully find a linear functional obeying the constraints when $\Delta_0^{\min} = 0$ this represents an upper bound on the lightest charged operator, and similarly when $\Delta_0^{\min} = \Delta_Q^{\min}$ we get a bound on the lightest local operator. Either of these bounds may be optimized, to within a small numerical tolerance, to obtain the final bounds, which are shown in Figure 2.2. This concludes our description of our modifications to the usual modular bootstrap procedure.

2.5 Conclusion

In this work, we take an additional step towards constraining the space of $(1{+}1)d$ bosonic CFTs with finite global symmetries and anomalies. To this end, we incorporate a more complete picture of the symmetry properties of defect operators into the modular bootstrap, exploiting the delicate balance between the spectrum of defect operators and local operators. We make the relationship between the spectra of defect and local operators quantitatively precise using conformal bootstrap techniques, and in the end obtain universal bounds on the spectrum of local operators. Our primary result is a generalization of the main results of Refs. [99, 100] that $\mathbb{Z}_N$ anomalies imply the presence of light, charged operators in a CFT. What we show is that this statement continues to hold for a class of $\mathbb{Z}_N^3$ anomalies that, in some cases, do not lead to any non-trivial spin selection rule for certain defect operators. The particular symmetries and anomalies that we study occur in physically relevant situations such as spin chains obeying LSM-type constraints, and in somewhat more fine-tuned situations such as multicritical points of $(1{+}1)d$ SPT phases. Of course, our bounds also apply to the gapless boundary theories of in-cohomology $(2{+}1)d$ SPT phases protected by $\mathbb{Z}_N^3$ symmetry with 3-cocycle ω given by (2.14).

A question that motivated this work is how, if at all, the central charge of a $(1{+}1)d$ CFT is bounded from below by its discrete symmetries and anomalies. As far as symmetry goes, it is known that a CFT with a finite global symmetry whose faithfully realized part

is a group larger than $\mathbb{Z}_2$ or S_3 must have $c \geq 1$[128]. Further, the Sugawara construction provides a formula for the minimum central charge needed to accommodate continuous global symmetries, which is generally even larger than $c = 1$ [52]. Thus, restricting to general finite symmetries, we are interested in the question of whether any lower bound $c > 1$ can be proven when the symmetry is anomalous.

Consequently, another goal of our work was to search for numerical bootstrap evidence that could test whether certain suggested lower bounds are reasonable. Some of our calculations seem to suggest that existing, proposed bounds are not quantitatively correct. Specifically, in the case $N = 5$ that we study, there is a prominent kink in our plot, but it does not obviously correspond to any known theory. The location of the kink is nearly coincident with the WZW CFT $(\mathfrak{g}_2)_1$, which has central charge $c = 14/5$, but upon doing more careful numerics we were able to place this theory outside of the allowed region. Since bootstrap calculations can only rigorously show what is disallowed, it is difficult to make any statements about features in the allowed region when they do not appear to correspond to known theories. In the future, it will be interesting to explore more carefully the region near this kink to look for other signatures that can explain the kink as an actual theory. We expect that using a mixed correlator bootstrap setup will especially help in this direction, which we are actively investigating. More generally, we are hopeful that future analysis, guided by the evidence provided here, together with additional analytic or numerical calculations, will produce the types of central charge bounds that we desire.

There are various exciting avenues for future study that we would like to mention. First, we can consider technical improvements to the calculations that were done in this work. Among them are, first, using Virasoro conformal blocks for the correlator bootstrap constraints; this would quantitatively improve the bounds and is also a way to directly incorporate the central charge into the correlator bootstrap calculations without needing to assume a non-generic gap in the spectrum of symmetric local operators. Second, we think it would be very interesting to consider the problem of bootstrapping correlation functions of defect operators with fractional spin, which could produce bootstrap bounds on defect operators in

the most general setting. The aforementioned improvements would open up the possibility of obtaining current state-of-the-art universal bounds for completely general finite global symmetries and anomalies. This seems especially interesting when the symmetry is described by a fusion category with some non-invertible TDLs. There are countless examples of interesting theories with such non-invertible symmetries, especially in the context of $(1{+}1)d$ CFT, so exploring the space of CFTs with such symmetries using bootstrap is a natural future direction. This story has been initiated in [101], and we expect more general cases to be improved by the techniques introduced in this work.

Generalizations of our story to CFTs in higher dimensions seem especially interesting, albeit seemingly in the absence of a useful analog of modular invariance [14]. Some progress in this direction has been made already [98], but accounting for the complete picture of symmetries[5] and anomalies in higher dimensions within bootstrap remains a challenge. There is significant condensed matter theory motivation to incorporate anomalies into bootstrap, since, for instance, it could provide another way to explore the properties of exotic gapless states (see i.e. [164, 84]).

How might such higher-dimensional generalizations be achieved? In $(1{+}1)d$, there is a clear relationship between defect operators and local operators since both sets of operators contribute to the twisted torus partition function, and the OPE of defect operators may contain local operators. In contrast, defect operators corresponding to 0-form global symmetries in dimensions $d{+}1 > 2$ are extended objects, given by conformal defects attached to codimension-1 topological hypersurfaces (for example, in the $3d$ Ising CFT an example of this is the disorder operator, sometimes known as the twist defect). Such conformal defects host localized operators that have reduced conformal symmetry. Perhaps, then, the implications of anomalies can be reduced to some properties of these operators. There has been much study of such extended objects using a wide range of techniques [153, 154], including via conformal field theory techniques and bootstrap [22, 74, 21], so including anomalies into the

[5]Symmetry in QFT in higher dimensions is an active area of study. See i.e. Refs. [73, 46, 15, 18] for recent progress.

story seems like a natural next step. There are, however, some technical issues that seem to prohibit the most direct generalizations of our work to cases involving extended defects—see i.e. Ref. [133]. Additionally, as already pointed out in Ref. [99], anomalies of finite 0-form symmetries in bosonic CFTs in dimensions $d+1 > 2$ can be saturated by gapped topological theories, which have a unique ground state on the spatial sphere. This eliminates the possibility that such anomalies can lead to refined bounds on the spectrum of local operators since any CFT can be made to have any anomaly in this class via stacking gapped degrees of freedom. For such anomalies, it then seems that the questions that bootstrap may be able to answer are those concerning the properties of the extended defects. However, there are several classes of anomalies that ensure gaplessness in higher dimensions, including anomalies for continuous symmetries and even cases involving discrete symmetries [47, 48]. It thus seems promising to continue to develop new ways to incorporate the constraints of such symmetries and anomalies into bootstrap.

Acknowledgements

This work was facilitated through the use of advanced computational, storage, and networking infrastructure provided by the Hyak supercomputer system and funded by the Student Technology Fee at the University of Washington. We thank Tyler Ellison, Justin Kaidi, Ho Tat Lam, Sahand Seifnashri, Shu-Heng Shao, and Nathanan Tantivasadakarn for helpful discussions. We especially thank Tyler Ellison, Justin Kaidi, and Shu-Heng Shao for comments on an initial draft of this work. We thank Mocho Go and Yuji Tachikawa for their assistance with `autoboot`. RL thanks the 2021 annual meeting for the Simons Collaboration on Non-Perturbative bootstrap, as well as the Simons Center for Geometry and Physics at Stony Brook University, for hospitality. RL and LF are supported by NSF DMR-1939864.

Chapter 3

BOOTSTRAPPING THE MAGNETIC LINE DEFECT OF THE ISING CFT

The contents of this chapter will be submitted for publication after the submission of this thesis.
Based on joint work with Shang Liu and Max Metlitski.

3.1 Introduction

The critical phenomena of defects and impurities has been a subject of long-standing interest in theoretical physics [93, 156, 9, 114, 150, 22, 49]. When an impurity is introduced into a gapless system, remnants of the impurity degrees of freedom can potentially survive at long distances, leading to new impurity universality classes. A basic question is whether a given impurity becomes screened or not. In certain situations, such as when the bulk is described by a conformal field theory and the impurity in the UV corresponds to a clean bulk perturbed by a relevant operator

$$S = S_{\text{bulk}} + \lambda \int \mathcal{O}(x(\sigma))\, d\sigma, \tag{3.1}$$

the answer is guaranteed to be no due to the so-called g-theorem, which is a recently-proved monotonicity theorem concerning RG flows on line defects [2, 28, 51]. Line defects are pertinent in the context of impurities in a quantum-mechanical system described by a CFT since they can be thought of as representing the worldline of the impurity. Non-topological line defects in CFTs, which break spacetime symmetries of the bulk system, will be the main focus of this chapter.

The study of defects poses many challenges as a problem in CFT, and QFT more broadly. The problem of studying a defect embedded in a higher-dimensional bulk system is perhaps the simplest setting where RG is applicable [156]. At a CFT fixed point in the presence of

a defect away from a fixed point, the defect can flow under RG while the bulk remains unchanged. The simplest examples of CFTs in higher dimensions are the $O(N)$ Wilson-Fisher (WF) theories [157], describing the fluctuations of an order parameter near a second-order transition between ordered and disordered phases. Indeed, in various past works there have been efforts to perturbatively understand the simplest defect present in these theories, which can be created by applying a small pinning field perturbation along a line and studying the resulting RG flow [7, 49]. Additionally, various numerical approaches have been utilized to study this problem, ranging from Monte-Carlo simulations to the new fuzzy sphere regularization technique [6, 116, 87, 162]. The fuzzy sphere approach has been applied to study this kind of defect so far to the case of the Ising CFT in $D = 3$ Euclidean spacetime dimensions, providing the most accurate estimates to date for various quantities characterizing the defect. In this chapter, we will also study the pinning field defect of the Ising CFT.

While approaches using the techniques mentioned so far offer an excellent window into the defect's properties, few so far have made use of the significant developments in CFT tools that have been developed over the past decade or so with the advent of the numerical conformal bootstrap [124, 60, 61]. A few works have obtained interesting bootstrap results for line defects in various instances [74, 97, 77, 76], but none so far have managed to incorporate detailed information about the properties of the bulk CFTs whose defects these studies have targeted. This crucial step will be made in this work to achieve new, detailed predictions for a number of quantities characterizing the Ising pinning field defect.

The key new ingredient that facilitates our bootstrap study is the addition of defect-changing operators into the set of primary operators studied in the four-point functions we bootstrap. In general, the presence of a conformal line defect induces an explicit breaking of the bulk conformal symmetry down to a subgroup containing at least $SL(2,\mathbb{R})$, representing conformal transformations preserving the location of a straight line. The fact that the bulk symmetries are broken produces a new set of primary operators under this $SL(2,\mathbb{R})$ that are localized on the defect, whose scaling dimensions are in general distinct from those in the bulk. Defect-changing operators are special kinds of operators that live at a junction

between line defects of different types, which generalize the notion of boundary-condition changing operators in two-dimensional theories [26]. If we denote different line defects of a given CFT by $\mathcal{D}^a, \mathcal{D}^b$ etc., we will denote the defect-changing operators by e.g. ϕ_i^{ab}. We will explain the properties of these operators in more detail later. The reason that the defect-changing operators are such a useful ingredient in this work is that they facilitate a direct connection between the bulk and defect operators that can be readily exploited in numerical bootstrap. The key observation is that, for line defects $\mathcal{D}^a$ that can end[1], the endpoints are a special class of defect-changing operators, which we denote ϕ_i^{0a}. By taking two endpoints close together in different ways, either with the defects attached to the endpoints extending off to infinity or not, we can fuse the endpoints into bulk operators or operators that are localized on the non-trivial defect. These two different expansions turn out to be related by a certain crossing symmetry, so the content of these OPEs may be constrained rigorously using numerical bootstrap techniques [131]. We find this approach to be very effective at extracting a number of the scaling dimensions of defect-changing operators, in addition to the defect g-function and other OPE coefficients.

Beyond the question of wanting to gain a deeper quantitative understanding of the pinning field defect, there are additional physical questions that motivate this work. It is well known that local, finite-temperature, reflection-positive, classical systems in one dimension cannot exhibit spontaneous symmetry breaking (SSB)[2]. In the case of discrete symmetry, the physical mechanism is the proliferation of domain walls between symmetry breaking domains. The reason may be understood heuristically using the Peierls argument, which explains the dominance of entropy over energy in computing the free energy difference associated with a domain wall configuration relative to a fully ordered one. For quantum systems in 0+1 dimensions, the situation can be different: domain wall operators (corresponding to tunnelling between different "symmetry broken" ground states) can be charged under part

[1]Examples of line defects that cannot end are those that are protected by a one-form symmetry [73] or, relatedly, are attached to a topological surface such as in the case of a monodromy/disorder defect.

[2]There are additional caveats that are technically required for this to hold, such as finiteness of the energy difference between configurations that differ only locally in a lattice system.

of the symmetry group and disallowed, resulting in protected degeneracy of the ground-state subspace. Upon breaking some of these assumptions, the possibility of an ordered phase can be restored in standalone classical one-dimensional systems [58]. Long-range interactions can cause the energy cost of a domain wall pair to grow with their separation, suppressing the possibility of domain wall proliferation. We ask in this work whether it is impossible to induce a sufficiently long-range interaction via coupling a defect to a higher-dimensional bulk system. The intuition for why this could be expected to happen is that the relatively slow decay of the bulk degrees of freedom can induce an effective long-range interaction on the defect.

We make progress on this question in the simplest case of $\mathbb{Z}_2$ SSB by obtaining bounds on a certain defect-changing operator ϕ_0^{+-} representing a domain wall between pinning field defects of opposite sign. In a certain setup where one considers making the sign of the pinning field dynamical, one can construct a new line defect from the pinning field defects with a two-fold degenerate vacuum and a long-range decaying order parameter, reminiscent of higher-dimensional systems that spontaneously break a $\mathbb{Z}_2$ symmetry. We show that this defect, in the absence of some symmetry obstruction [148], in fact does not support spontaneous symmetry breaking due to the tendency of domain walls to proliferate. This occurs because, as we show, the scaling dimension of ϕ_0^{+-} is less than one and therefore relevant.

3.1.1 Universal bounds on symmetry-breaking line defects

A much simpler version of the setup we use to derive bounds on the pinning field defect of the $3d$ Ising CFT can be used to extract bounds that apply to any CFT with *stable* ($\Delta_1^{++} \geq 1$) conformal line defects $\mathcal{D}^{\pm}$ that break a $\mathbb{Z}_2$ symmetry, shown in Fig. 3.1. These bounds, while they do little to shed light on any particular line defect, demonstrate a few interesting and general features. We compute these universal bounds for CFTs in $D = 2, 3, 4$, which enters through the minimum scaling dimension allowed in the calculation in the bulk

operator channels, which is set by the unitarity bound

$$\Delta \geq \frac{D-2}{2}. \tag{3.2}$$

We thus expect the bounds to become stronger as the ambient spacetime dimension increases simply because of the stronger gap assumptions. The bounds are derived by imposing crossing symmetry on correlation functions of the leading endpoint primaries $\phi_0^{0\pm}$ using the techniques described in Sec. 3.3.

There are a few general results that we can extract from these bounds. Recall that, roughly speaking, g quantifies how many degrees of freedom are carried by a defect relative to the clean bulk: $g < 1$ indicates that the defect contains fewer degrees of freedom and vice versa. Excluding $D = 2$ where we only bound g from above, we obtain non-trivial two-sided bounds on g for stable, $\mathbb{Z}_2$-breaking line defects as a function of the scaling dimension of an endpoint operator Δ^{0+}[3]. Via the state-operator correspondence, we can associate Δ^{0+} with the energy of placing a single defect on a spatial sphere S^{D-1} via $E \sim \Delta^{0+}/R$. An interesting way to read our bounds on g is to consider the inverse plot, which is a *lower* bound on Δ^{0+} as a function of g: what is the minimum energy cost required to add/remove degrees of freedom in a localized region in a CFT? In $D = 2$ we thus find that it only necessarily costs energy to increase g, while in $D > 2$ we see that tuning away from $g = 1$ in either direction always has finite energy cost. Our bound in $D = 2$ is complementary to bounds on g computed by imposing open/closed duality of the annulus partition function, where it was also found that an *upper* bound on g exists for stable boundary conditions (suitably interpreted using the folding trick to apply to line defects) as a function only of the bulk central charge c [45].

We can also read off general constraints on when SSB can be potentially supported on a conformal line defect via the bound on Δ_0^{+-} of Fig. 3.1. As we explain in more detail later, any defect that explicitly breaks a $\mathbb{Z}_2$ symmetry can be promoted to a non-simple "SSB defect" with the potential to break $\mathbb{Z}_2$ spontaneously. If the leading domain wall operator

[3]In this simple calculation, it is not possible to encode the assumption that the external endpoint operator has the lowest scaling dimension amongst all other endpoint operators.

D	3	4
Δ^{0+}_{min}	0.1209	0.2259

Table 3.1: Universal lower bound on endpoint operator scaling dimension for $\mathbb{Z}_2$ symmetry-breaking conformal line defects, in any CFT, satisfying $\Delta_1^{++}, \Delta_0^{+-} \geq 1$ in $D = 3, 4$.

is relevant with $\Delta_0^{+-} < 1$, then the SSB defect is unstable and SSB is forbidden without fine-tuning. Our calculation reveals monotonically increasing upper bounds on Δ_0^{+-} as a function of the scaling dimension of an endpoint operator, except in $D = 2$ where our setup does not produce a non-trivial bound. From these bounds, we conclude that in order for SSB on a line defect to be possible, the dimension of any endpoint operator must satisfy the bounds from below listed in Tab. 3.1 for which the leading domain wall operator is not forced to be relevant.

3.1.2 Bootstrap bounds on the 3d Ising pinning field defect

Our main results are more specialized bootstrap calculations that aim to extract tight bounds on various quantities characterizing the $3d$ Ising pinning field defect. The most important among these are tight bounds on the defect g-function and the scaling dimension of the leading domain wall primary, plotted in Fig. 3.2. The latter, in addition to more convincing evidence we show later, demonstrates convincingly that the pinning field defect of the $3d$ Ising CFT does not give rise to a stable SSB defect. The question of whether such a defect exists in principle is still left open, but our bounds prove that such a defect must be fully non-perturbative (in the sense that it is not a direct sum of perturbative defects such as the pinning field) since the only defect-relevant bulk operator is σ, which is used to create the pinning field defect. Further, our bounds give us a very accurate estimate of the scaling dimension of the leading endpoint primary operator Δ_0^0. Numerically, we predict

$$g = 0.6056(32) \qquad \Delta_0^{0+} = 0.1079(19) \qquad \Delta_0^{+-} = 0.818(28).$$

In the main text, we also obtain bounds on other quantities such as OPE coefficients and dimensions of other defect operators.

3.1.3 Outline

The remainder of this chapter is structured as follows. In section 3.2 we will discuss generalities about line defects that break a $\mathbb{Z}_2$ symmetry from a symmetry point of view. We will also discuss in some detail the case of the two-dimensional pinning field defect, both as an interesting example and as a consistency check of our derivation of the various crossing symmetry rules. In section 3.3 we will describe our numerical bootstrap approach and present the bounds we derived on the defect conformal data of the $3d$ Ising pinning field defect. Finally, in section 3.4 we will discuss various directions for future research.

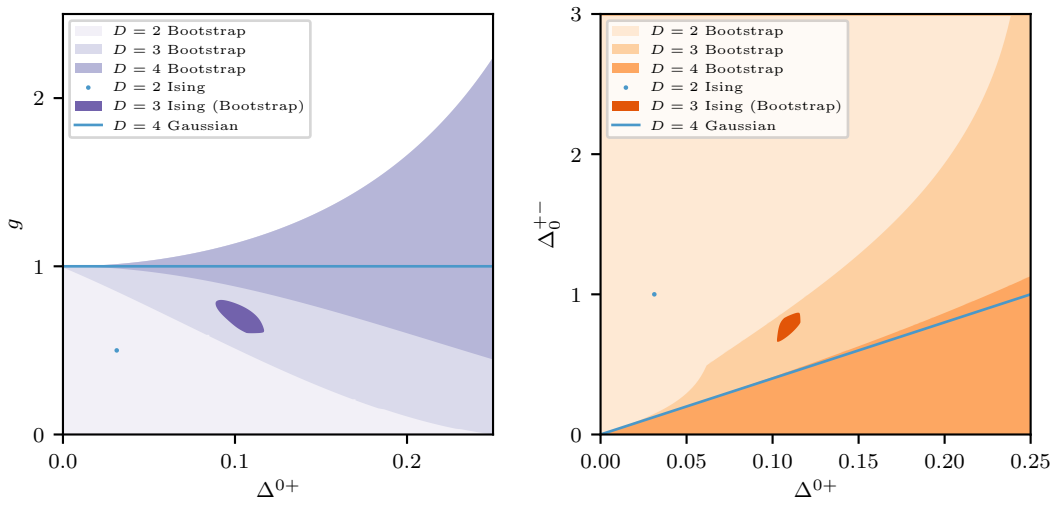

Figure 3.1: Universal bounds on stable ($\Delta_1^{++} \geq 1$) conformal line defects that explicitly break a $\mathbb{Z}_2$ symmetry in $D = 2, 3, 4^-$ compared with our most general bootstrap bounds for the $3d$ Ising pinning field defect. The shaded regions are allowed by bootstrap at derivative order $\Lambda = 45$. For the $D = 3$ Ising bootstrap bounds, we only plot the island expected to contain the pinning field defect created by a bulk σ perturbation. There is a larger allowed region beyond the island that we do not show for clarity. **Left:** Universal lower and upper bounds on the defect g-function. For $D = 2$ we do not find a non-trivial lower bound. The $D = 2$ Ising point lies at $(\Delta_0^{0+}, g)_{2d} = (1/32, 1/2)$. In the $D = 4$ Gaussian theory Δ_0^{0+} may take any positive real value with $g_{4d} = 1$. For the $3d$ Ising bootstrap result we plot the allowed region where only $\Delta_1^{++} \geq 1$ is assumed. **Right:** Universal bounds on the leading domain wall primary operator Δ_0^{0+}. In $D = 2$ Ising we have $\Delta_0^{+-} = 1$ and in the $D = 4$ Gaussian fixed point we have $\Delta_0^{+-} = 4\Delta_0^{0+}$. The $D = 3$ Ising bootstrap island is computed assuming $\Delta_1^{++} \geq 1$ and $\Delta_1^{+-} \geq 1$.

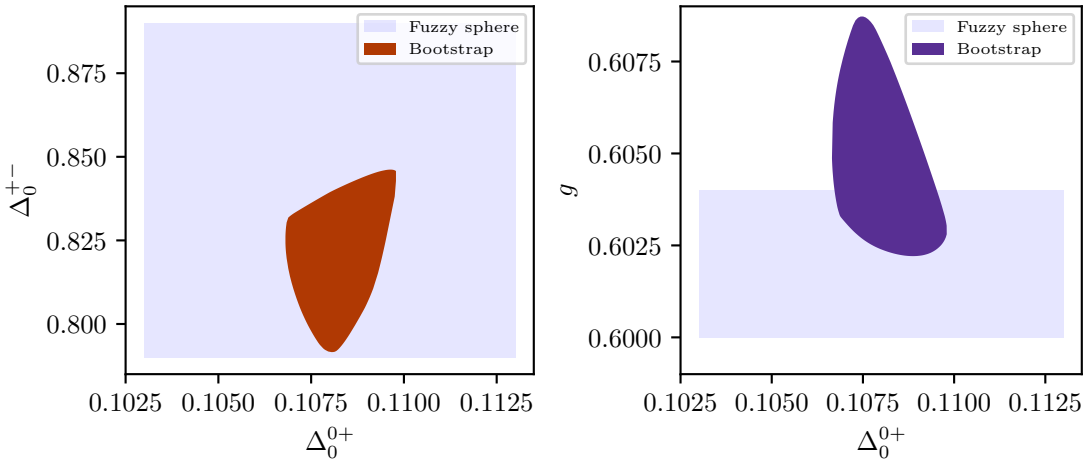

Figure 3.2: Bootstrap allowed regions for the scaling dimension of the leading domain wall primary Δ_0^{0+} and the defect g function at $\Lambda = 45$, each computed as a function of the scaling dimension of the leading endpoint operator Δ_0^{0+}. For comparison, we show estimates of the same quantities computed via the fuzzy sphere regularization technique of [161]. The bounds are obtained using non-generic gap assumptions in the defect-changing sectors. In each bound it is assumed that $\Delta_1^{++} \geq 1.4$, $\Delta_0^{+-} \geq 0.6$, and $\Delta_1^{0+} \geq \Delta_0^{0+} + 1.5$. The calculations use input from the OPE ratio bounds of Fig. 3.9, discussed in Sec. 3.3.3. To obtain the bound on Δ_0^{+-}, we further assume that there is only one relevant domain wall operator, i.e. $\Delta_1^{+-} \geq 1$.

3.2 $\mathbb{Z}_2$ symmetry-breaking conformal line defects

Here we make general remarks, from the point of view of symmetry, about conformal line defects that break a $\mathbb{Z}_2$ symmetry, either explicitly or spontaneously. We will provide a definition of spontaneous symmetry-breaking that is appropriate in the context of a line defect embedded within in a gapless CFT, setting up our ability to later derive general constraints on when this is allowed using numerical bootstrap. This discussion will naturally lead us to more carefully introduce the notions of defect-changing operators and the defect g-function. We will finally examine the consequences of the internal and spacetime symmetries for correlation functions of defect-changing operators, deriving various selection rules that will later enter our bootstrap analysis.

We will consider throughout this work the situation where the combined bulk and defect system is described by a defect CFT (dCFT) in the IR. This situation is characterized by the partial breaking of the bulk conformal symmetry by degrees of freedom localized on the defect. For instance, when the geometry of the defect is a straight, infinite line, which we will henceforth take to be placed along the τ axis in coordinates $(\tau, x_1, ..., x_{D-1}) \in \mathbb{R}^D$, the minimal set of conformal symmetry generators required to have a dCFT describing a line defect are those generating dilatations $\hat{D}$, translations along the τ axis $\hat{P} \equiv \hat{P}^\tau$, and special conformal transformations along the τ axis $\hat{K} \equiv \hat{K}^\tau$. We will also assume invariance under the transverse rotations and reflections preserving the τ axis, which we denote $O(D-1)_T$. We denote the transverse rotation generators as $\hat{M}_{ij}$ and reflection generators as $\hat{R}_\mu$, including also reflections about a plane perpendicular to the τ axis. Altogether, this leads us to assume the spacetime symmetry group $SL^\pm(2,\mathbb{R}) \times O(D-1)_T$ where $SL^\pm(2,\mathbb{R})$ denotes the set of real 2×2 matrices M with $\det M = \pm 1$. We will denote the $\hat{R}^\tau$ eigenvalues by $r^\mu = \pm 1$. We will mainly be interested in the case $D = 3$, in which case we denote the $SO(3)$ and $SO(2)_T$ spins of bulk and defect operators living on a straight, infinite defect by ℓ and s, respectively.

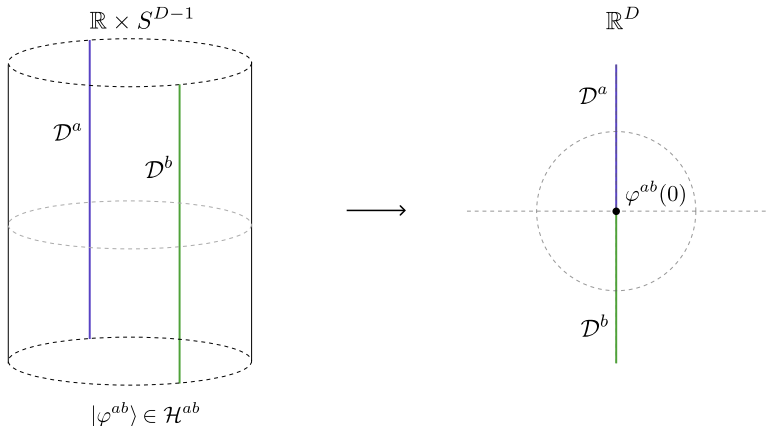

Figure 3.3: A schematic illustration of the operator-state mapping with conformal defects.

3.2.1 Defect-changing operators

Let us consider a CFT placed on $\mathbb{R} \times S^{D-1}$. The CFT may contain various non-trivial line defects of distinct types a, which we label $\mathcal{D}^a$. We now imagine placing two, possibly distinct, conformal defects $\mathcal{D}^a, \mathcal{D}^b$ at the north and south poles of the S^{D-1} that extend all throughout the $\mathbb{R}$ direction, which we choose as defining imaginary time. We denote the Hilbert space of states describing the quantization on S^{D-1} with the pair of defects as $\mathcal{H}^{ab}$, which we will call the *defect-changing Hilbert space*. The usual Weyl transformation that implements the state-operator map between $\mathbb{R} \times S^{D-1}$ and $\mathbb{R}^D$ brings this defect configuration to a straight, infinite line defect in $\mathbb{R}^D$ containing a point-like junction at the origin accross which the defect type changes, illustrated in Fig. 3.3. We will refer to the operators hosted at these junctions *defect-changing operators*.

The notion of a defect-changing operator bears close resemblance with that of a boundary condition-changing operator in two dimensional theories. Of course, in two dimensions a defect-changing operator may be viewed as a boundary condition-changing operator via the folding trick. Much of the formalism used to describe correlation functions of boundary condition-changing operators in two dimensions carries over directly to our setting, since the $SL(2, \mathbb{R})$ conformal symmetry, which plays a significant role in determining the functional

form of correlation functions involving operators on the defect, is present regardless of the ambient spacetime dimension.

Indeed, defect-changing operators may be organized into primary and descendant operators under the $SL(2,\mathbb{R})$ subgroup of the conformal symmetry preserved by the defect. We will label the defect-changing primaries and their scaling dimensions by ϕ_i^{ab} and Δ_i^{ab}, respectively, letting ϕ_0^{ab} be the operator with lowest scaling dimension in $\mathcal{H}^{ab}$ and ordering $\Delta_i^{ab} < \Delta_j^{ab}$ for $i < j$. We note a slight subtlety in defining the $SL(2,\mathbb{R})$ charges of defect-changing operator. The subtlety comes from the fact that performing the naive integral of the dilatation current $x_\mu T^{\mu\nu}$ around a sphere containing some primary operator will have additional UV-divergent contributions when the stress tensor insertion approaches the defect. These UV-divergent contributions do not contribute to the scaling dimension, representing instead a contribution coming from the "defect mass", so we thus *define* the defect-changing scaling dimension as the cutoff-independent piece in this scheme.

We will from now on assume the defect-changing Hilbert spaces furnish a representation of the one-dimensional conformal symmetry algebra, generated by operators acting on the defect-changing Hilbert spaces $\hat{D}^{ab}, \hat{P}^{ab}, \hat{K}^{ab}$, with the defect-changing operators transforming in the usual way

$$\begin{aligned}
[\hat{D}^{ab}, \mathcal{O}^{ab}(\tau)] &= (\tau\partial_\tau + \Delta)\mathcal{O}^{ab}(\tau) \\
[\hat{P}^{ab}, \mathcal{O}^{ab}(\tau)] &= \partial_\tau \mathcal{O}^{ab}(\tau) \\
[\hat{K}^{ab}, \mathcal{O}^{ab}(\tau)] &= (\tau^2\partial_\tau + 2\Delta\tau)\mathcal{O}^{ab}(\tau)
\end{aligned}$$

In general, under a spacetime orientation-reversing transformation a line defect $\mathcal{D}^a$ can map to its orientation-reversed partner $\mathcal{D}^{\bar{a}}$, but in this work we will always have $a = \bar{a}$ corresponding to orientationless defects. For the remainder of the work, we will also only deal with defect-changing operators having $s = 0$. Since there are thus no charges that transform non-trivially under complex conjugation, we take Hermitian conjugation to act as

$$(\phi_i^{ab}(\tau))^\dagger = \tau^{2\Delta_i^{ab}} \phi_i^{ba}(1/\tau). \tag{3.3}$$

3.2.2 Defect g-function

The most fundamental quantity characterizing a conformal line defect is the value of its defect g-function, which can be defined as the vacuum expectation value of the defect on an S^D spacetime where the defect is placed on an equator of S^D

$$g_a \equiv Z^a_{S^D}/Z^0_{S^D}, \tag{3.4}$$

with $Z^a_{S^D}$ denoting the partition function of the theory in the presence of the defect $\mathcal{D}^a$. Upon subtracting off any cosmological constant ambiguities, this quantity has been shown to be a RG monotone in $D \geq 2$ [67, 28, 51], and may be identified with the quantum dimension in the case when $\mathcal{D}^a$ is topological. By performing a conformal map to flat space that maps the defect to an infinite line, we alternatively may interpret g_a as the expectation value of the identity primary operator in the presence of the defect in radial quantization around a point on the defect

$$g_a = \langle I^{aa} \rangle, \tag{3.5}$$

where we use I^{aa} to denote the identity operator in the defect Hilbert space $\mathcal{H}^{aa}$.

In equating (3.4) and (3.5), there is a subtlety related to the choice of infrared regulator; implicitly, the relation assumes that we regulate the point at infinity as if, globally, we take flat space to be $\mathbb{R}^D \cup \{\infty\}$. This choice of infrared regulator is standard if we require special conformal symmetry, which is strictly ill-defined on $\mathbb{R}^D$. When points at infinity are not all identified, this different choice of infrared regulator can indeed produce different results for the straight and circular defects in certain examples [54, 64]. From now on we will simply refer to flat space as $\mathbb{R}^D$, but the reader should keep in mind that we assume the choice of regulator is such that the equality of (3.4) and (3.5) makes sense. We will see in the next section how g_a enters inside correlation functions of defect-changing operators.

3.2.3 Correlation functions of defect-changing operators

Again, we will work in flat space with all defects placed along the τ axis in $\mathbb{R}^D$. Correlation functions of defect-changing operators may be described using very similar formalism to the $D = 2$ case of correlation functions of boundary condition changing operators [95, 129], except that in higher dimensions there is no Virasoro symmetry. As with local operators, there is a notion of an operator product expansion (OPE) of defect-changing operators. Let us consider a configuration where two defect-changing operators ϕ_i^{ab}, ϕ_j^{bc} are inserted at nearby points, contained within a sphere without other operator insertions. At long distances, this creates a new operator in the $\mathcal{H}^{ac}$ defect Hilbert space. The OPE may be expressed as a sum over primary and descendant operators of the form (assuming $\tau > 0$)[4]

$$\phi_i^{ab}(\tau) \times \phi_j^{bc}(0) = \delta_{ij}\delta_{ac}\alpha_i^a I^{aa} + \sum_k \lambda_{kij}^{abc} \tau^{\Delta_k^{ac} - \Delta_i^{ab} - \Delta_j^{bc}} \sum_{n=0}^{\infty} \tau^n \beta_{kij}^{(n)} \mathcal{O}_k^{ac,(n)}(0) \tag{3.6}$$

with $|\phi_i^{ab,(n)}\rangle \equiv \hat{P}^n |\phi_i^{ab}(0)\rangle$, where the coefficients $\beta_{kij}^{(n)}$ are fixed by $SL(2,\mathbb{R})$ symmetry to be[5]

$$\beta_{kij}^{(n)} = \frac{(\Delta_k^{ac} + \Delta_i^{ab} - \Delta_j^{bc})_n}{n!(2\Delta_{\mathcal{O}})_n}. \tag{3.7}$$

One issue we must take care with is the normalization of defect-changing operators. A general two-point function of defect-changing primary operators takes the form

$$\langle \phi_i^{ab}(\tau_1) \phi_i^{ba}(\tau_2) \rangle = \frac{g_a \alpha_i^a}{\tau_{12}^{2\Delta_\phi}}. \tag{3.8}$$

where $\tau_{12} = \tau_1 - \tau_2$ and we assume $\tau_1 > \tau_2$. Note that in general, we will use a τ-ordering convention inside correlation functions. Next we observe that the $SL(2,\mathbb{R})$ conformal symmetry may be used to cyclically permute the operators inside a correlation function, which allows us to swap the location of the operators in (3.8), leading to the relation

$$g_a \alpha_i^a = g_b \alpha_i^b \tag{3.9}$$

[4] Note here we do not demand unit-normalization of the operators appearing on the right-hand side.

[5] $(a)_n$ denotes the Pochhammer symbol.

One solution is to choose $\alpha_i^a = g_a^{-1}$, which leads to unit-normalization of non-trivial defect-changing primaries.

Continuing, a general 3-point function involving non-trivial defect-changing operators takes the form (assuming $\tau_i > \tau_{i+1} > 0$)

$$\langle \phi_i^{ab}(\tau_1)\phi_j^{bc}(\tau_2)\phi_k^{ca}(\tau_3)\rangle = \frac{\lambda_{ijk}^{bca}}{\tau_{12}^{\Delta_{ijk}^{abc}}\tau_{13}^{\Delta_{ikj}^{bca}}\tau_{23}^{\Delta_{jki}^{bca}}} \qquad \Delta_{ijk}^{bca} = \Delta_i^{ab} + \Delta_j^{bc} - \Delta_k^{ca} \tag{3.10}$$

Using again the $SL(2,\mathbb{R})$ symmetry to cyclically permute the operators in (3.10) leads to the relations

$$\lambda_{ijk}^{bca} = \lambda_{jki}^{cab} = \lambda_{kij}^{abc}. \tag{3.11}$$

At this point it is also appropriate to mention the constraint coming from the $\hat{R}^\tau$ reflection symmetry. We assume that the $\hat{R}^\tau$ reflection leads to a relation

$$\langle \phi_i^{ab}(\tau_1)\phi_j^{bc}(\tau_2)\phi_k^{ca}(\tau_3)\rangle = e^{i\pi\left(\theta_i^{ab}+\theta_j^{bc}+\theta_k^{ca}\right)}\langle \phi_k^{ac}(-\tau_3)\phi_j^{cb}(-\tau_2)\phi_i^{ba}(-\tau_1)\rangle \tag{3.12}$$

for three-point functions. An operator $\phi_i^{ab}(0)$ cannot be associated with a definite $\hat{R}^\tau$ eigenvalue since the reflection acts as a map between different defect Hilbert spaces and θ_i^{ab} reflects an ambiguity in the choice of basis, except when $a = b$ and $e^{i\pi\theta_i^{aa}}$ is physically meaningful. The fact that $(\hat{R}^\tau)^2 = I$ leads to the relation

$$\theta_i^{ab} + \theta_i^{ba} = 0 \mod 2, \tag{3.13}$$

but in this work we may simply set $\theta_i^{ab} = 0$ for $a \neq b$. Another important symmetry to impose at this point is the $\mathbb{Z}_2^\tau$ unitary reflection symmetry, implemented by $\hat{R}^\tau$. These considerations, combined with those following from Hermitian conjugation, yield

$$\lambda_{ijk}^{abc} = e^{i\pi(\theta_i^{ab}+\theta_j^{bc}+\theta_k^{ca})}\lambda_{kji}^{bac} = (\lambda_{kji}^{bac})^*.$$

With these relations we are now prepared to discuss four-point functions, which are the main objects of study in our bootstrap calculations. A four-point function of defect-changing

operators, as dictated by the $SL(2,\mathbb{R})$ symmetry, takes the general form

$$\langle \phi_i^{ab}(\tau_1)\phi_j^{bc}(\tau_2)\phi_k^{cd}(\tau_3)\phi_l^{da}(\tau_4)\rangle = \left(\frac{|\tau_{24}|}{|\tau_{14}|}\right)^{\Delta_{ij}^{abc}} \left(\frac{|\tau_{14}|}{|\tau_{13}|}\right)^{\Delta_{kl}^{cda}} \frac{G_{ijkl}^{abcd}(x)}{|\tau_{12}|^{\Delta_i^{ab}+\Delta_j^{bc}}|\tau_{34}|^{\Delta_k^{cd}+\Delta_l^{da}}} \tag{3.14}$$

where $x = \frac{\tau_{12}\tau_{34}}{\tau_{13}\tau_{24}}$ and

$$G_{ijkl}^{abcd}(x) = \sum_m \frac{\lambda_{ijm}^{bca}\lambda_{mkl}^{cda}}{\langle \phi_m^{ca}|\,\phi_m^{ca}\rangle} g_{\Delta_m^{ca}}^{\Delta_{ij}^{abc},\Delta_{kl}^{cda}}(x) \qquad \Delta_{ij}^{abc} = \Delta_i^{ab} - \Delta_j^{bc}. \tag{3.15}$$

The functions $g_\Delta^{\Delta_{12},\Delta_{34}}(x)$ are $1d$ conformal blocks, given by

$$g_\Delta^{\Delta_{12},\Delta_{34}}(x) = x^\Delta {}_2F_1(\Delta-\Delta_{12},\Delta+\Delta_{34},2\Delta,x).$$

It is worth pointing out now how the g-function enters as a non-trivial ingredient in four-point functions. Assuming all primary operators other than the identity are unit-normalized, we may expand (3.15) as

$$G_{ijkl}^{abcd}(x) = \frac{\delta_{ac}}{g_a} g_0^{\Delta_{ij}^{abc},\Delta_{kl}^{cda}}(x) + \sum_{\substack{m \\ \phi_m^{ca}\neq I^{aa}}} \lambda_{ijm}^{bca}\lambda_{mkl}^{cda} g_{\Delta_m^{ca}}^{\Delta_{ij}^{abc},\Delta_{kl}^{cda}}(x) \tag{3.16}$$

Thus, the g-function appears as the coefficient of the identity operator when the exchanged operators are genuine defect operators. Intuitively, since g measures the number of degrees of freedom on the defect, having $g<1$ enhances the contribution of the vacuum sector.

Finally, four-point functions of defect-changing operators are subject to crossing symmetry, which again amounts to a cyclic permutation of the operator labels in addition to a change in the cross-ratio $x \to 1-x$. Explicitly, crossing symmetry becomes the statement that

$$(1-x)^{\Delta_j^{bc}+\Delta_k^{cd}} G_{ijkl}^{abcd}(x) = x^{\Delta_i^{ab}+\Delta_j^{bc}} G_{lijk}^{dabc}(1-x). \tag{3.17}$$

We define for later convenience a modified set of conformal blocks that have definite crossing parity

$$F_{\Delta,\pm}^{\phi_i^{ab}\phi_j^{bc}\phi_k^{cd}\phi_l^{da}}(x) = (1-x)^{\Delta_j^{bc}+\Delta_k^{cd}} g_\Delta^{\Delta_{ij}^{abc},\Delta_{kl}^{cda}}(x) \pm x^{\Delta_j^{bc}+\Delta_k^{cd}} g_\Delta^{\Delta_{\phi_i\phi_j},\Delta_{\phi_k\phi_l}}(1-x). \tag{3.18}$$

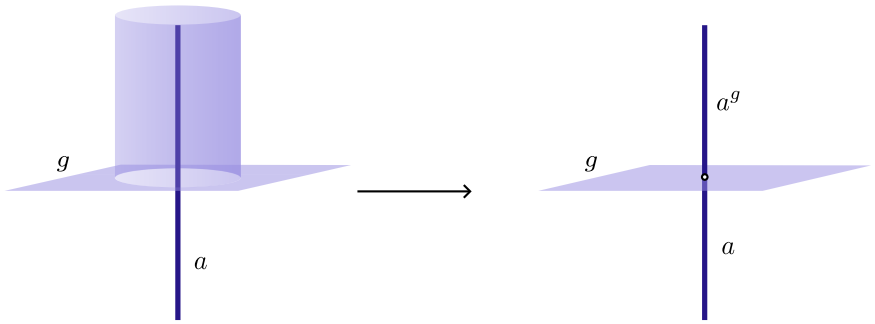

Figure 3.4: A topological surface operator for a symmetry group element g that surrounds a line defect can be shrunk down onto the line a, implementing a symmetry transformation of the line leading to a potentially new line a^g. This process may also be done partially, as shown, to create a topological junction between the topological surface and the line defects a, a^g.

In terms of the blocks in (3.18), the statement of crossing symmetry (leaving the x dependence implicit) becomes

$$\begin{aligned} 0 = \frac{\delta_{ac}}{g_a} F_{0,\mp}^{\phi_i^{ab}\phi_j^{bc}\phi_k^{cd}\phi_l^{da}} \pm \frac{\delta_{db}}{g_d} F_{0,\mp}^{\phi_l^{da}\phi_i^{ab}\phi_j^{bc}\phi_k^{cd}} \\ + \sum_{\substack{m \\ \phi_m^{ca} \neq I^{aa}}} \lambda_{ijm}^{bca}\lambda_{mkl}^{cda} F_{\Delta,\mp}^{\phi_i^{ab}\phi_j^{bc}\phi_k^{cd}\phi_l^{da}} \pm \sum_{\substack{m \\ \phi_m^{bd} \neq I^{bb}}} \lambda_{li\mathcal{O}}^{abd}\lambda_{mjk}^{bcd} F_{\Delta,\mp}^{\phi_l^{da}\phi_i^{ab}\phi_j^{bc}\phi_k^{cd}} . \end{aligned} \tag{3.19}$$

From (3.19), it is clear why the g-function has not made it into prior bootstrap studies involving correlation functions of defect operators, since if line defects of only a single type are considered then multiplying the above expression by g will lead to a crossing equation with a conventional contribution from the identity operator and further cannot modify any positivity properties. With the introduction of multiple defect types, where defect-changing operators become involved, then g can enter and we may constrain the physically allowed values, as we will later demonstrate.

3.2.4 Explicit and spontaneous symmetry breaking on line defects

Defects generally break the symmetries of the bulk, as we saw before in the case of spacetime symmetries. Unsurprisingly, defects can also break global, internal symmetries. The partic-

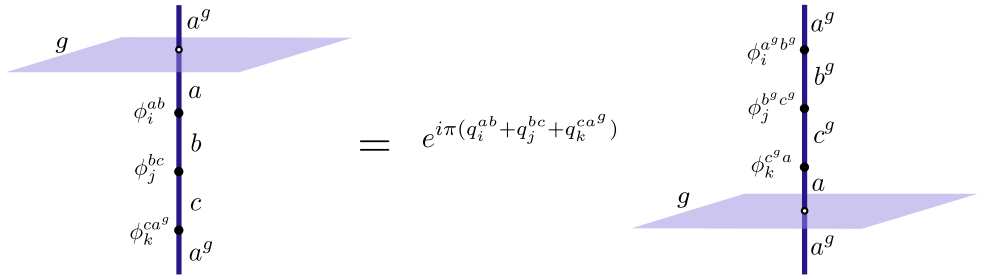

Figure 3.5: Sweeping the $\mathbb{Z}_2$ Ising topological surface defect past defect-changing operators inserted in a correlation function gives a constraint on three-point functions, illustrated here graphically.

ular pattern of symmetry breaking gives rise to constraints on correlation functions involving defect-changing operators, as we will see. The general mathematical structure describing the interplay between non-topological defects and topological symmetry defects implementing finite symmetries is a developing subject, but for the simple case of a $\mathbb{Z}_2$ symmetry, which we study in this work, an intuitive description suffices. For recent work describing this structure in category-theoretic language, see e.g. [19, 12]. In two-dimensions, one can use the mathematical language of module categories over fusion categories to describe the interplay of finite symmetries with boundaries/defects [66, 91, 89, 43].

We first describe the consequences of global symmetry for defects that explicitly break the $\mathbb{Z}_2$ symmetry, such as the Ising pinning field defect in any dimension. To create the pinning field defect, we can imagine starting from a clean system and making a perturbation

$$\delta S = h \int \sigma(\tau, 0)\, d\tau \tag{3.20}$$

to the effective action. This kind of perturbation explicitly breaks the $\mathbb{Z}_2$ symmetry; consequently, in the IR we may end up at one of two defect fixed points, which we call $\mathcal{D}^{\pm}$, depending on the sign of h.

In general, the bulk global symmetries act on the space of defects. For an invertible G symmetry, we can abstractly define an action of $g \in G$ on the space of defect labels via $a^g \equiv g \cdot a$, making the space of defect labels a kind of G-module. The full structure needed to

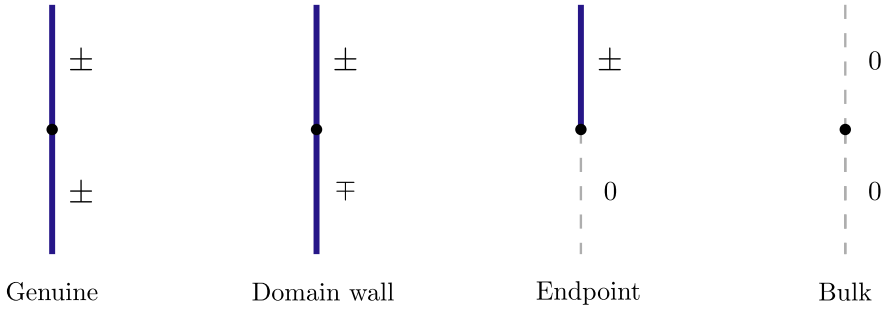

Figure 3.6: An illustration of the four types of defect-changing operators considered in this work.

describe a symmetry action on a defect, however, is more sophisticated than a G-module since it contains additional information about properties of junctions between the topological and non-topological defects. It is interesting to note that, in the event that $a^g = a$, the symmetry must act trivially on the defect as an object that can be inserted in a correlation function $g : \mathcal{D}^a \to \mathcal{D}^a$ whenever its defect g-function obeys $g_a > 0$.

For the specific case of the pinning field defect, we have two defect labels $\pm$ which are mapped to each other by the generator g of the $\mathbb{Z}_2$ symmetry $\pm^g = \mp$. We also will consider the trivial defect label 0, which obviously obeys $0^g = 0$. By considering making the perturbation (3.20) non-uniform along τ, we can create other kinds of defect configurations with new excitation types such as domain walls and endpoints, illustrated in Fig. 3.6. Accordingly, the defect-changing operators transform as $g : \phi_i^{ab} \to e^{i\pi q_i^{ab}} \phi_i^{a^g b^g}$, illustrated in Fig. 3.5 for a case of multiple defect-changing operator insertions. Akin to the case of the spacetime reflection symmetry mentioned previously, when $(a, b) \neq (a^g, b^g)$ the quantities q_i^{ab} represent the freedom to perform a change of basis by an overall phase, and otherwise q_i^{ab} is physically meaningful and represents the $\mathbb{Z}_2$ charge. A slight exception to this are domain wall operators. For a domain wall operator, we can consider the combined action of the R^τ reflection and internal $\mathbb{Z}_2$ symmetry. Since applying this combination twice must do nothing[6], we conclude that $\theta_i^{\pm\mp} + q_i^{\mp\pm} = 0 \mod 1$, representing a conserved charge.

[6]We assume we work in a basis in which both symmetries do not act on any internal quantum numbers,

In the cases we will consider, however, operators with a non-trivial value of this charge in the domain wall channel may not appear so we will again set $q_i^{ab} = 0$ whenever a or b are non-trivial.

The constraints coming from the Ising symmetry in correlation functions are encoded in relations between OPE coefficients

$$\lambda_{ijk}^{\pm\pm\pm} = \lambda_{ijk}^{\mp\mp\mp} \qquad \lambda_{ijk}^{\pm\mp\pm} = \lambda_{ijk}^{\mp\pm\mp}$$
$$\lambda_{ijk}^{\pm 0\pm} = \lambda_{ijk}^{\mp 0\mp} \qquad \lambda_{ijk}^{\pm 0\mp} = \lambda_{ijk}^{\mp 0\pm}$$
$$\lambda_{ijk}^{0\pm 0} = e^{i\pi q_i^{00}} \lambda_{ijk}^{0\mp 0} \qquad \lambda_{ijk}^{000} = e^{i\pi(q_i^{00}+q_j^{00}+q_k^{00})} \lambda_{ijk}^{000}$$

and permutations thereof, which follow from the relation illustrated in Fig. 3.5. We have only listed the examples relevant for correlation functions of endpoint operators and bulk operators. These relations will enter later when we derive the crossing equations.

So far we have discussed properties of line defects that explicitly break the $\mathbb{Z}_2$ symmetry. We will see now that the construction introduced so far naturally leads to a notion of spontaneous symmetry breaking for line defects. We will first discuss the properties that we expect for such a line defect, and then show how we may construct such a defect via a defect that explicitly breaks the symmetry.

Our starting assumption is that we have a bulk CFT with an unbroken $\mathbb{Z}_2$ symmetry. We will also assume the theory possesses a line defect $\mathcal{D}^l$ with long-range order (LRO) of the $\mathbb{Z}_2$ symmetry, in a sense that we will describe. We will call this kind of defect an *LRO defect* without regard to its stability, which is an additional physical consideration that determines whether the defect would naturally be realized in the setting of a UV completion of the CFT without fine-tuning. When $\mathcal{D}^l$ is stable, we will refer to it as an *SSB* defect.

First, the combined bulk and defect system still preserves the $\mathbb{Z}_2$ symmetry, implying for instance that all $\mathbb{Z}_2$-odd local operators have a vanishing expectation value with or without $\mathcal{D}^l$. For there to be long-range order of the $\mathbb{Z}_2$ symmetry, there necessarily exists some $\mathbb{Z}_2$-odd

---

which is allowed since the internal $\mathbb{Z}_2$ and reflection symmetries commute.

defect primary operator $\phi^{ll}_{0,-}$ whose *connected* two-point function obeys

$$\lim_{\tau\to\infty}\langle\phi^{ll}_{0,-}(\tau)\phi^{ll}_{0,-}(0)\rangle \sim \text{const.} \tag{3.21}$$

and thus represents the order parameter on the defect. Consistency with scale invariance thus dictates that $\Delta^{ll}_{0,-}=0$, implying that it is a topological local operator. This additional topological local operator, which is distinct from the trivial operator since it carries $\mathbb{Z}_2$ charge, indicates that $\mathcal{D}^l$ is *non-simple*. A consequence of the non-simplicity and the additional non-trivial operator with $\Delta=0$ is a twofold degeneracy of scaling dimensions of every operator on $\mathcal{D}^l$, since fusing any operator on $\mathcal{D}^l$ with $\phi^{ll}_{0,-}$ will give a distinct operator with the opposite $\mathbb{Z}_2$ charge. The presence of $\phi^{ll}_{0,-}$ will also generally lead bulk $\mathbb{Z}_2$-odd operators to acquire LRO of their connected two-point functions when measured parallel to the defect, which can be seen by noting that $\phi^{ll}_{0,-}$ would generally give the leading contribution to the defect operator expansion (DOE) of such an operator. We do not want to claim, however, that the presence of a defect order parameter with LRO is sufficient to claim that $\mathcal{D}^l$ supports SSB—we also require that $\mathcal{D}^l$ be stable.

To discuss the stability requirements, let us now explain how to describe the excitations of the LRO defect $\mathcal{D}^l$ in terms of defect-changing operators introduced before in the context of a defect that explicitly breaks $\mathbb{Z}_2$. Consider again the radial quantization picture on the spacetime $\mathbb{R}\times S^{D-1}$. In a phase where a $\mathbb{Z}_2$ symmetry is spontaneously broken, an infinitesimal perturbation of the system that explicitly breaks the symmetry will drive the system towards one of the two vacuum sectors with a fixed sign. In defect terminology, we thus expect the SSB defect to flow to pinning field defects $\mathcal{D}^{\pm}$. The non-simplicity implies that we may write $\mathcal{D}^l=\mathcal{D}^+\oplus\mathcal{D}^-$, resulting in a Hilbert space that decomposes as

$$\mathcal{H}=\mathcal{H}^{++}\oplus\mathcal{H}^{+-}\oplus\mathcal{H}^{-+}\oplus\mathcal{H}^{--}. \tag{3.22}$$

On $\mathbb{R}\times S^{D-1}$, these sectors in which the Hilbert space decomposes represent the choice of how we pin the sign of the defect at the north and south poles. The different types of excitations are distinguished by whether the defects at the north/south poles have the same sign or opposite sign.

For a LRO defect, the operators in the $\mathcal{H}^{\pm\pm}$,$\mathcal{H}^{\pm\mp}$ sectors are all genuine dynamical excitations, whereas for $\mathcal{D}^{\pm}$ the allowed excitations are captured only by $\mathcal{H}^{\pm\pm}$ and those in $\mathcal{H}^{\pm\mp}$ should be thought of as point-like defects that may only be generated by hand. Conversely, this suggests that if we are given any defect with explicitly-broken $\mathbb{Z}_2$ symmetry we may formally construct an SSB defect by, for instance, coupling the sign of the pinning field to a pair of dynamical classical spins at the north/south poles in the $\mathbb{R} \times S^{D-1}$ picture, recovering both the defect and domain wall sectors as dynamical excitations. The question now is whether this way of constructing an SSB defect is stable. Since for the non-simple SSB defect both defect and domain-wall excitations are allowed, stability requires that the scaling dimension of the lightest non-trivial operator in either sector must be irrelevant with scaling dimension $\Delta > 1$.

3.2.5 Implementing selection rules in OPEs

In our bootstrap calculations, we will consider correlation functions involving the leading endpoint operator ϕ_0^{0+} with transverse $SO(2)_T$ spin $s = 0$ together with the leading bulk, scalar primary operators σ and ε of the $3d$ Ising CFT. Having described the various symmetries and selection rules applicable for general $\mathbb{Z}_2$-breaking line defects and their defect-changing operators, we now demonstrate how the OPEs of these operators are constrained.

Let us assign some labels to the different sets of operators appearing in the dCFT scenario that we consider, refined by the symmetry charges and defect labels. We will assume further that each set only contains operators appearing in the OPEs of ϕ_0^{0+}, σ and ε. Recall again that all operators under consideration must be $SO(2)_T$ singlets and must also be even under reflections about the transverse directions, so we do not label the quantum numbers associated with these symmetries. We denote the set of bulk $SL(2,\mathbb{R})$ primary operators with $\mathbb{Z}_2$ charge q and $\mathbb{Z}_2^\tau$ charge r^τ by $\mathfrak{B}^{q,r^\tau}$. We denote the sets of endpoint, defect, and domain wall operators by $\mathfrak{D}^{0+}$, $\mathfrak{D}^{++}$ and $\mathfrak{D}^{+-}$, respectively. We do not need to additionally specify the $\mathbb{Z}_2$ or $\mathbb{Z}_2^\tau$ charges of operators in these sectors since the $\mathbb{Z}_2$ symmetry is broken and the $\mathbb{Z}_2^\tau$ symmmetry is unbroken only for defect operators, as discussed above, but all

such operators appearing in the OPEs under consideration will be even under $\mathbb{Z}_2^\tau$ reflections whenever they correspond to a defect-changing operator involving a non-trivial defect.

The step that requires the most care is classifying bulk $SL(2,\mathbb{R})$ primary operators by their $\hat{R}^\tau$ parity. In some instances such operators will be bulk descendant operators, so their $\hat{R}^\tau$ parity can differ from their parent primary operator. This analysis will later help us to decide in which OPE channels bulk descendant operators that are $SL(2,\mathbb{R})$ primaries may appear.

If we consider a bulk traceless symmetric tensor primary operator[7] $\mathcal{O}_a$, with a representing its $SO(3)$ indices, with $SO(3)$ spin ℓ, parity p, and scaling dimension Δ, a $\mathbb{Z}_2^\tau$ transformation acts as

$$\mathbb{Z}_2^\tau : \mathcal{O}_a(\tau,\vec{x}) \to (-1)^{p+n_\tau}\mathcal{O}_a(-\tau,\vec{x}),$$

where we use n_τ to denote the number of components set to point along the τ direction, giving $r^\tau = p + n_\tau$. Tracelessness and the requirement of being an $SO(2)_T$ singlet implies that at bulk descendant level zero $\mathcal{O}_a$ appears only with all its free indices set to τ, which will apply for the rest of this discussion. There are a few ways that we can generate $SL(2,\mathbb{R})$ primaries that are bulk conformal descendant operators.

First let us assume that $\mathcal{O}_a$ is a scalar operator $\mathcal{O}$ with $\ell = 0$ and scaling dimension Δ. In this case, we may construct $SO(2)_T$ singlet operators that are $SL(2,\mathbb{R})$ descendants by considering operators of the form

$$\tilde{\mathcal{O}}^{(N,i)}(x) = \sum_{n=0}^{N} a_n^i (\partial_\tau)^{2n} (\partial_i \partial^i)^{N-n} \mathcal{O}(x). \tag{3.23}$$

Such operators have scaling dimensions $\Delta + 2N$ and $r^\tau = 0$. It is not possible to obtain an operator at odd descendant level for such a scalar operator that satisfies all of our symmetry requirements, so we cannot construct any descendants from $\mathcal{O}$ with $r^\tau = 1$. If $\mathcal{O}_a$ has $\ell > 0$, it is possible again to find $SL(2,\mathbb{R})$ primaries amongst the bulk descendant operators using

[7] We will not need to consider pseudo-tensor operators and their descendants since they always violate the transverse parity symmetries.

the same construction as in (3.23) with scaling dimensions $\Delta+2N$, in addition to others that come from contracting an even number of derivatives with the $SO(3)$ indices of $\mathcal{O}_a$ in a way that preserves $SO(2)_T$ invariance. All such operators will have $r^\tau = \ell \mod 2$ matching $\mathcal{O}_a$. When $\ell > 0$, it is also possible to construct descendant operators that are $SL(2,\mathbb{R})$ primaries with the opposite r^τ eigenvalue while still maintaining the other symmetry requirements. This can be done, for instance, by contracting an odd number of derivatives with the $SO(3)$ indices of $\mathcal{O}_a$ in an $SO(2)_T$-invariant way. This leads to operators with scaling dimensions $\Delta + 2N + 1$ and $r^\tau = \ell + 1 \mod 2$.

To summarize, we see that for spin-ℓ traceless symmetric tensor operators $\mathcal{O}_a$ with $\mathbb{Z}_2$ charge q we have

$$\mathfrak{B}^{q,0} \ni \begin{cases} \partial^{2N}\mathcal{O}_a, & \ell \in 2\mathbb{Z} \\ \partial^{2N+1}\mathcal{O}_a, & 0 < \ell \in 2\mathbb{Z}+1 \end{cases} \qquad \mathfrak{B}^{q,1} \ni \begin{cases} \partial^{2N}\mathcal{O}_a, & \ell \in 2\mathbb{Z}+1 \\ \partial^{2N+1}\mathcal{O}_a, & 0 < \ell \in 2\mathbb{Z} \end{cases}$$

where we use the shorthand $\partial^n\mathcal{O}_a$ to denote an arbitrary $SL(2,\mathbb{R})$ primary at bulk descendant level n in the conformal tower of $\mathcal{O}_a$. For later use, we will also introduce the notation

$$\mathfrak{B}^{q,r^\tau}_{3d,\ell} = \{\mathcal{O}_a \in \mathfrak{B}^{q,r^\tau} : \ell_\mathcal{O} = \ell, K^\mu |\mathcal{O}\rangle = 0\} \tag{3.24}$$

containing only $3d$ bulk primaries with spin ℓ.

In total, we may finally express the content of each of the OPEs as

$$\begin{aligned} \phi^{+0}\times\phi^{0+} &\subset \mathfrak{D}^{++} & \sigma\times\phi^{0+} &\subset \mathfrak{D}^{0+} \\ \phi^{+0}\times\phi^{0-} &\subset \mathfrak{D}^{+-} & \varepsilon\times\phi^{0+} &\subset \mathfrak{D}^{0+} \\ \phi^{0+}\times\phi^{+0} &\subset \mathfrak{B}^{0,0}\cup\mathfrak{B}^{1,0} & \sigma\times\varepsilon &\subset \mathfrak{B}^{1,0}\cup\mathfrak{B}^{1,1} \\ \varepsilon\times\varepsilon &\subset \mathfrak{B}^{0,0} & \sigma\times\sigma &\subset \mathfrak{B}^{0,0} \end{aligned} \tag{3.25}$$

In the above discussion, we have only treated operators as being primary with respect to the residual $SL(2,\mathbb{R})$ conformal symmetry preserved by the defect. However, an essential ingredient that connects the bulk and defect together in our bootstrap calculations is to include four-point functions of defect-changing operators involving non-trivial conformal

defects together with bulk operators. But the OPE of bulk operators $\mathcal{O}_a, \mathcal{O}_b$ is constrained by the full $SO(D+1,1)$ symmetry

$$\mathcal{O}_a(x) \times \mathcal{O}_b(0) = \sum_c C^{3d}_{cab}(x, \partial_\mu)\mathcal{O}_c(0) \tag{3.26}$$

where $\mathcal{O}_c$ is a bulk $SO(D+1,1)$ primary operator and $C^{3d}_{cab}(x,\partial_\mu)$ is a differential operator which exactly determines the contributions of descendant operators of $\mathcal{O}_c$ given the OPE coefficient λ_{cab}. There is no known closed-form expression for $C^{3d}_{bac}(x,\partial_\mu)$ in $D=3$, the dimension mainly study in this work, but it can be computed up to arbitrary high descendant level in various ways.

We will consider correlation functions of bulk operators that are always inserted along the τ axis. In this limit, we can make use of the OPE of the form (3.6) for the special case of bulk operators, which contains less structure than (3.26) but, as we will see, is necessary to consider a mixed bootstrap system of endpoint operators and bulk operators. The fact that some $SO(D+1,1)$ descendant operators can be primary with respect to $SL(2,\mathbb{R})$ means, in a completely generic CFT, the OPE coefficients of such primaries appearing in (3.6) will be fixed in terms of the OPE coefficients λ_{cab}, and we can make use of this information to give stronger bounds in bootstrap.

Let us consider some bulk primary operator $\mathcal{O}_*$ and let $\tilde{\mathcal{O}}^{(n),i}_*$ label bulk descendants at descendant level n that are primary with respect to $SL(2,\mathbb{R})$. Let us consider just the operators ϕ_0^{0+}, ϕ_0^{+0} and σ, and suppose that

$$\sigma \times \sigma \ni \mathcal{O}_*$$
$$\phi_0^{0+} \times \phi_0^{+0} \ni \mathcal{O}_*.$$

Let us illustrate how to incorporate the information about the OPE coefficients of bulk descendant operators in our setup. First we define

$$\alpha^{(n),i}_{\mathcal{O}_r\mathcal{O}_p\mathcal{O}_q} \equiv \frac{\lambda_{\tilde{\mathcal{O}}^{(n),i}_r\mathcal{O}_p\mathcal{O}_q}}{\lambda_{\mathcal{O}_r\mathcal{O}_p\mathcal{O}_q}}, \tag{3.27}$$

which are completely fixed by the $SO(D+1,1)$ conformal symmetry. Let us next consider a simple system of four-point functions where $\mathcal{O}_*$ and its descendants appear as exchanged primary operators, which we may write as

$$G^{0+0+}_{0000}(x) = \sum_{n=0}^{\infty}\sum_{i}(\lambda^{0+0}_{\tilde{\mathcal{O}}^{(n),i}_{*}00})^2 g^{0,0}_{\Delta_{\mathcal{O}_*}+n}(x) + \sum_{\mathcal{O}}(\lambda^{0+0}_{\mathcal{O}00})^2 g^{0,0}_{\Delta_{\mathcal{O}}}(x) \tag{3.28}$$

$$G^{0+00}_{00\sigma\sigma}(x) = \lambda_{\mathcal{O}_*\sigma\sigma}\sum_{n=0}^{\infty}\sum_{i}\lambda^{0+0}_{\tilde{\mathcal{O}}^{(n),i}_{*}00}\alpha^{(n),i}_{\mathcal{O}_*\sigma\sigma} g^{0,0}_{\Delta_{\mathcal{O}_*}+n}(x) + \sum_{\mathcal{O}}\lambda^{0+0}_{\mathcal{O}00}\lambda_{\mathcal{O}\sigma\sigma} g^{0,0}_{\Delta_{\mathcal{O}}}(x) \tag{3.29}$$

$$G^{0000}_{\sigma\sigma\sigma\sigma}(x) = \lambda^2_{\mathcal{O}_*\sigma\sigma}\sum_{n=0}^{\infty}\sum_{i}(\alpha^{(n),i}_{\mathcal{O}_*\sigma\sigma})^2 g^{0,0}_{\Delta_{\mathcal{O}_*}+n}(x) + \sum_{\mathcal{O}}(\lambda_{\mathcal{O}\sigma\sigma})^2 g^{0,0}_{\Delta_{\mathcal{O}}}(x). \tag{3.30}$$

It is straightforward now to make use of the knowledge of $\alpha^{(n),i}_{\mathcal{O}_r\mathcal{O}_p\mathcal{O}_q}$ in our bootstrap setup. In our numerical calculations, we may treat the OPE coefficients appearing in the crossing equations as unknowns and the fact that the crossing equations can be expressed as quadratic forms in these unkowns permits the use of semidefinite programming techniques. That is, a generic crossing equation will take the form[8]

$$\sum_{\mathcal{O}}\mathrm{Tr}\left(P_{\mathcal{O}}\mathbf{V}^{\mathcal{O}}_{\Delta_{\mathcal{O}}}(x)\right) = 0 \qquad P_{\mathcal{O}} = \vec{\lambda}_{\mathcal{O}}\cdot\vec{\lambda}^{\mathsf{T}}_{\mathcal{O}} \tag{3.31}$$

where $\vec{\lambda}_{\mathcal{O}}$ is a vector of OPE coefficients in which $\mathcal{O}$ appears and the crossing vectors $\mathbf{V}^{\mathcal{O}}_{\Delta_{\mathcal{O}}}(x)$ have entries that are matrices. Such a crossing equation can be derived easily from (3.28–3.30). A bulk operator distinct from $\mathcal{O}_*$, which we will consider only as an $SL(2,\mathbb{R})$ primary, can have its contributions to (3.28–3.30) accounted for as in (3.31), writing the contribution

[8]The product is taken treating $P_{\mathcal{O}}$ as a scalar with the scalar multiplication replaced with matrix multiplication, and the trace is taken element-wise in the crossing vector.

also using crossing parity-definite blocks (3.18) and using shorthand ϕ for ϕ_0^{0+}, ϕ_0^{+0},

$$\mathbf{V}_\Delta(x) = \begin{pmatrix} \begin{pmatrix} F^{\phi\phi\phi\phi}_{\Delta,-} & 0 \\ 0 & 0 \end{pmatrix} \\ \begin{pmatrix} F^{\phi\phi\phi\phi}_{\Delta,+} & 0 \\ 0 & 0 \end{pmatrix} \\ \begin{pmatrix} 0 & \frac{1}{2}F^{\phi\phi\sigma\sigma}_{\Delta,-} \\ \frac{1}{2}F^{\phi\phi\sigma\sigma}_{\Delta,-} & 0 \end{pmatrix} \\ \begin{pmatrix} 0 & \frac{1}{2}F^{\phi\phi\sigma\sigma}_{\Delta,+} \\ \frac{1}{2}F^{\phi\phi\sigma\sigma}_{\Delta,+} & 0 \end{pmatrix} \\ \begin{pmatrix} 0 & 0 \\ 0 & F^{\sigma\sigma\sigma\sigma}_{\Delta,-} \end{pmatrix} \end{pmatrix} \qquad \vec{\lambda}_{\mathcal{O}} = \begin{pmatrix} \lambda^{0+0}_{\mathcal{O},00} \\ \lambda_{\mathcal{O}\sigma\sigma} \end{pmatrix} \tag{3.32}$$

In contrast, since the OPE coefficients of $SL(2,\mathbb{R})$ primaries that are bulk descendants of the operator $\mathcal{O}_*$ when it appears in $\sigma \times \sigma$ are known exactly up to $\lambda_{\mathcal{O}\sigma\sigma}$, their contribution will take a different form. However, to use these relations we must ultimately truncate the number of descendant operators whose OPE coefficients we use explicitly to some maximum level K. This is because the dimension of the OPE vector $\vec{\lambda}_{\mathcal{O}_*}$ grows with K since each $\lambda^{0+0}_{\tilde{\mathcal{O}}^{(n),i}00}$ is not obviously related by symmetry to $\lambda^{0+0}_{\mathcal{O}00}$. The upshot is that with some choice of K we may derive an analogous, but more complicated, crossing vector akin to (3.32) involving the OPE vector

$$\lambda^{(K)}_{\mathcal{O}} = \left(\lambda^{0+0}_{\mathcal{O}_*00} \quad \lambda_{\mathcal{O}_*\sigma\sigma} \quad \bigoplus_{n=1}^{K} \bigoplus_i \lambda^{0+0}_{\tilde{\mathcal{O}}_*^{(n),i}00}\right)^{\mathsf{T}}$$

that will intertwine the contributions of $\mathcal{O}_*$ and its descendants.

From this discussion we see why it is not possible to allow four-point functions only involving bulk operators to be taken away from the collinear limit at this stage. This would involve using full $3d$ conformal blocks, which automatically sum up these $SL(2,\mathbb{R})$ primaries that, as we showed, in this problem must be carefully intertwined with their contributions to the $\phi^{0+} \times \phi^{+0}$ OPE. However, the $3d$ conformal block decomposition can be used as long as the purely bulk four-point functions are included twice, once as in the above discussion using

the decomposition into $SL(2,\mathbb{R})$ primaries and again using the full $SO(D+1,1)$ primary decomposition. It is easy to see then that this would lead to a setup in which it is possible to achieve violations of crossing symmetry with semidefinite programming. This would generate additional computational cost, since one will then need to account for the different $SO(3)$ spin sectors, but this would make the sensitivity to the bulk operator spectrum at least as sensitive as the standard $3d$ bootstrap of local operators, which is highly desirable.

For simplicity, we will take into account knowledge of the descendant OPE coefficients only for level-two descendant operators of bulk scalar primaries. Our first task is to determine, for a given bulk, scalar primary, what are the corresponding level-two $SL(2,\mathbb{R})$ primaries. Since ultimately we will consider four-point functions where all external bulk operators are parity-even scalars inserted collinearly, we only need the level-two bulk descendants that are $SO(D-1)$ transverse spin and transverse reflection singlets. A general level two descendant operator of a bulk, scalar primary satisfying the spin and parity constraints takes the form

$$|\mathcal{O}^{(2)}\rangle = (a\,P_\tau^2 + b\,P_i^2)\,|\mathcal{O}\rangle \tag{3.33}$$

The constraint that $|\mathcal{O}^{(2)}\rangle$ is an $SL(2,\mathbb{R})$ primary is equivalent to demanding

$$0 = \lim_{\vec{x}\to 0}\langle \mathcal{O}^{(2)}(\tau,\vec{x})\mathcal{O}(0,0)\rangle = \lim_{\vec{x}\to 0}(a\,\partial_\tau^2 + b\,\vec{\nabla}_{D-1}^2)\frac{1}{|x|^{2\Delta}} = \frac{2\Delta(a(2\Delta+1)-b(D-1))}{\tau^{2\Delta+2}}$$

which yields

$$a = \frac{D-1}{2\Delta+1}b. \tag{3.34}$$

We will define $|\tilde{\mathcal{O}}^{(2)}\rangle \equiv b\left(\frac{D-1}{2\Delta+1}P_\tau^2 + P_i^2\right)|\mathcal{O}\rangle$. The normalization of this state, which we will also need, may be easily computed using the conformal symmetry algebra to be

$$b = \sqrt{\frac{2\Delta+1}{8(D-1)\Delta(\Delta+1)(2(\Delta+1)-D)}} \tag{3.35}$$

which ensures that $|\tilde{\mathcal{O}}^{(2)}\rangle$ is a unit-normalized $SL(2,\mathbb{R})$ primary. We lastly determine the OPE coefficient of $\tilde{\mathcal{O}}^{(2)}$ appearing in the OPE of bulk, scalar primaries $\mathcal{O}_1, \mathcal{O}_2$, relative to

$\lambda_{\mathcal{O}\mathcal{O}_1\mathcal{O}_2}$. To do this, we compute (assuming $\tau > 1$)

$$\begin{aligned}\lim_{\vec{x}\to 0}\langle\tilde{\mathcal{O}}^{(2)}(\tau,\vec{x})\mathcal{O}_1(1,0)\mathcal{O}_2(0,0)\rangle &= \lim_{\vec{x}\to 0}(a\partial_\tau^2 + b\vec{\nabla}^2_{D-1})\langle\mathcal{O}(\tau,\vec{x})\mathcal{O}_1(1,0)\mathcal{O}_2(0,0)\rangle \\ &= -b(D-1)\frac{(\Delta+\Delta_{12})(\Delta-\Delta_{12})}{2\Delta+1}\frac{\lambda_{\mathcal{O}\mathcal{O}_1\mathcal{O}_2}}{(\tau-1)^{\Delta+2+\Delta_{12}}\tau^{\Delta+2-\Delta_{12}}}\end{aligned} \tag{3.36}$$

Note that the above functional form serves as an independent check that we correctly identified $\tilde{\mathcal{O}}^{(2)}$ as an $SL(2,\mathbb{R})$ primary. From (3.36) and comparing with (3.10) we extract

$$\alpha^{(2)}_{\mathcal{O}\mathcal{O}_1\mathcal{O}_2} \equiv \frac{\lambda_{\tilde{\mathcal{O}}^{(2)}\mathcal{O}_1\mathcal{O}_2}}{\lambda_{\mathcal{O}\mathcal{O}_1\mathcal{O}_2}} = -b(D-1)\frac{(\Delta+\Delta_{12})(\Delta-\Delta_{12})}{2\Delta+1}$$

3.2.6 Crossing equations

Having accounted for the various symmetry constraints and selection rules, we are ready to express the system of crossing symmetry constraints in a manner suitable for our bootstrap analysis. To do so, we must enumerate all four-point functions involving the external operators ϕ_0^{0+}, σ, and ε, and impose the crossing symmetry relation (3.19). Suppressing the coordinate dependence, the four-point functions that we consider are

$$\langle\phi^{+0}\phi^{0+}\phi^{+0}\phi^{0+}\rangle, \langle\phi^{+0}\phi^{0-}\phi^{-0}\phi^{0+}\rangle, \langle\sigma\phi^{0+}\phi^{+0}\sigma\rangle, \langle\epsilon\phi^{0+}\phi^{+0}\sigma\rangle, \langle\epsilon\phi^{0+}\phi^{+0}\epsilon\rangle,$$
$$\langle\sigma\sigma\sigma\sigma\rangle, \langle\sigma\sigma\epsilon\epsilon\rangle, \langle\sigma\epsilon\sigma\epsilon\rangle, \langle\epsilon\epsilon\epsilon\epsilon\rangle.$$

All others are related to the above set by crossing symmetry. We could also imagine augmenting the above set of correlators by other important operators in the game such as the displacement operator D_i, or the other leading primary operators such as ϕ_1^{++} or ϕ_0^{+-}. These larger systems of correlators certainly deserve more study in the future. We list the decomposition of the above four-point functions into conformal blocks in Appendix B, and present

here the result in a compactified form

$$0 = g^{-1}\mathbf{V}_0^{++} + \mathrm{Tr}(C^1_{3\times 3}V_0^{0,0}) + \mathrm{Tr}(P_T\mathbf{V}_T) + \mathrm{Tr}(P_{\sigma\varepsilon}\mathbf{V}_{\sigma\varepsilon}) + \sum_{\substack{I\neq\mathcal{O}\in\mathfrak{B}^{0,0}_{3d,0}\\ \ell=0,\Delta\leq 6}} \mathrm{Tr}(P_{\mathcal{O},\mathrm{scal}}\mathbf{V}_\Delta^{0,0,\mathrm{scal}})$$
$$+ \sum_{\substack{\mathcal{O}\in\mathfrak{B}^{1,0}_{3d,0}\\ \ell=0,\Delta\leq 6}} \mathrm{Tr}(P_{\mathcal{O},\mathrm{scal}}\mathbf{V}_\Delta^{1,0,\mathrm{scal}}) + \sum_{m>0}(\lambda^{+0+}_{m00})^2\mathbf{V}_\Delta^{++} + \sum_{m}(\lambda^{+0-}_{m00})^2\mathbf{V}_\Delta^{+-} + \sum_{m>0}\mathrm{Tr}(P_m^{0+}\mathbf{V}_\Delta^{0+})$$
$$+ \sum_{I\neq\mathcal{O}\in\mathfrak{B}^{0,0}} \mathrm{Tr}(P^{0,0}_{\mathcal{O}}\mathbf{V}^{0,0}_\Delta) + \sum_{\mathcal{O}\in\mathfrak{B}^{1,0}} \mathrm{Tr}(P^{1,0}_{\mathcal{O}}\mathbf{V}^{1,0}_\Delta) + \sum_{\mathcal{O}\in\mathfrak{B}^{1,1}} |\lambda_{\mathcal{O}\sigma\varepsilon}|^2\mathbf{V}^{1,1}_\Delta. \tag{3.37}$$

where $C^1_{3\times 3}$ is the 3×3 constant matrix with all elements equal to unity. The OPE vectors appearing in (3.37) are

$$\vec{\lambda}_T = \begin{pmatrix}\lambda^{0+0}_{T00} & \lambda_{T\sigma\sigma}\end{pmatrix}^{\mathsf{T}} \qquad \vec{\lambda}_{\sigma\varepsilon} = \begin{pmatrix}\lambda^{0+0}_{\sigma 00} & \lambda^{0+0}_{\varepsilon 00} & \lambda_{\varepsilon\sigma\sigma} & \lambda^{0+0}_{\tilde{\sigma}^{(2)}00} & \lambda^{0+0}_{\tilde{\varepsilon}^{(2)}00}\end{pmatrix}^{\mathsf{T}}$$
$$\vec{\lambda}^{0,0}_{\mathcal{O},\mathrm{scal}} = \begin{pmatrix}\lambda^{0+0}_{\mathcal{O}00} & \lambda_{\mathcal{O}\sigma\sigma} & \lambda_{\mathcal{O}\varepsilon\varepsilon} & \lambda_{\tilde{\mathcal{O}}^{(2)}00}\end{pmatrix}^{\mathsf{T}} \qquad \vec{\lambda}^{1,0}_{\mathcal{O},\mathrm{scal}} = \begin{pmatrix}\lambda^{0+0}_{\mathcal{O}00} & \lambda_{\mathcal{O}\sigma\varepsilon} & \lambda_{\tilde{\mathcal{O}}^{(2)}00}\end{pmatrix}^{\mathsf{T}}$$
$$\vec{\lambda}^{0+}_m = \begin{pmatrix}\lambda^{+00}_{m\sigma\sigma} & \lambda^{+00}_{m\varepsilon\varepsilon}\end{pmatrix}^{\mathsf{T}} \qquad \vec{\lambda}^{0,0}_{\mathcal{O}} = \begin{pmatrix}\lambda^{0+0}_{\mathcal{O}00} & \lambda^{0+0}_{\mathcal{O}\sigma\sigma}\lambda^{0+0}_{\mathcal{O}\varepsilon\varepsilon}\end{pmatrix}^{\mathsf{T}} \qquad \vec{\lambda}^{1,0}_{\mathcal{O}} = \begin{pmatrix}\lambda^{0+0}_{\mathcal{O}00} & \lambda^{0+0}_{\mathcal{O}\sigma\varepsilon}\end{pmatrix}^{\mathsf{T}}$$

3.2.7 Example: pinning field in $D = 2$

In two dimensions, the pinning field defect of the Ising CFT can be studied exactly using bCFT techniques. As a sanity check to confirm our above analysis about selection rules and crossing symmetry, we compute four-point functions of the endpoints of the pinning field defect both with and without bulk operators. Studying the case of $D = 2$, rather than $D = 4$ which also may be exactly solved, is especially useful for the purpose of verifying how g enters in four-point functions. This is because for $D = 4$ the pinning field defect has $g = 1$, resembling the case of local operators, and is thus less illuminating.

In $D = 2$, the study of line defects is equivalent to the study of conformal interfaces between a given CFT $\mathcal{T}$ and itself, which is yet still equivalent to the study of conformal boundary conditions of $\mathcal{T}\otimes\bar{\mathcal{T}}$ via the folding trick. A special class of conformal interfaces are *factorized* interfaces, which correspond to separately imposing conformal boundary conditions on $\mathcal{T}$ and $\bar{\mathcal{T}}$ in the folded theory. It turns out that the pinning field line defect of the

$2d$ Ising CFT is an example of a factorized interface, obtained by imposing a the continuum version of a fixed-spin boundary condition on each copy. We will for the rest of this section use $\mathcal{T}$ to denote the $2d$ Ising CFT.

Recall that the $2d$ Ising CFT supports three simple conformal boundary conditions, which may be described in the Cardy state formalism via

$$|\pm\rangle = \frac{1}{\sqrt{2}}|I\rangle\rangle + \frac{1}{\sqrt{2}}|\varepsilon\rangle\rangle \pm \frac{1}{2^{1/4}}|\sigma\rangle\rangle$$
$$|f\rangle = |I\rangle\rangle - |\varepsilon\rangle\rangle.$$

The states $|\mathcal{O}\rangle\rangle$ are known as Ishibashi states, satisfying the condition $(L_n - \bar{L}_{-n})|\mathcal{O}\rangle\rangle$. For a conformal boundary condition B, its boundary g-function may be defined as the overlap of the vacuum state with the corresponding Cardy state $|B\rangle$

$$g = \langle 0|B\rangle, \tag{3.38}$$

which has the interpretation of the disc partition function. In the folded theory, the pinning field defect corresponds to the Cardy state

$$|\mathcal{D}^{\pm}\rangle = |\pm\rangle \otimes |\pm\rangle \tag{3.39}$$

from which it is straightforwrard to extract $g = 1/2$. The determination of other pieces of dCFT data is accomplished straightforwardly, for the most part, using tricks associated with the factorized nature of the pining field defect. A generic line defect of the $2d$ Ising CFT may be described using the description of $\mathcal{T} \otimes \bar{\mathcal{T}}$ as an orbifold of a compact boson and studying the corresponding set of conformal boundary conditions.

We now show how to compute additional pieces of dCFT data for the pinning field defect, which will make extensive use of the following trick. Consider placing a single copy of $\mathcal{T}$ on the upper half plane (UHP), and impose the "+" boundary condition without loss of generality. Next note that a $z \mapsto z^2$ coordinate transformation maps the negative real line onto the positive real line, which in turn corresponds to placing the pinning field defect along the positive real line with endpoints at the origin and at infinity. Since we did not place a

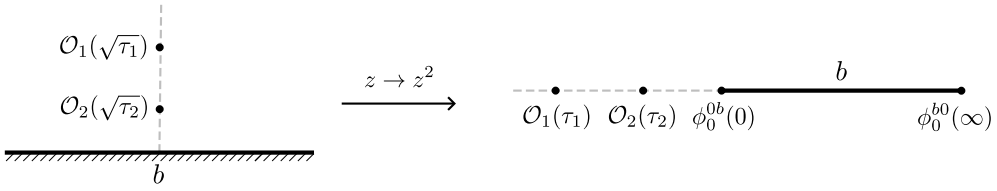

Figure 3.7: The coordinate transformation $z \to z^2$ folds an arbitrary conformal boundary condition b into a semi-infinite line defect, which we denote with the same label for such factorized line defects. In the presence of additional bulk operator insertions, this prepares a correlation function of the bulk operators in addition to the leading boundary operator

non-trivial boundary primary operator at the origin or at infinity, this procedure produces endpoint primary operators with the lowest scaling dimension ϕ_0^{0+}. With this trick, a general four-point function involving two endpoint primaries, as above, and two bulk operators can be computed as follows. To compare the results with the setup we outlined earlier, we will take the bulk operators to be inserted colinearly with the defect, which amounts to taking the bulk operators to be inserted along the imaginary axis before the $z \mapsto z^2$ transformation. Thus, let $z = \sqrt{\tau}$ for real $\tau < 0$. For a general four-point function involving bulk scalar operators $\mathcal{O}_1, \mathcal{O}_2$, we then have

$$\langle \phi_0^{0+} | \mathcal{O}_1(\tau_1) \mathcal{O}_2(\tau_2) | \phi_0^{0+} \rangle = \frac{\langle \mathcal{O}_1(\sqrt{\tau_1}) \mathcal{O}_2(\sqrt{\tau_2}) \rangle_+}{2^{\Delta_1+\Delta_2} |\tau_1|^{\frac{\Delta_1}{2}} |\tau_2|^{\frac{\Delta_2}{2}}}. \tag{3.40}$$

Note that we only use a single complex coordinate to specify the positions of operators, defining $\mathcal{O}(z) \equiv \mathcal{O}(z, z^*)$, since in the presence of a boundary only a single copy of the Virasoro algebra is preserved.

Let us use this result to compute various quantities for the case of the $2d$ Ising pinning field defect. First we consider the case where both $\mathcal{O}_1$ and $\mathcal{O}_2$ are trivial, which yields the norm of the leading endpoint primaries

$$\frac{1}{2} = g_+ = \langle I \rangle_+ = \langle \phi_0^{0+} | \phi_0^{0+} \rangle,$$

where we use $\langle . \rangle_B$ to denote expectation value in the presence of the boundary condition B on the UHP. From now on we will take ϕ_0^{0+} to be unit-normalized, which amounts to taking

$\langle I \rangle_+ = 1$ in the remaining calculations.

We next use (3.40) to extract the scaling dimension of the leading endpoint primary ϕ_0^{0+}. For the present case of a factorized defect, this turns out to be a universal quantity that only depends on central charge $\Delta = \frac{c}{16}$, giving the result $\Delta_0^{0+} = \frac{1}{32}$ for the Ising pinning field defect. To see this, we consider a slight modification of the relation (3.40) to account for the anomalous transformation of the stress tensor under conformal transformations. Noting that $\langle T(z) \rangle_B = 0$ for any conformal boundary condition B, only the Schwarzian derivative term from the stress tensor conformal transformation contributes to the three-point function of two endpoints and $T(z)$

$$\langle \phi_0^{0+} | T(\tau) | \phi_0^{0+} \rangle = \frac{c}{12} \{\sqrt{\tau}; \tau\} = \frac{1}{64} \frac{1}{|\tau|^2}. \tag{3.41}$$

Along with the identical result from the antiholomorphic component of the stress tensor, we may read off $\Delta_0^{0+} = 1/32$.

We next compute OPE coefficients of σ, ε in the OPE of the endpoint operators. This is done using the general form of the one-point function of a bulk primary operator (which must have $s = 0$ to have a non-vanishing one-point function) in the presence of a boundary

$$\langle \mathcal{O}(z) \rangle_B = \frac{a_{\mathcal{O}}^B}{|z - z^*|^\Delta} \implies \langle \phi_0^{0+} | \mathcal{O}(\tau) | \phi_0^{0+} \rangle = \frac{a_{\mathcal{O}}^+}{2^{2\Delta}} \frac{1}{|\tau|^\Delta}. \tag{3.42}$$

Using $\Delta_\sigma = 1/8$, $\Delta_\varepsilon = 1$, $a_\sigma^+ = 2^{1/4}$, and $a_\varepsilon^+ = 1$ we find $\lambda_{\sigma 00}^{0+0} = 1$ and $\lambda_{\varepsilon 00}^{0+0} = 1/4$ [27].

The dCFT quantities computed above will help to verify the crossing symmetry of four-point functions involving the endpoint operators, as we now demonstrate. To compute four-point functions involving two endpoints and two bulk operators, we need first to know the two-point functions of bulk operators in the presence of the fixed boundary condition. A general such two-point function has the form

$$\langle \mathcal{O}_1(z_1) \mathcal{O}_2(z_2) \rangle_B = \frac{G^B_{\mathcal{O}_1 \mathcal{O}_2}(\xi)}{|z_1 - z_1^*|^{\Delta_1} |z_2 - z_2^*|^{\Delta_2}} \qquad \xi = \frac{|z_1 - z_2|^2}{|z_1 - z_1^*||z_2 - z_2^*|}. \tag{3.43}$$

For the $2d$ Ising CFT with fixed-spin boundary, we have [52]

$$G^{+}_{\sigma\sigma}(\xi) = \sqrt{\left(\frac{\xi}{1+\xi}\right)^{1/4} + \left(\frac{\xi}{1+\xi}\right)^{-1/4}} \tag{3.44}$$

$$G^{+}_{\varepsilon\sigma}(\xi) = \frac{1}{2^{3/4}}\left(\left(\frac{\xi}{1+\xi}\right)^{1/2} + \left(\frac{\xi}{1+\xi}\right)^{-1/2}\right) \tag{3.45}$$

$$G^{+}_{\varepsilon\varepsilon}(\xi) = \frac{1+\xi+\xi^2}{\xi(1+\xi)} \tag{3.46}$$

Now consider (3.14) in the limit where $\tau_1 \to \infty$ and $\tau_4 \to 0$

$$\langle \phi_i^{ba} | \phi_j^{bc}(\tau_2) \phi_k^{cd}(\tau_3) | \phi_l^{da} \rangle = \frac{G^{abcd}_{ijkl}(x)}{|\tau_1|^{\Delta_j^{bc}-\Delta_i^{ab}} |\tau_2|^{\Delta_k^{cd}+\Delta_l^{da}}} \qquad x = \frac{\tau_3}{\tau_2}. \tag{3.47}$$

In the τ coordinates, we also have

$$\xi = \frac{1}{4}\left(x^{1/4} - x^{-1/4}\right)^2.$$

Finally comparing (3.47) with (3.40) for the specific case of the pinning field defect with two bulk operator insertions, we get

$$G^{+00+}_{0\mathcal{O}_1\mathcal{O}_20}(x) = \frac{x^{1/32}}{4^{\Delta_1+\Delta_2}} G^{+}_{\mathcal{O}_1\mathcal{O}_2}\left(\frac{1}{4}\left(x^{1/4} - x^{-1/4}\right)^2\right).$$

Using (3.44–3.46) and expanding in small x, which corresponds to the OPE limit of the bulk operators approaching the endpoint operators, we see that in terms of $SL(2,\mathbb{R})$ blocks in the endpoint channel we have

$$G^{+00+}_{0\sigma\sigma0}(x) = g^{-3/32,3/32}_{1/32}(x) + \frac{1}{136} g^{-3/32,3/32}_{65/32}(x) + O(x^{97/32}) \tag{3.48}$$

$$G^{+00+}_{0\varepsilon\sigma0}(x) = \frac{1}{4}\left(g^{-31/32,3/32}_{1/32}(x) - \frac{2}{17} g^{-31/32,3/32}_{65/32}(x) + O(x^{97/32})\right) \tag{3.49}$$

$$G^{+00+}_{0\varepsilon\varepsilon0}(x) = \frac{1}{16}\left(g^{-31/32,31/32}_{1/32}(x) + \frac{32}{17} g^{-31/32,31/32}_{65/32}(x) + O(x^{97/32})\right). \tag{3.50}$$

We see that the endpoint Virasoro primaries appear with the correct OPE coefficients that

were derived above. Using the crossing relation (3.17) we can also derive

$$G^{0++0}_{00\sigma\sigma}(x) = 1 + \frac{1}{128} g_2^{0,0}(x) + \frac{1}{8}\left(g_1^{0,0}(x) + \frac{1}{384} g_3^{0,0}(x) \right) + O(x^4) \tag{3.51}$$

$$G^{0++0}_{00\varepsilon\sigma}(x) = \frac{1}{2}\left(g_{1/8}^{0,7/8}(x) + \frac{1}{20} g_{17/8}^{0,7/8}(x) + O(x^{33/8}) \right) \tag{3.52}$$

$$G^{0++0}_{00\varepsilon\varepsilon}(x) = 1 + \frac{1}{16} g_2^{0,0}(x) + O(x^4) \tag{3.53}$$

Here we see the expected expansion into operators in the bulk channel, noting additionally that $\lambda_{\varepsilon\varepsilon\varepsilon} = 0$ and $\lambda_{\varepsilon\sigma\sigma} = 1/2$. An additional consistency check is that in (3.51) and (3.53) $SL(2,\mathbb{R})$ primaries appear only at even Virasoro descendant levels, consistent with the fact that these correlators respect the parity symmetries $\hat{R}^\tau$ which act on the *bulk* Virasoro generators as $(L_n, \bar{L}_n) \to (\bar{L}_n, L_n)$ and $(L_n, \bar{L}_n) \to ((-1)^n L_n, (-1)^n \bar{L}_n)$.

The final, more non-trivial case is the four-point function involving only endpoint operators where the trick used above is no longer applicable. This was computed in a general setting in [45] from which we quote

$$G^{0+0\pm}_{0000}(x) = \left(\frac{x^2}{2^8(1-x)} \right)^{\frac{1}{48}} Z^{\text{cl}}_{+\pm}\left(t(x)\right) \qquad t(x) = \frac{{}_2F_1(1/2,1/2,1;1-x)}{{}_2F_1(1/2,1/2,1;x)} \tag{3.54}$$

where $Z^{\text{cl}}_{+\pm}(t)$ is the closed-channel annulus partition function of the Ising CFT

$$Z^{\text{cl}}_{+\pm}(t) = \frac{1}{2}\chi_0(t) + \frac{1}{2}\chi_{1/2}(t) \pm \frac{1}{\sqrt{2}}\chi_{1/16}(t). \tag{3.55}$$

The functions $\chi_h(t)$ are the $c = 1/2$ Virasoro characters, and we will need the few q-series terms in their q-series expansions [52]

$$\chi_0(\tau) = q^{-1/48} + q^{95/48} + q^{143/48} + O(q^{49/16}) \tag{3.56}$$

$$\chi_{1/16}(\tau) = q^{1/24} + q^{25/24} + q^{49/24} + O(q^{73/24}) \tag{3.57}$$

$$\chi_{1/2}(\tau) = q^{23/48} + q^{71/48} + q^{119/48} + O(q^{167/48}). \tag{3.58}$$

where $q = e^{2\pi i \tau}$. The limit $x \to 0$ is controlled by the OPE where the endpoints shrink down to bulk operators. Indeed, the expansion in this limit may be carried out for a few terms to check for the expected appearance of the bulk Virasoro primaries. The regime of small x in

$\chi_h(t(x))$ is dominated by the terms with the smallest powers of q. Expanding in small x and writing the result as a sum of $SL(2,\mathbb{R})$ blocks gives

$$G_{0000}^{0+0\pm}(x) = \frac{1}{2}\left(1 \pm g_{1/8}^{0,0}(x) + \frac{1}{16}g_1^{0,0}(x) + \frac{1}{512}g_2^{0,0}(x) + O(x^{17/8})\right). \tag{3.59}$$

In the above, the leading contribution of each Virasoro primary is exactly in agreement with our predictions from our calculations of the OPE coefficients, multiplied by a common factor of the defect g-function $g = 1/2$. To be sure that everything works as expected, in particular that the contribution from the identity operator is consistent with crossing in the crossed channel, we also compute the conformal block expansion in the crossed channel where the endpoint operators are expanded in defect/domain wall operators. This can be done by noting that $t(x) = 1/t(1-x)$ and using $Z_{+\pm}^{\text{cl}}(1/t) = Z_{+\pm}^{\text{op}}(t)$ with

$$Z_{++}^{\text{op}}(t) = \chi_0(t) \tag{3.60}$$

$$Z_{+-}^{\text{op}}(t) = \chi_{1/2}(t) \tag{3.61}$$

the open-channel partition functions in the presence of equal or mixed fixed boundary conditions. Again making use of (3.17) we obtain

$$G_{0000}^{+0+0}(x) = 1 + \frac{1}{512}g_2^{0,0}(x) + O(x^4) \tag{3.62}$$

$$G_{0000}^{-0+0}(x) = \frac{1}{16}\left(g_1^{0,0}(x) + \frac{1}{1536}g_3^{0,0}(x) + O(x^5)\right) \tag{3.63}$$

We thus see that the contributions from the identity operators in the two OPE channels differ by a factor of g. To have g appear as in (3.16) we can everywhere divide by g. Implementing this in (3.63) allows us to extract the OPE coefficient of the domain wall Virasoro primary $\lambda_{000}^{+0-} = \frac{1}{2\sqrt{2}}$ in the OPE of the endpoints.

3.3 Bootstrap bounds on symmetry-breaking defects

We now discuss the conformal bootstrap approach to studying the pinning field defect in the $D = 3$ Ising CFT, with the goal of both obtaining bounds on the leading defect CFT

data and presenting the results of spectrum extraction on the higher operator spectrum from g-minimization.

Our bootstrap analysis proceeds using the standard formulation of numerical conformal bootstrap problems as polynomial-matrix problems (PMPs), which are internally converted to semidefinite programming problems (SDPs) and solved using the solver `SDPB` [131]. These techniques will allow us to numerically impose necessary conditions that any hypothetical set of CFT data must satisfy, and to optimize quantities of our choosing subject to the constraints.

The calculations involve numerically searching for a linear functional α of the form

$$\alpha[\mathbf{V}] = \sum_{m=0}^{\Lambda} \sum_{i} a_m^i \partial_x^m [\mathbf{V}(x)]_i \Big|_{x=\frac{1}{2}} \tag{3.64}$$

that acts on the space of crossing vectors and satisfies certain positive-semidefiniteness constraints. The output of α acting on a crossing vector is a matrix whose entries are, usually[9], polynomials in the scaling dimension of exchanged operators. We refer to the maximum number of derivatives Λ as the *derivative order*, which we may increase to yield stronger bounds. The task of searching for α is performed using the `SDPB`. There is a further truncation parameter, which we call κ, which represents the order to which we approximate the $SL(2,\mathbb{R})$ blocks as polynomials in the cross ratio, which yields a rational function of Δ when evaluated at the crossing-symmetric point $x = 1/2$

$$g_\Delta^{\Delta_{12},\Delta_{34}}(x) \approx \frac{x^\Delta}{\chi_\kappa(\Delta)} P_\kappa(x; \Delta_{12}, \Delta_{34}, \Delta) \tag{3.65}$$

where $\chi_\kappa(x)$ is chosen to factor out all poles and $P_\kappa(x; \Delta_{12}, \Delta_{34}, \Delta)$ is a degree-κ polynomial. We will choose $\kappa = \Lambda + 10$ throughout this work. Importantly, χ_κ is positive for $\Delta \geq 0$, allowing us to express all positivity constraints only in terms of P_κ whenever Δ is not explicitly fixed, suitable for input into `SDPB`. Depending on the particular calculation, we will require α to satisfy different constraints, which we will outline in the following subsections in addition to discussing our bounds.

[9] We will shortly discuss constraints for which we assign a different meaning to the continuous parameter in `SDPB`.

3.3.1 Incorporating 3d Ising CFT data

One the main goals of our work is to develop the ability to study conformal defects in a way that can effectively and rigorously incorporate details about the bulk operator spectrum. To accomplish this, we take advantage of the wealth of information known about the local operator spectrum of the $D = 3$ Ising CFT to study its pinning-field defect. Firstly, the scaling dimensions and OPE coefficients involving the leading $\mathbb{Z}_2$-odd and even scalar primaries σ, ε are known to high precision from previous conformal bootstrap calculations, taking values

$$(\Delta_\sigma, \Delta_\varepsilon, \lambda_{\varepsilon\sigma\sigma}, \lambda_{\varepsilon\varepsilon\varepsilon}) = (0.5181489(\mathbf{10}), 1.412625(\mathbf{10}), 1.0518537(\mathbf{41}), 1.532435(\mathbf{19})) \tag{3.66}$$

where the bold uncertainties represent rigorous errors [94]. In our setup, σ and ε appear both as external and exchanged primary operators in the four-point functions we consider. The fact that these operators are external in our setup makes it somewhat difficult to fully account for the uncertainty in $(\Delta_\sigma, \Delta_\varepsilon)$, since this would involve performing a scan over these quantities during the optimization of any defect quantity. Recently, the navigator bootstrap method has been developed to efficiently deal precisely this type of problem [126, 102]. However, the precision we are able to achieve for any defect quantity is many orders of magnitudes less than the precision of quantities in (3.67), making the error introduced by fixing the values of these quantities insignificant for the purposes of this work. We postpone a more sophisticated navigator bootstrap treatment to future work, opting instead to choose values from the navigator bootstrap minimum of [134]

$$(\Delta_\sigma, \Delta_\varepsilon, \lambda_{\varepsilon\sigma\sigma}, \lambda_{\varepsilon\varepsilon\varepsilon}) = (0.518148884, 1.41262383, 1.05185442, 1.53243407) \tag{3.67}$$

for all bootstrap calculations performed in our work, unless otherwise stated. The OPE coefficients $\lambda_{\varepsilon\sigma\sigma}, \lambda_{\varepsilon\varepsilon\varepsilon}$ enter through their ratio in our calculations through the parameter $r_{\sigma\varepsilon} = \lambda_{\varepsilon\varepsilon\varepsilon}/\lambda_{\varepsilon\sigma\sigma}$.

Beyond the leading bulk operator data, scaling dimensions of subleading operators of the Ising CFT have been estimated using a variety of methods [132, 125, 163]. Our strategy will be to explicitly assume that a subset of relatively low-lying bulk operators appear as internal

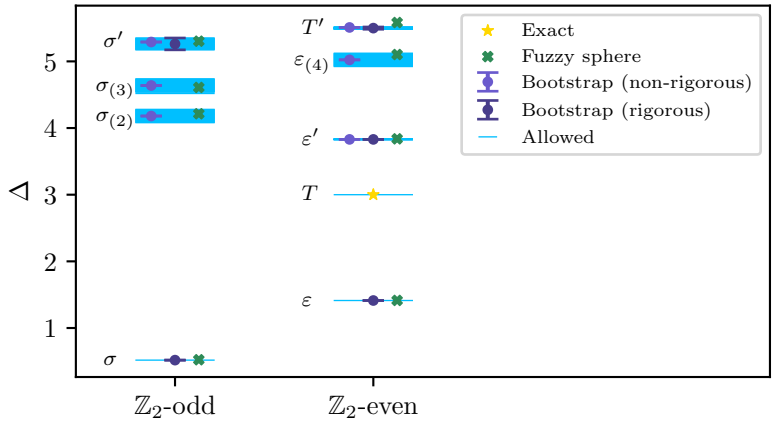

Figure 3.8: A graphical illustration of the discrete bulk primary spectrum included in our numerical bootstrap calculations. We use $(\sigma_{(\ell)}, \varepsilon_{(\ell)})$ to denote the leading $\mathbb{Z}_2$-(odd,even) spin-ℓ traceless symmetric tensor operator of the $3d$ Ising CFT in the instances where the operator does not have a more conventional symbol. Each horizontal light blue line represents an operator dimension explicitly allowed to appear in the crossing equation, whose values we choose based on the available bootstrap/fuzzy sphere data shown in the scattered points. The fuzzy sphere data are taken from [163] and the bootstrap data with (non)-rigorous error are taken from ([132])[125]. For clarity, we only explicitly mark operators that are bulk primaries; their descendants also appear as explained in the main text.

operators in our crossing equation (3.37), allowing also for uncertainty in the exact values of the scaling dimensions of these operators. We note that an analogous strategy was used to study the space of boundary conditions of specific rational CFTs, where it is especially effective since all bulk operator dimensions are known exactly [45]. In our context, while it will be essential to make discrete bulk spectrum assumptions to yield strong bounds on the defect CFT data, we must exercise caution in how much we assume[10].

First, excluding the cases where rigorous errors have been obtained [125], the errors in the scaling dimensions of the remaining sub-leading bulk operators from bootstrap techniques

[10]In practice we found relatively little sensitivity to the precise choices of subleading operator dimensions of our bounds on defect quantities, but it difficult to do a careful analysis since there are a large number of parameters.

are non-rigorous [132]. Another issue is the possibility that the set of operators present in the OPEs $\sigma \times \sigma$, $\sigma \times \epsilon$, and $\epsilon \times \epsilon$, which are the only OPEs studied in [132], does not exhaust the complete set of low-lying bulk operators. The main reason this is a possibility is because pseudotensor operators and $\mathbb{Z}_2$-even tensor operators with odd ℓ are kinematically excluded from these OPEs, and in principle our setup would be sensitive to the latter set[11].

In light of these uncertainties about the bulk operator spectrum, we will work with the following set of assumptions about the scaling dimensions of low-lying bulk primaries of the $D = 3$ Ising CFT. The recent results from the fuzzy sphere regularization technique seem to account for all operators predicted in [132] with $\Delta \leq 7$ and $\ell \leq 4$ [163], and further do not uncover any additional operators in this range, giving justification to our assumption that all operators in this range are known. An example of such a potential unknown operator is the leading $\mathbb{Z}_2$-even, vector primary, whose scaling dimension is now expected to be at least $\Delta \geq 7$ [105, 163]. Since there is no existing data that could completely cover the spectrum of operators with $\ell \geq 5$ within some higher range of Δ, we will assume a completely general spectrum of operators with $\Delta \geq 6$, coinciding with the $\ell = 5$ unitarity bound $\Delta \geq \ell + 1$ in $D = 3$.

Our task now is to incorporate the known bulk operators with $\Delta < 6$ and $\ell \leq 4$ into our setup. Our spectrum assumptions in this regime are illustrated graphically in Fig. 3.8. For each subleading bulk primary $\mathcal{O}$ with scaling dimension $\Delta_{\mathcal{O}}$, we let δ represent the error in $\Delta_{\mathcal{O}}$ and further use a small discrete sampling width of at most $\epsilon = 0.002$. We set δ according to the rigorous error of $\Delta_{\mathcal{O}}$ whenever possible, and otherwise we uniformly choose $\delta = 0.1$, which is roughly one to four orders of magnitude larger than any non-rigorous error. As seen in Fig. 3.8, this choice includes both the bootstrap and fuzzy sphere predictions for all operator dimensions with non-rigorous error to be allowed in the crossing equation.

In addition to each bulk primary operator, we also must consider the contributions of its complete set of descendant operators, some of which will be $SL(2, \mathbb{R})$ primary operators as

[11] In the latter case, more precisely our setup is sensitive to descendants of such operators.

we discussed before. Altogether, this leads to a number of constraints that are fixed accross all of our calculations

$$\alpha[\mathbf{V}^{0,0,\text{scal}}_{\Delta_{\mathcal{O}}+n\epsilon_{\mathcal{O}}}] \succeq 0 \qquad \varepsilon \neq \mathcal{O} \in \mathfrak{B}^{0,0}_{3d,0}, \Delta_{\mathcal{O}} \leq 6 \tag{3.68}$$

$$\alpha[\mathbf{V}^{0,0}_{\Delta}] \succeq 0 \qquad \Delta \in \{\Delta_\varepsilon + 4\} \cup \{\Delta_{\mathcal{O}} + n\epsilon_{\mathcal{O}} + 2m : \mathcal{O} \in \mathfrak{B}^{0,0}_{3d,\ell}, \ell > 0, m \in \mathbb{N}_0\} \cup [6, \infty) \tag{3.69}$$

$$\alpha[\mathbf{V}^{1,0,\text{scal}}_{\Delta_{\mathcal{O}}+n\epsilon_{\mathcal{O}}}] \succeq 0 \qquad \sigma \neq \mathcal{O} \in \mathfrak{B}^{3d,0}_{1,0}, \Delta_{\mathcal{O}} \leq 6 \tag{3.70}$$

$$\alpha[\mathbf{V}^{1,0}_{\Delta}] \succeq 0 \qquad \Delta \in \{\Delta_\sigma + 4\} \cup \{\Delta_{\mathcal{O}} + n\epsilon_{\mathcal{O}} + 2m : \mathcal{O} \in \mathfrak{B}^{1,0}_{3d,\ell}, \ell > 0, m \in \mathbb{N}_0\} \cup [6, \infty) \tag{3.71}$$

$$\alpha[\mathbf{V}^{1,0}_{\Delta}] \succeq 0 \qquad \Delta \in \{\Delta_{\mathcal{O}} + n\epsilon_{\mathcal{O}} + 2m + 1 : \mathcal{O} \in \mathfrak{B}^{1,1}_{3d,\ell}, \ell > 0, m \in \mathbb{N}_0\} \tag{3.72}$$

$$\alpha[\mathbf{V}^{1,1}_{\Delta}] \succeq 0 \qquad \Delta \in \{\Delta_{\mathcal{O}} + n\epsilon_{\mathcal{O}} : \mathcal{O} \in \mathfrak{B}^{1,1}_{3d,\ell}, \ell > 0\} \cup [6, \infty) \tag{3.73}$$

$$\alpha[\mathbf{V}^{1,1}_{\Delta}] \succeq 0 \qquad \Delta \in \{\Delta_{\mathcal{O}} + n\epsilon_{\mathcal{O}} + 2m + 1 : \mathcal{O} \in \mathfrak{B}^{1,0}_{3d,\ell}, \ell > 0, m \in \mathbb{N}_0\} \tag{3.74}$$

where in all the above we take $n \in \mathbb{Z}$ with $|n\epsilon_{\mathcal{O}}| \leq \delta_{\mathcal{O}}$. Further, note that when $\mathcal{O} = \varepsilon', T'$ in the above we incorporate the rigorous errors on the ratio of OPE coefficients $\lambda_{\varepsilon'\varepsilon\varepsilon}/\lambda_{\varepsilon'\sigma\sigma}$ and $\lambda_{T'\varepsilon\varepsilon}/\lambda_{T'\sigma\sigma}$ [125]. We also introduce the ratio $r_T = \lambda_{T\varepsilon\varepsilon}/\lambda_{T\sigma\sigma} = \Delta_\varepsilon/\Delta_\sigma$.

Finally, we mention in passing that we also could have used a continuous interval positivity constraint to account for uncertainties instead of a discrete sampling [5], but for some bulk operators we will use such a continuous interval constraint for ratios of OPE coefficients, as we will explain shortly, and it is not as straightforward to combine these distinct continuous constraints in `SDPB`. We find very little sensitivity in our setup to changes in ϵ or δ, so the discrete sampling is sufficient for our purposes.

3.3.2 Defect gap assumptions

Having outlined the spectrum assumptions we make about the set of bulk operators, we now turn to describing our limited set of assumptions about defect-changing operators. Recall that our main goal is to describe the IR fixed-point of a defect RG flow triggered by a relevant, explicit $\mathbb{Z}_2$ symmetry-breaking perturbation. This physical scenario implies two

main consequences for the low-lying defect CFT data:

1. The IR defect fixed-point lacks a non-trivial, relevant defect operator preserving both parity/reflection and $SO(2)_T$ spacetime symmetries. Our setup is not sensitive to parity/reflection and $SO(2)_T$ violating operators, so we assume $\Delta_1^{++} \geq 1$.

2. The defect g-theorem guarantees that $g < 1$ at the IR defect fixed-point.

The first consequence will be explicitly assumed, and the second consequence will guide our search for finding the physical values of the Ising pinning field defect's CFT data based on those that *imply* $g < 1$ as a non-trivial consequence of imposing crossing symmetry.

Based on these simple physical consequences, we impose the following set of constraints on α in the most general setting. All of our calculations will begin with the assumption that there exists an endpoint operator ϕ_0^{0+} with lowest scaling dimension Δ_0^{0+}. Then the constraints on α become

$$\alpha[\mathbf{V}_\Delta^{0+}] \succeq 0 \qquad \Delta \geq \Delta_{1,\text{min}}^{0+} \tag{3.75}$$

$$\alpha[\mathbf{V}_\Delta^{++}] \succeq 0 \qquad \Delta \geq \Delta_{1,\text{min}}^{++} \tag{3.76}$$

$$\alpha[\mathbf{V}_\Delta^{+-}] \succeq 0 \qquad \Delta \geq \Delta_{0,\text{min}}^{+-}. \tag{3.77}$$

The most general gap choices for the gap assumptions are $\Delta_{1,\text{min}}^{0+} = \Delta_0^{0+}$, $\Delta_{1,\text{min}}^{++} = 1$, and $\Delta_{0,\text{min}}^{+-} = 0$. We will also later make various stronger, non-generic gap assumptions in the defect-changing operator sectors to obtain stronger bounds.

3.3.3 Δ_0^{0+} *island and bounds on* $|\lambda_{\varepsilon 00}^{0+0}/\lambda_{\sigma 00}^{0+0}|$

The first set of bounds we present constrain the ratio of the OPE coefficients $\lambda_{\sigma 00}^{0+0}$ and $\lambda_{\varepsilon 00}^{0+0}$, shown in Fig. 3.9. The reason to introduce these bounds first is because we will use the results in all of our subsequent calculations as a way to encode information about the lack of degeneracy of operators with scaling dimension equal to Δ_σ or Δ_ε appearing in the $\phi_0^{0+} \times \phi_0^{+0}$

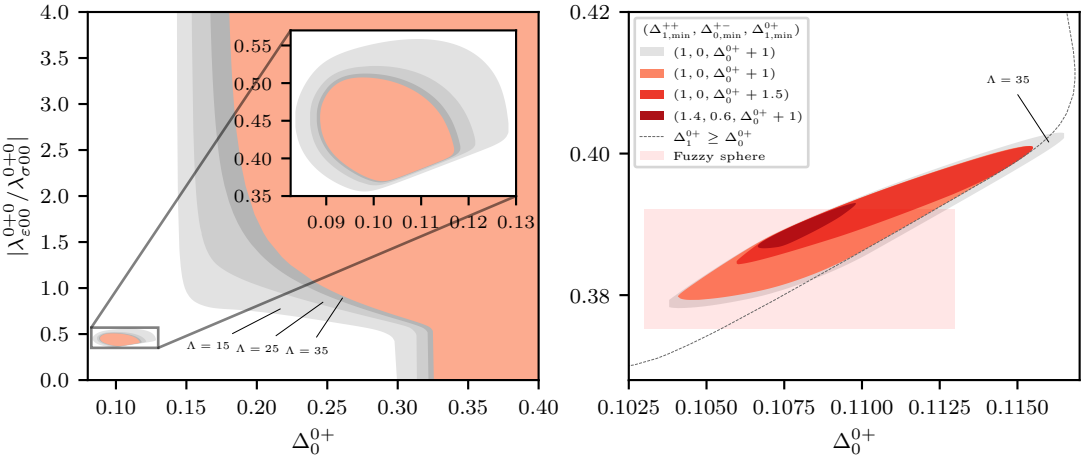

Figure 3.9: Bounds on the ratio of OPE coefficients of the $3d$ Ising pinning field endpoint primaries ϕ_0^{0+} fusing to ε and σ. We compute this for various gap assumptions and choices of Λ. Unless otherwise indicated the bounds are computed with $\Lambda = 45$. **Left:** The most general bound where only $\Delta_1^{++} \geq 1$ is assumed. **Right:** The same calculation with stronger gap assumptions. We show the $\Lambda = 35$ bound to demonstrate that the stable region lies in the interior of the most general bound once a non-trivial Δ_1^{0+} gap is assumed, which is outlined in the same plot.

OPE. The main effect of this additional assumption will be to give a stronger restriction on the allowed values of Δ_0^{0+}.

There are a few main takeaways from the bounds of Fig. 3.9. First, they reveal an island of allowed values of Δ_0^{0+} that is separated from the remaining allowed values, even when no non-trivial gap assumptions for defect-changing operators are made[12]. We claim that this island indeed contains the physical pinning-field defect solution (up to our fixed assumptions about the bulk) based on the additional evidence that we will summarize from our other bounds, and also the fact that the fuzzy sphere estimate of Δ_0^{0+} and $r_{\sigma\varepsilon}^{\phi_0^{0+}}$ agree very well with the values contained within the island. It is further noteworthy that the allowed "continent" that exists for values of Δ_0^{0+} exceeding those contained in the island does not

[12]The existence of an island in the allowed region does not require the extra assumption encoded by computing this OPE ratio, but its width in Δ_0^{0+} is reduced.

seem to possess any feature that is robust to an increase in Λ. This makes it difficult to say whether any potentially new physical solutions lie in this region.

We now describe how the bounds on are derived. Let us consider the contribution of σ, ε to the crossing equation (3.37) as internal operators, given by $\vec{\lambda}_{\sigma\epsilon}^{\mathsf{T}} \cdot \mathbf{V}^{\sigma\varepsilon}(x) \cdot \vec{\lambda}_{\sigma\epsilon}$. Recall that the OPE vector $\vec{\lambda}_{\sigma\varepsilon}$ is given by

$$\vec{\lambda}_{\sigma\varepsilon} = \begin{pmatrix} \lambda_{\sigma 00}^{0+0} & \lambda_{\varepsilon 00}^{0+0} & \lambda_{\varepsilon\sigma\sigma} & \lambda_{\tilde{\sigma}^{(2)}00}^{0+0} & \lambda_{\tilde{\varepsilon}^{(2)}00}^{0+0} \end{pmatrix}^{\mathsf{T}} \tag{3.78}$$

As was pointed out in [94], if in some calculation we only impose $\alpha[\mathbf{V}^{\sigma\varepsilon}(x)] \succeq 0$, this allows for solutions to crossing containing contributions of the form

$$\sum_i (\vec{\lambda}_{\sigma\varepsilon}^i)^{\mathsf{T}} \cdot \mathbf{V}^{\sigma\varepsilon}(x) \cdot \vec{\lambda}_{\sigma\varepsilon}^i, \tag{3.79}$$

which has the interpretation that multiple operators appear with dimensions equal to $\Delta_\sigma, \Delta_\varepsilon$, each with their own distinct OPE vector $\vec{\lambda}_{\sigma\varepsilon}^i$ of the form (3.78). Clearly then the uniqueness of the operators with scaling dimensions equal to $\Delta_\sigma, \Delta_\varepsilon$ is not encoded in this treatment. The uniqueness of σ, ε is an important physical assumption, so imposing it can potentially eliminate unphysical solutions and give stronger bounds.

We will extract consequences of the uniqueness of σ, ε appearing in the $\phi^{0+} \times \phi^{+0}$ OPE by explicitly fixing $|\lambda_{\varepsilon 00}^{0+0}/\lambda_{\sigma 00}^{0+0}|$ to different values and determining which choices are disallowed by crossing symmetry. Note that we bound only the absolute value because for any solution where $\lambda_{\varepsilon 00}^{0+0}/\lambda_{\sigma 00}^{0+0}$ is allowed $\lambda_{\varepsilon 00}^{0-0}/\lambda_{\sigma 00}^{0-0} = -\lambda_{\varepsilon 00}^{0+0}/\lambda_{\sigma 00}^{0+0}$ must also be allowed by symmetry. Thus, we may assume $\lambda_{\varepsilon 00}^{0+0}/\lambda_{\sigma 00}^{0+0} > 0$ without loss of generality. The main external scanning parameter in our problem is the dimension of the leading endpoint operator Δ_0^{0+}. For any given Δ_0^{0+}, we compute upper and lower bounds on $|\lambda_{\varepsilon 00}^{0+0}/\lambda_{\sigma 00}^{0+0}|$ using a "cutting-curve" algorithm adapted from an essentially identical algorithm introduced in [40], which we describe in Appendix C.

To implement this scan, we fix some $\theta_{\sigma\varepsilon}^{\phi_0^{0+}}$ [13] and let

$$(\lambda_{\sigma 00}^{0+0}, \lambda_{\varepsilon 00}^{0+0}) = |\lambda_{\sigma 00}^{0+0}|(\sin\theta_{\sigma\varepsilon}^{\phi_0^{0+}}, \cos\theta_{\sigma\varepsilon}^{\phi_0^{0+}}). \tag{3.80}$$

Substituting (3.80) into $\vec{\lambda}_{\sigma\varepsilon}$, we define the reduced OPE vector

$$\vec{\lambda}_{\sigma\varepsilon}^{\theta} \equiv \begin{pmatrix} |\lambda_{\sigma 00}^{0+0}| & \lambda_{\varepsilon\sigma\sigma} & \lambda_{\tilde{\sigma}^{(2)}00}^{0+0} & \lambda_{\tilde{\varepsilon}^{(2)}00}^{0+0} \end{pmatrix}^{\mathsf{T}} = M^{\theta}(\theta_{\sigma\varepsilon}^{\phi_0^{0+}}) \cdot \vec{\lambda}_{\sigma\varepsilon}$$

$$M^{\theta}(\theta_{\sigma\varepsilon}^{\phi_0^{0+}}) = \begin{pmatrix} \sin\theta_{\sigma\varepsilon}^{\phi_0^{0+}} & \cos\theta_{\sigma\varepsilon}^{\phi_0^{0+}} & 0 & 0 \\ 0 & 0 & 1 & 0 \\ 0 & 0 & 0 & 1 \end{pmatrix}.$$

We finally replace

$$(\vec{\lambda}_{\sigma\varepsilon})^{\mathsf{T}} \cdot \mathbf{V}_{\sigma\varepsilon}(x) \cdot \vec{\lambda}_{\sigma\varepsilon} \to (\vec{\lambda}_{\sigma\varepsilon}^{\theta}(\theta_{\sigma\varepsilon}^{\phi_0^{0+}}))^{\mathsf{T}} \cdot \mathbf{V}_{\sigma\varepsilon}^{\theta}(x; \theta_{\sigma\varepsilon}^{\phi_0^{0+}}) \cdot \vec{\lambda}_{\sigma\varepsilon}^{\theta}(\theta_{\sigma\varepsilon}^{\phi_0^{0+}}) \tag{3.81}$$

with $\mathbf{V}_{\sigma\varepsilon}^{\theta}(x; \theta_{\sigma\varepsilon}^{\phi_0^{0+}}) = M^{\theta}(\theta_{\sigma\varepsilon}^{\phi_0^{0+}}) \cdot \mathbf{V}_{\sigma\varepsilon}(x) \cdot M^{\theta}(\theta_{\sigma\varepsilon}^{\phi_0^{0+}})^{\mathsf{T}}$ in the crossing equation to account for our explicit choice of $\theta_{\sigma\varepsilon}^{\phi_0^{0+}}$. To compute the bounds shown in Fig. 3.9, we run the "cutting curve" algorithm subject to (3.68–3.77) in addition to

$$\alpha[\mathbf{V}_0^{0,0}(x)] = 1 \tag{3.82}$$

$$\alpha[\mathbf{V}_0^{++}(x)] \succeq 0, \tag{3.83}$$

as our normalization and to account for the identity operator in the defect channel with unspecified g, and finally

$$\alpha[\mathbf{V}_{\sigma\varepsilon}^{\theta}(x; \theta_{\sigma\varepsilon}^{\phi_0^{0+}})] \succeq 0 \tag{3.84}$$

where $\theta_{\sigma\varepsilon}^{\phi_0^{0+}}$ takes the role of the parameter γ in the notation of Appendix C.

In calculations of other defect quantities, we will make use of the bounds of Fig. 3.9 in the following way. Again, without using a more sophisticated setup such as the navigator method, it is somewhat impractical to scan over fixed values of $\theta_{\sigma\varepsilon}^{\phi_0^{0+}}$ as we did above when

[13] The trigonometric parameterization is convenient for the purpose of bounding $|\lambda_{\varepsilon 00}^{0+0}/\lambda_{\sigma 00}^{0+0}|$ since it makes the scanning region bounded.

computing bounds on other quantities. We settle instead for allowing $|\lambda^{0+0}_{\varepsilon 00}/\lambda^{0+0}_{\sigma 00}|$ to take any values within the allowed regions implied by Fig. 3.9. In SDPB each constraint supports up to one continuous parameter that appears polynomially. The continuous parameter usually takes the role of the scaling dimension of an exchanged primary operator, but since in $\mathbf{V}_{\sigma\varepsilon}(x)$ all operator dimensions are fixed we are free to use $r^{\phi_0^{0+}}_{\sigma\varepsilon} \equiv |\lambda^{0+0}_{\varepsilon 00}/\lambda^{0+0}_{\sigma 00}|$ as a continuous parameter. It is straightforward to modify the derivation of the constraint $\mathbf{V}^{\theta}_{\sigma\varepsilon}(x, \theta^{\phi_0^{0+}}_{\sigma\varepsilon})$ to arrive on one that depends directly on $r^{\phi_0^{0+}}_{\sigma\varepsilon}$

$$\mathbf{V}^{r}_{\sigma\varepsilon}(x, r^{\phi_0^{0+}}_{\sigma\varepsilon}) = M^{r}(r^{\phi_0^{0+}}_{\sigma\varepsilon}) \cdot \mathbf{V}_{\sigma\varepsilon}(x) \cdot M^{r}(r^{\phi_0^{0+}}_{\sigma\varepsilon})^{\mathsf{T}} \qquad M^{r}(r^{\phi_0^{0+}}_{\sigma\varepsilon}) = \begin{pmatrix} 1 & r^{\phi_0^{0+}}_{\sigma\varepsilon} & 0 & 0 \\ 0 & 0 & 1 & 0 \\ 0 & 0 & 0 & 1 \end{pmatrix}, \tag{3.85}$$

which enters in the crossing equation via the term

$$(\vec{\lambda}^{r}_{\sigma\varepsilon}(r^{\phi_0^{0+}}_{\sigma\varepsilon}))^{\mathsf{T}} \cdot \mathbf{V}^{r}_{\sigma\varepsilon}(x, r^{\phi_0^{0+}}_{\sigma\varepsilon}) \cdot \vec{\lambda}^{r}_{\sigma\varepsilon}(r^{\phi_0^{0+}}_{\sigma\varepsilon}) \qquad \vec{\lambda}^{r}_{\sigma\varepsilon}(r^{\phi_0^{0+}}_{\sigma\varepsilon}) = \begin{pmatrix} \lambda^{0+0}_{\sigma 00} & \lambda_{\varepsilon\sigma\sigma} & \lambda^{0+0}_{\tilde{\sigma}^{(2)}00} & \lambda^{0+0}_{\tilde{\varepsilon}^{(2)}00} \end{pmatrix}.$$

Note that $r^{\phi_0^{0+}}_{\sigma\varepsilon}$ appears quadratically in $\mathbf{V}^{r}_{\sigma\varepsilon}(x; r^{\phi_0^{0+}}_{\sigma\varepsilon})$. We would like to impose

$$r^{\phi_0^{0+}}_{\sigma\varepsilon}(\Delta_0^{0+}) \in [r_{\min}(\Delta_0^{0+}), r_{\max}(\Delta_0^{0+})],$$

where the upper and lower bounds are set by Fig. 3.9 and depend on the choices of Λ and gap assumptions made in a particular calculation. In SDPB, however, the continuous parameter is assumed to take values in $y \in [0, \infty)$. By letting

$$r^{\phi_0^{0+}}_{\sigma\varepsilon}(\Delta_0^{0+}) = r_{\min}(\Delta_0^{0+}) + \left(r_{\max}(\Delta_0^{0+}) - r_{\min}(\Delta_0^{0+})\right) \frac{y}{1+y} \tag{3.86}$$

we can convert the interval constraint on $r^{\phi_0^{0+}}_{\sigma\varepsilon}$ to a form suitable for input to SDPB, further without introducing any discretization error, which would otherwise be required. Upon making the substitution (3.86) the crossing vector $\mathbf{V}^{r}_{\sigma\varepsilon}(x, r^{\phi_0^{0+}}_{\sigma\varepsilon})$ depends non-polynomially on y, which is not suitable for input to SDPB. This is easily fixed by choosing $1/(1+y)^2$ as a positive prefactor, and imposing

$$\begin{aligned} \alpha[(1+y)^2 \mathbf{V}^{r}_{\sigma\varepsilon}(x, y)(\Delta_0^{0+}))] &\succeq 0 \\ r^{\phi_0^{0+}}_{\sigma\varepsilon}(\Delta_0^{0+}) &\in [r_{\min}(\Delta_0^{0+}), r_{\max}(\Delta_0^{0+})] \end{aligned} \tag{3.87}$$

in our subsequent calculations. With this strategy, the uniqueness of σ, ε in the $\phi_0^{0+} \times \phi^{+0}$ OPE is only partially accounted for, since again solutions with multiple OPE vectors in the spirit of (3.79) are allowed, but this nonetheless gives improved constraining power in our other bounds.

3.3.4 Bounds on g-function

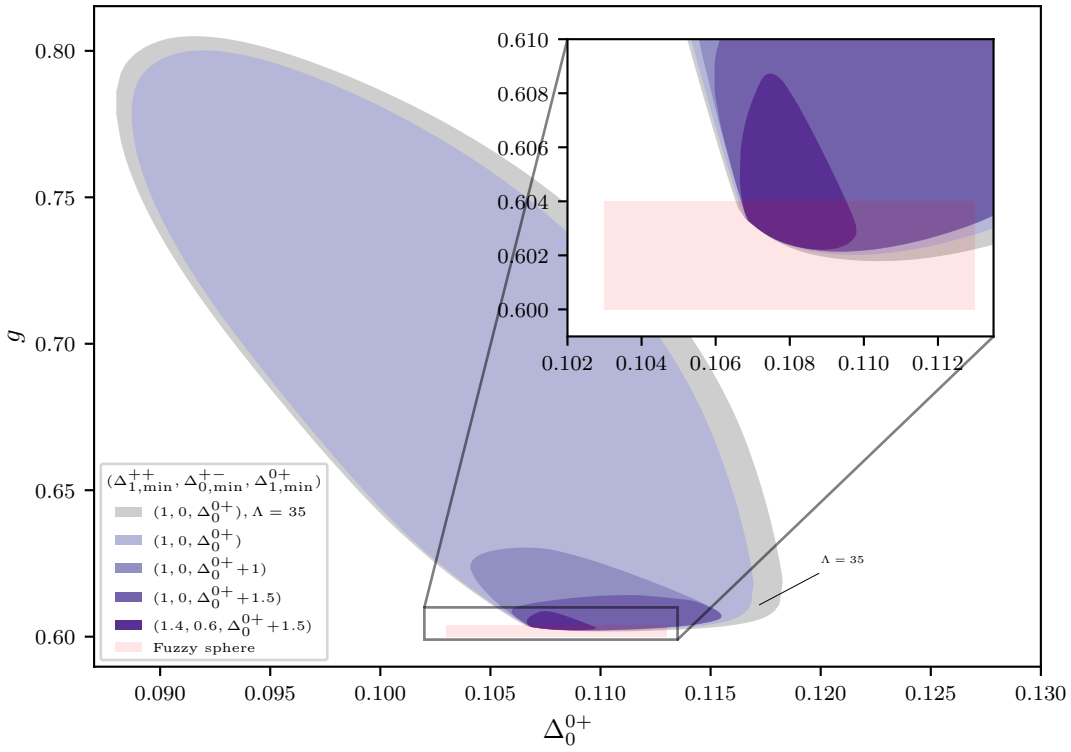

Figure 3.10: Bounds on the defect g-function with various defect spectrum assumptions. The bounds are obtained using $\Lambda = 45$, unless otherwise indicated.

Next we explore bounds on the defect g-function, which are shown in Fig. 3.10. A number of interesting physical implications follow from these bounds. First, we learn that all values of Δ_0^{0+} sitting within the islands of Fig. 3.9, even for the range obtained with no non-trivial assumptions about the defect operator spectrum, are inconsistent with $g \geq 1$. This means that a generic point within the island will satisfy all of the necessary requirements we expect

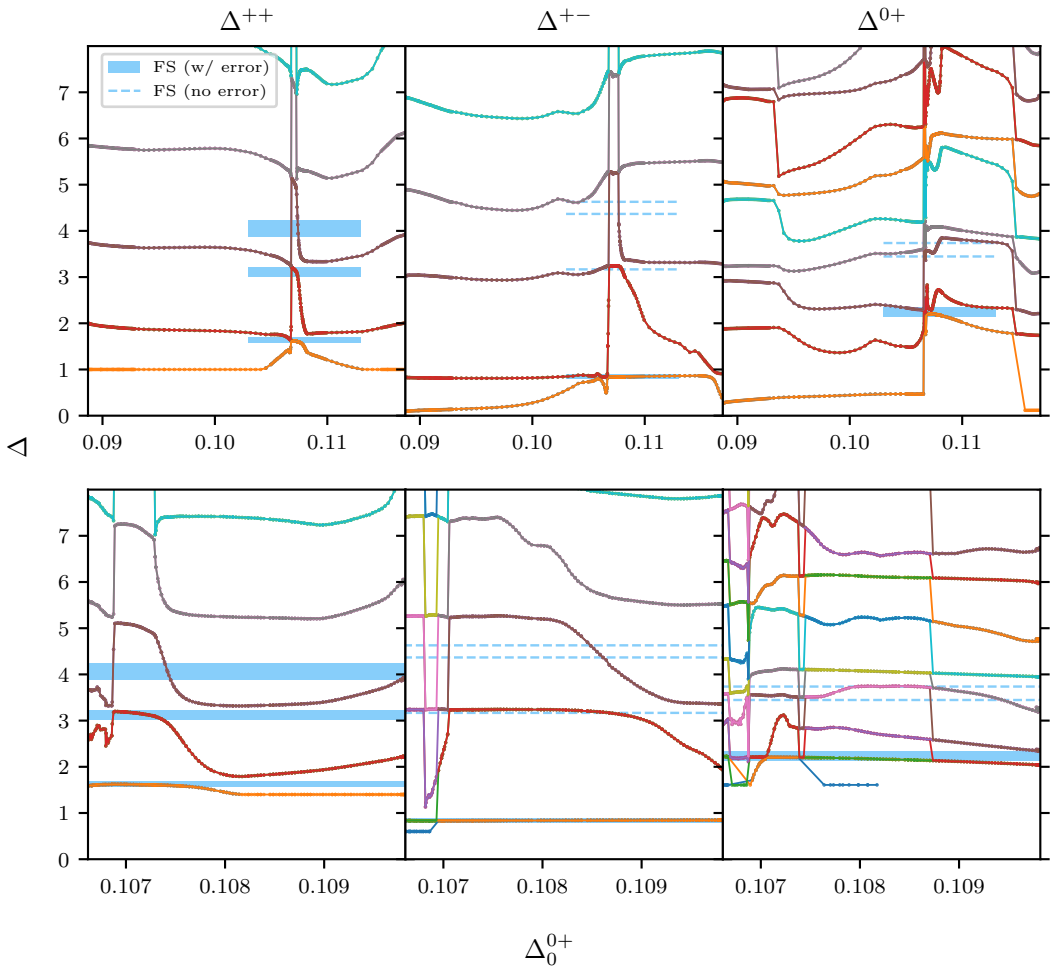

Figure 3.11: Zeros of the optimal functional obtained from g-minimization at $\Lambda = 45$ for the defect, domain wall, and endpoint spectra, going from left to right. The spectra in the upper subplot were obtained upon minimizing g with no assumptions on the defect-changing spectrum other than $\Delta_1^{++} \geq 1$. The spectra in the lower row were obtained assuming $\Delta_1^{++} \geq 1.4$, $\Delta_0^{+-} \geq 0.6$, and $\Delta_1^{0+} \geq \Delta_0^{0+} + 1.5$. We also present the corresponding operator dimensions computed with the fuzzy sphere regularization for comparison, whose values we list in Tab.

of the true pinning field defect. Together with existing analytical and numerical evidence, which predict values for Δ_0^{0+} and g that are overall very consistent with the island seen in Fig. 3.10, we can safely reason that the physical solution is indeed responsible for the island. Another interesting feature is that $g < 1/2$ is totally ruled out. This is significant because it means that the non-simple SSB defect $\mathcal{D}^+ \oplus \mathcal{D}^-$ *can* flow to the trivial defect, since this defect would have $g_{\text{SSB}} = 2g_\pm > 1$. If $g < 1/2$ were allowed, then we would not have ruled out the scenario where domain wall proliferation drives the non-simple defect fixed point to a non-trivial symmetry-preserving defect with $g < 1$. This scenario would be very surprising, since it would require the existence of a stable, symmetry-preserving line defect of the $3d$ Ising CFT, but we know of no evidence supporting the existence of such an object. In principle, given our bounds, it is still possible that domain walls drive the SSB defect to a non-trivial (non-perturbative) $g > 1$ defect, but this scenario is quite unlikely for the same reason.

Another interesting feature of our bound on g is the region where the bounds have appeared to saturate. We can see that there is a kink in the island along its lower edge, and there is a sizeable region near this kink where the lower bound on g is essentially insensitive to increasing Λ and imposing stronger gap assumptions. This behavior serves as strong evidence that our setup is close to saturating the physical value of g, which we expect to live near this kink.

A further indication that the physical dCFT data lie near the kink comes from the spectra produced during g minimization. When g is minimized, the functional α^* which produces the optimal bound also produces a unitary solution to the crossing equations for free [59, 132]. We show the spectra of defect-changing operators implied from α^* in Fig. 3.11. When we choose Δ_0^{0+} to be near the kink, the low-lying spectra predicted shows excellent agreement with the fuzzy sphere predictions. We see very close agreement between our predictions and those of the fuzzy sphere for Δ_1^{++}, Δ_2^{++}, Δ_0^{+-}, Δ_1^{+-}, Δ_0^{0+}[14], and Δ_1^{0+}. Unfortunately, looking

[14] ϕ_0^{0+} is an external operator. Since the OPE coefficients involving ϕ_0^{0+} are accounted for in the discrete constraint $\mathbf{V}^r_{\sigma\varepsilon}$, we do not expect it to necessarily appear as a zero of $\alpha[\mathbf{V}_\Delta^{0+}(x)]$.

beyond these low-lying operators, the fuzzy sphere appears to predict a few operators that we do not find, so our ability to make comparison is rather limited. There are a few reasons that could explain why we seem to miss these operators. One explanation is that we have not yet included enough constraints in our setup. We have not yet included constraints coming from using the displacement operator or ϕ_0^{+-}, ϕ_1^{++} as external operators, which would allow more physical assumptions to be made. We also could include more constraints about the bulk, such as fixing more of the bulk descendant OPE coefficients or fully incorporating $3d$ conformal blocks, as we will discuss later. A final possibility is that we have chosen bulk CFT data that are too far from their physical values. It will be interesting in the future to implement these improvements to learn more about the higher operator spectrum.

We finally mention how we obtain the bounds on g, which follows the standard technique to optimize OPE coefficients. To briefly recall how this works, we first act on the crossing equation with a linear functional α and write the result as

$$\frac{1}{g}\alpha[\mathbf{V}_0^{++}] + \alpha[\mathbf{V}_0^{0,0}] + \sum_i \vec{\lambda}_i^{\mathsf{T}} \cdot \alpha[\mathbf{V}_i] \cdot \vec{\lambda}_i = 0 \tag{3.88}$$

where $\mathbf{V}_i$ runs over all crossing vectors included in (3.68–3.77) in addition to (3.87), representing the remaining terms in the crossing equation. Setting $\alpha[\mathbf{V}_0^{0,0}] = \pm 1$ and imposing $\alpha[\mathbf{V}_i] \succeq 0$ allows us to derive

$$\alpha[\mathbf{V}_0^{++}] \leq \mp g, \tag{3.89}$$

which means $\mp\alpha[\mathbf{V}_0^{++}]$ yields a valid upper/lower bound on g, and we use `SDPB` to find an α saturating the optimal bound subject to the constraints.

3.3.5 Defect-changing operator dimensions

We next discuss our bounds on the scaling dimensions of various defect-changing operators. Our most general results are upper bounds on Δ_1^{++}, Δ_0^{+-}, and Δ_1^{0+} as a function of Δ_0^{0+}, where we make no assumptions about the defect-changing spectrum other than $\Delta_1^{++} \geq 1$. These bounds are obtained by imposing (3.68–3.77), (3.87), and (3.83) and finding the

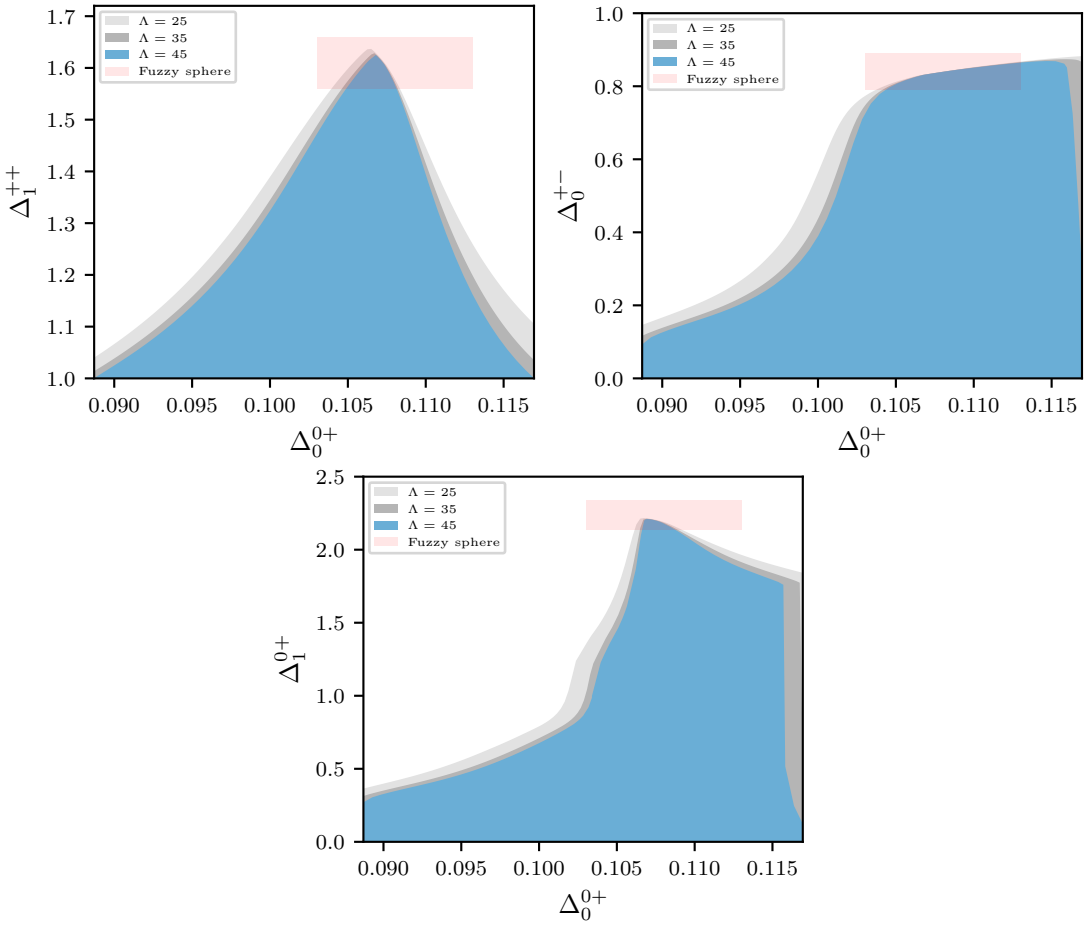

Figure 3.12: Upper bounds on the scaling dimension of the lightest non-trivial defect primary Δ_1^{++}, the lightest domain wall primary Δ_0^{+-}, and the second-lightest endpoint primary Δ_1^{0+}. The only assumption about the defect-changing operator spectra is $\Delta_1^{++} \geq 1$, which is also encoded in the bound on $|\lambda_{\varepsilon 00}^{0+0}/\lambda_{\sigma 00}^{0+0}|$.

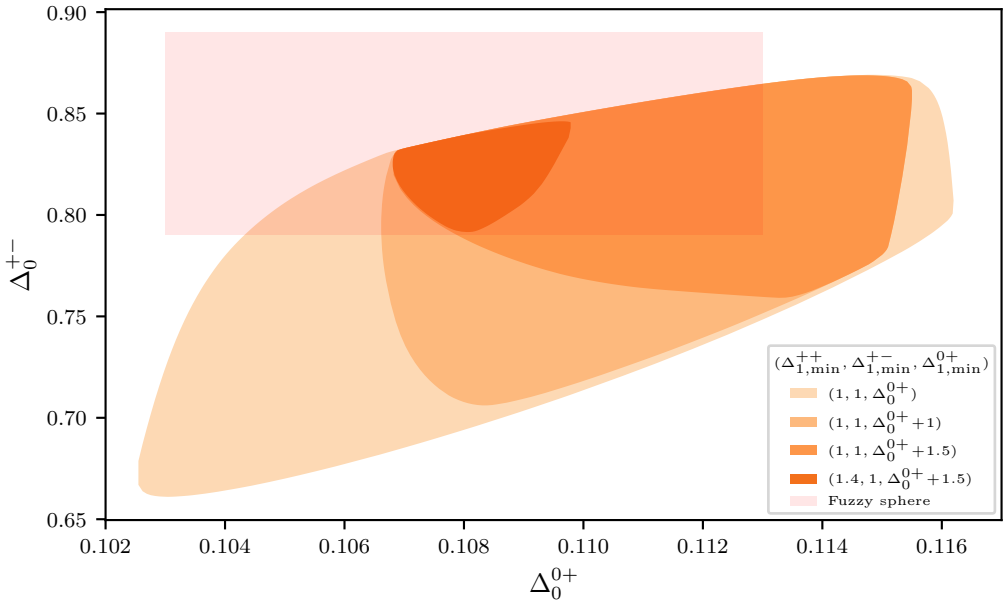

Figure 3.13: Allowed region for the leading domain wall operator with various non-generic gap assumptions. In all instances, we compute a bound assuming only a single relevant domain wall operator.

smallest disallowed choices of the gaps in the defect-changing sectors using a binary search. The bounds are shown in Fig. 3.12 and lead to the following general bounds

$$1 \leq \Delta_1^{++} \leq 1.625 \qquad \Delta_0^{+-} \leq 0.870 \qquad \Delta_1^{0+} \leq 2.210.$$

The values at which the above bounds are saturated, as a function of increasing Λ, agree well with the values predicted by the fuzzy sphere [161]

$$(\Delta_1^{++}, \Delta_0^{+-}, \Delta_1^{0+}) = (1.61(5), 0.84(5), 2.24(10)).$$

The most interesting consequence of these bounds is the proof, with no non-trivial defect-changing spectrum assumptions, that ϕ_0^{+-} is a *relevant* operator of the $\mathcal{D}^+ \oplus \mathcal{D}^-$ fixed point, thus ruling out this non-simple defect from supporting stable spontaneous symmetry breaking. This likely proves that there is no conformal line defect of the $3d$ Ising CFT that

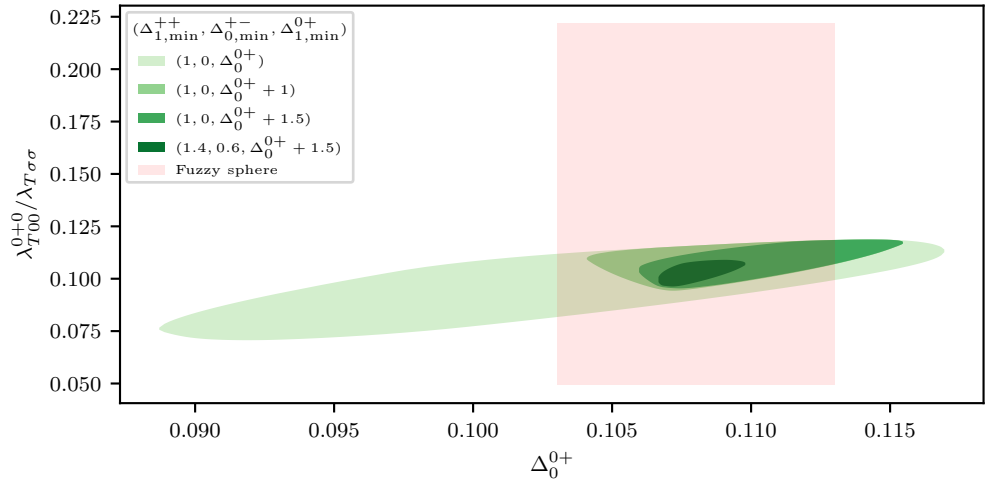

Figure 3.14: The allowed region for the ratio of OPE coefficients $\lambda^{0+0}_{T00}/\lambda_{T\sigma\sigma}$. The bounds are computed at $\Lambda = 45$.

can support SSB, but in principle there can exist defects without any obvious perturbative description where SSB occurs, which our results do not technically rule out.

To obtain more refined estimates of Δ_0^{+-}, we further impose $\Delta_1^{+-} \geq 1$, amounting to assuming only a single relevant domain wall is present. The new allowed region in Δ_0^{+-} is now bounded from below due to these secondary gap assumptions. These gap assumptions are implemented by respectively replacing (3.77) with

$$\alpha[\mathbf{V}^{+-}_{\Delta_0^{+-}}] \geq 0 \tag{3.90}$$

$$\alpha[\mathbf{V}^{+-}_{\Delta}] \geq 0 \qquad \Delta \geq 1. \tag{3.91}$$

All the other constraints are imposed in the same way as before, and we use the "cutting curve" algorithm again to obtain the final islands using Δ_0^{+-} as scanning parameters.

3.3.6 Stress tensor OPE ratio

A final quantity that we bound is $\lambda^{0+0}_{T00}/\lambda_{T\sigma\sigma}$, representing the ratio of OPE coefficients of the stress tensor appearing in the endpoint vs. σ OPEs. We obtain the bound in an essentially identical manner as described earlier in the case of $|\lambda^{0+0}_{\varepsilon 00}/\lambda^{0+0}_{\sigma 00}|$, except we scan over $\theta^T_{\phi_0^{0+}\sigma} = \lambda^{0+0}_{T00}/\lambda_{T\sigma\sigma}$ using the crossing vector $\mathbf{V}_T(x, \theta^T_{\phi_0^{0+}\sigma})$, defined as

$$\mathbf{V}_T(x, r^T_{\phi_0^{0+}\sigma}) = M_T(\theta^T_{\phi_0^{0+}\sigma}) \cdot \mathbf{V}_T(x) \cdot M_T(\theta^T_{\phi_0^{0+}\sigma})^{\mathsf{T}} \qquad M_T(\theta^T_{\phi_0^{0+}\sigma}) = \begin{pmatrix} \sin\theta^T_{\phi_0^{0+}\sigma} & \cos\theta^T_{\phi_0^{0+}\sigma}. \end{pmatrix} \tag{3.92}$$

The results are shown in Fig. 3.14.

3.4 Discussion

In this chapter, we have demonstrated the power of modern numerical conformal bootstrap tools to probe the properties of conformal line defects in specific CFTs in higher dimensions. We focused on the case of the pinning field defect in the $3d$ Ising CFT, giving essentially rigorous bounds on a variety of the most important quantities characterizing this defect. Our most physically important result is the proof that the non-simple "LRO defect" $\mathcal{D}^+ \oplus \mathcal{D}^-$ related to the pinning field defect cannot support stable spontaneous symmetry breaking due to the RG-relevance of the domain-wall creation operator, under the assumption that the bootstrap island we find is indeed due to the $3d$ Ising pinning field defect.

There are a number of interesting directions that are worth more study in the future. One direction is to pursue improvements to our setup. Some options that stand out are firstly to include more external defect-changing operators such as the displacement operator, Δ_1^{++}, or Δ_0^{+-}. While the dimensions of these operators are quite large compared to that of ϕ_0^{0+}, making them generally somewhat less constraining, including them allows more physical assumptions to be encoded, such as the uniqueness of these operators. Hopefully, these additional operators make way for a more accurate picture of the higher operator spectrum, which we were not able to achieve in this work beyond the first two operators in each defect-changing sector. Another interesting possibility is to include the full $3d$ conformal

blocks in correlation functions that only contain bulk operators. While this likely comes at a significantly higher computational cost, sensitivity beyond that of the pure bulk $3d$ Ising bootstrap would be achieved, which would be a significant advantage compared with our setup. Conversely, one can fantasize that, since augmenting the $3d$ bulk Ising bootstrap setup with the defect-changing operators of the pinning field strictly strengthens any bulk bounds in principle, the complete system of bulk and defect-changing operators could lead to a shrinkage of the $3d$ Ising bulk bootstrap allowed region compared with the existing, purely bulk results [94]. To attempt this, it will be important to also upgrade to a navigator bootstrap setup to more efficiently scan over the rather large number of parameters that could be involved [126].

Beyond the $3d$ Ising pinning field, which is the simplest example of a line defect in a strongly coupled CFT in higher dimensions, a rich set of defects exist in other CFTs as well that merit future study. Spin impurities are a particularly physical example of a line defect, naturally appearing in e.g. the $O(N)$ WF theories, but are difficult to study analytically due to quantum effects [150, 103, 50]. Bootstrap does not suffer from issues due to being in a strong-coupling regime like in perturbation theory, so our method seems like an especially effective way to study these defects. Other theories that deserve attention from the perspective taken in this work are conformal gauge theories. The problem of bootstrapping such gauge theories has already proved to be a challenge; the problem can be set up in a similar fashion to simpler theories, but the results are not nearly as strong compared with e.g. the $O(N)$ CFTs [41, 5, 83]. One natural guess as to why previous bootstrap studies of gauge theories have not had as much success is that, when they have a flavor symmetry such as $SU(N)$, the flavor fundamental can be missing from the spectrum of local operators. An operator in the fundamental representation can fuse to create operators in the other representations, so it should be more constraining from a bootstrap point of view. However, in these gauge theories the Wilson line can often carry such a fundamental rep. operator at its endpoint. Using the techniques developed here, we hope that a deeper understanding of conformal gauge theories could be achieved.

Finally, we mention that the problem of studying line defects in two-dimensional theories is still quite open. It has proven extremely difficult to solve conformal boundary conditions beyond the rational boundaries of rational models and toroidal compactifications, so numerical bootstrap techniques are a natural next resort. There are a much richer set of constraints on line defects in two dimensions coming from the modular transformation properties of the annulus partition function [95], so combining these new consistency conditions in addition to those introduced in this chapter seems quite promising.

Appendix A

MODULAR BOOTSTRAP EQUATIONS

The reduced modular covariance equation reads

$$\tilde{\mathbf{Z}}_{\text{red}}(-1/\tau, -1/\bar{\tau}) = F_{\text{red}}\tilde{\mathbf{Z}}_{\text{red}}(\tau, \bar{\tau})$$

Here we list F_{ref} for each N along with the corresponding reduced partition function components.

A.0.1 $N \in 2\mathbb{Z}+1$

As discussed, when N is odd the LSM anomaly does not lead any $\mathbb{Z}_N$ subgroup to have a $\mathbb{Z}_N$ anomaly. When N is prime, such as in the cases we consider, the full orbit of the automorphism group of any non-trivial $g \in \mathbb{Z}_N^3$ contains all other non-trivial TDLs. Consequently, we may perform the maximal reduction and lose no generality. If we denote the trivial representation by ρ_1 and the trivial element of G by g_1 then

$$F_{\text{red}} = \begin{pmatrix} \frac{1}{|G|} & \frac{1}{|G|} & \frac{1}{|G|} \\ \frac{|G|-1}{|G|} & \frac{|G|-1}{|G|} & -\frac{1}{|G|} \\ |G|-1 & -1 & 0 \end{pmatrix} \tilde{\mathbf{Z}}_{\text{red}} = \begin{pmatrix} Z^{\rho_1} \\ \sum_{\rho_1 \neq \rho \in \text{Rep}(G)} Z^{\rho} \\ \sum_{g_1 \neq g \in G} Z_g \end{pmatrix}$$

A.0.2 $N \in 2\mathbb{Z}$

In the case of even N, the full reduction is no longer possible. However, by grouping together all TDLs with identical $\mathbb{Z}_M$ anomalies according to Table 2.1 we still may perform a non-trivial reduction.

$N = 2$

According to Table 2.1 there are two types of TDLs, both with order 2: non-anomalous or anomalous with $k = 1$. Denote the subset of G corresponding to the former as [2N] and the latter as [2A].

Next, denote representations of $\mathbb{Z}_N^3$ as vectors $\rho = [i, j, k]$. There are then two automorphism classes of representations induced by automorphisms preserving the spin selection rules of the LSM anomaly: a class [O] where an odd number of components of ρ is non-trivial and a class [E] where an even number is non-trivial. Then

$$F_{\text{red}} = \begin{pmatrix} \frac{1}{8} & \frac{1}{8} & \frac{1}{8} & \frac{1}{8} & \frac{1}{8} \\ \frac{3}{8} & \frac{3}{8} & \frac{3}{8} & \frac{3}{8} & -\frac{1}{8} \\ \frac{1}{2} & \frac{1}{2} & \frac{1}{2} & -\frac{1}{2} & 0 \\ 1 & 1 & -1 & 0 & 0 \\ 6 & -2 & 0 & 0 & 0 \end{pmatrix} \tilde{\mathbf{Z}}_{\text{red}} = \begin{pmatrix} Z^{\rho_1} \\ \sum_{\rho\in[\text{E}]} Z^{\rho} \\ \sum_{\rho\in[\text{O}]} Z^{\rho} \\ \sum_{g\in[\text{2A}]} Z_g \\ \sum_{g\in[\text{2N}]} Z_g \end{pmatrix}$$

$N = 4$

Table 2.1 indicates that there are three classes of TDLs. All order 2 TDLs are non-anomalous and we will denote the class of such TDLs by [2N]. Order 4 TDLs are either anomalous with $k = 2$ or non-anomalous, respectively denoted by [4A] and [4N]. There are also three classes of non-trivial representations. The first, denoted [2E], are representation vectors where an even number of components is equal to 2 and the rest are equal to 0. Then [2O] denotes the representation vectors where an odd number of components are equal to 2 and the rest are

0. Finally, [4] denotes all remaining, non-trivial representation vectors. These give

$$F_{\text{red}} = \begin{pmatrix} \frac{1}{64} & \frac{1}{64} & \frac{1}{64} & \frac{1}{64} & \frac{1}{64} & \frac{1}{64} & \frac{1}{64} \\ \frac{3}{64} & \frac{3}{64} & \frac{3}{64} & \frac{3}{64} & \frac{3}{64} & \frac{3}{64} & -\frac{1}{64} \\ \frac{1}{16} & \frac{1}{16} & \frac{1}{16} & \frac{1}{16} & \frac{1}{16} & -\frac{1}{16} & 0 \\ \frac{7}{8} & \frac{7}{8} & \frac{7}{8} & \frac{7}{8} & -\frac{1}{8} & 0 & 0 \\ 7 & 7 & 7 & -1 & 0 & 0 & 0 \\ 8 & 8 & -8 & 0 & 0 & 0 & 0 \\ 48 & -16 & 0 & 0 & 0 & 0 & 0 \end{pmatrix} \tilde{\mathbf{Z}}_{\text{red}} = \begin{pmatrix} Z^{\rho_1} \\ \sum_{\rho\in[2\text{E}]} Z^{\rho} \\ \sum_{\rho\in[2\text{O}]} Z^{\rho} \\ \sum_{\rho\in[4]} Z^{\rho} \\ \sum_{g\in[2\text{N}]} Z_g \\ \sum_{g\in[4\text{A}]} Z_g \\ \sum_{g\in[4\text{N}]} Z_g \end{pmatrix}$$

$N = 6$

Following a similar pattern as before, we label the classes of TDLs as $[2\text{N}], [2\text{A}], [3\text{N}], [6\text{N}], [6\text{A}]$ where the order 2 anomalous TDLs have $k = 1$ and the order 6 anomalous TDLs have $k = 3$. There are five classes of non-trivial representations. We denote the classes containing an even/odd number of components being equal to 3 as [3E]/[3O]. There is a class where each component is an even number, which we denote by [E]. There is a class containing only odd numbers with at least one component not equal to 3, denoted [O]. Finally, there is a class where the components are a mix of even and odd numbers, denoted [EO]. These give

$$F_{\text{red}} = \begin{pmatrix} \frac{1}{216} & \frac{1}{216} & \frac{1}{216} & \frac{1}{216} & \frac{1}{216} & \frac{1}{216} & \frac{1}{216} & \frac{1}{216} & \frac{1}{216} & \frac{1}{216} & \frac{1}{216} \\ \frac{1}{72} & \frac{1}{72} & \frac{1}{72} & \frac{1}{72} & \frac{1}{72} & \frac{1}{72} & \frac{1}{72} & -\frac{1}{216} & \frac{1}{72} & \frac{1}{72} & -\frac{1}{216} \\ \frac{1}{54} & \frac{1}{54} & \frac{1}{54} & \frac{1}{54} & \frac{1}{54} & \frac{1}{54} & -\frac{1}{54} & 0 & \frac{1}{54} & -\frac{1}{54} & 0 \\ \frac{13}{108} & \frac{13}{108} & \frac{13}{108} & \frac{13}{108} & \frac{13}{108} & \frac{13}{108} & \frac{13}{108} & \frac{13}{108} & -\frac{1}{216} & -\frac{1}{216} & -\frac{1}{216} \\ \frac{13}{36} & \frac{13}{36} & \frac{13}{36} & \frac{13}{36} & \frac{13}{36} & \frac{13}{36} & \frac{13}{36} & -\frac{13}{108} & -\frac{1}{72} & -\frac{1}{72} & \frac{1}{216} \\ \frac{13}{27} & \frac{13}{27} & \frac{13}{27} & \frac{13}{27} & \frac{13}{27} & \frac{13}{27} & -\frac{13}{27} & 0 & -\frac{1}{54} & -\frac{1}{54} & 0 \\ 1 & 1 & -1 & 1 & 1 & -1 & 0 & 0 & 0 & 0 & 0 \\ 6 & -2 & 0 & 6 & -2 & 0 & 0 & 0 & 0 & 0 & 0 \\ 26 & 26 & 26 & -1 & -1 & -1 & 0 & 0 & 0 & 0 & 0 \\ 26 & 26 & -26 & -1 & -1 & 1 & 0 & 0 & 0 & 0 & 0 \\ 156 & -52 & 0 & -6 & 2 & 0 & 0 & 0 & 0 & 0 & 0 \end{pmatrix} \tilde{\mathbf{Z}}_{\text{red}} = \begin{pmatrix} Z^{\rho_1} \\ \sum_{\rho\in[3\text{E}]} Z^{\rho} \\ \sum_{\rho\in[3\text{O}]} Z^{\rho} \\ \sum_{\rho\in[\text{E}]} Z^{\rho} \\ \sum_{\rho\in[\text{O}]} Z^{\rho} \\ \sum_{\rho\in[\text{EO}]} Z^{\rho} \\ \sum_{g\in[2\text{A}]} Z_g \\ \sum_{g\in[2\text{N}]} Z_g \\ \sum_{g\in[3\text{N}]} Z_g \\ \sum_{g\in[6\text{A}]} Z_g \\ \sum_{g\in[6\text{N}]} Z_g \end{pmatrix}$$

Appendix B

CROSSING EQUATIONS

In terms of conformal blocks (3.18), the full set of crossing equations is

$$0 = \left(\tfrac{1}{g} \pm 1\right) F^{\phi\phi\phi\phi}_{0,\mp}(x) + \sum_{\mathcal{O}\in[++;r^\tau=0]} (\lambda^{0++}_{\phi\phi\mathcal{O}})^2 F^{\phi\phi\phi\phi}_{\Delta,\mp}(x) \pm \sum_{\mathcal{O}\in\left[00;\substack{r^\tau=0\\q=0,1}\right]} (\lambda^{+00}_{\phi\phi\mathcal{O}})^2 F^{\phi\phi\phi\phi}_{\Delta,\mp}(x) \tag{B.1}$$

$$0 = \pm F^{\phi\phi\phi\phi}_{0,\mp}(x) + \sum_{\mathcal{O}\in[-+]} (\lambda^{0-+}_{\phi\phi\mathcal{O}})^2 F^{\phi\phi\phi\phi}_{\Delta,\mp}(x) \pm \sum_{\left[00;\substack{r^\tau=0\\q=0,1}\right]} (-1)^q (\lambda^{+00}_{\phi\phi\mathcal{O}})^2 F^{\phi\phi\phi\phi}_{\Delta,\mp}(x) \tag{B.2}$$

$$0 = \pm F^{\sigma\sigma\phi\phi}_{0,\mp}(x) + \sum_{\mathcal{O}\in[0+]} |\lambda^{00+}_{\sigma\phi\mathcal{O}}|^2 F^{\sigma\phi\phi\sigma}_{\Delta,\mp}(x) \pm \sum_{\mathcal{O}\in\left[00;\substack{r^\tau=0\\q=0}\right]} \lambda^{+00}_{\phi\phi\mathcal{O}}\lambda_{\sigma\sigma\mathcal{O}} F^{\sigma\sigma\phi\phi}_{\Delta,\mp}(x) \tag{B.3}$$

$$0 = \sum_{\mathcal{O}\in[0+]} \lambda^{00+}_{\epsilon\phi\mathcal{O}}(\lambda^{00+}_{\sigma\phi\mathcal{O}})^* F^{\epsilon\phi\phi\sigma}_{\Delta,\mp}(x) \pm \sum_{\mathcal{O}\in\left[00;\substack{r^\tau=0\\q=1}\right]} \lambda^{+00}_{\phi\phi\mathcal{O}}\lambda_{\epsilon\sigma\mathcal{O}} F^{\sigma\epsilon\phi\phi}_{\Delta,\mp}(x) \tag{B.4}$$

$$0 = \pm F^{\epsilon\epsilon\phi\phi}_{0,\mp}(x) + \sum_{\mathcal{O}\in[0+]} |\lambda^{00+}_{\epsilon\phi\mathcal{O}}|^2 F^{\epsilon\phi\phi\epsilon}_{\Delta,\mp}(x) \pm \sum_{\mathcal{O}\in\left[00;\substack{r^\tau=0\\q=0}\right]} \lambda^{+00}_{\phi\phi\mathcal{O}}\lambda_{\epsilon\epsilon\mathcal{O}} F^{\epsilon\epsilon\phi\phi}_{\Delta,\mp}(x) \tag{B.5}$$

$$0 = F^{\sigma\sigma\sigma\sigma}_{0,-}(x) + \sum_{\mathcal{O}\in\left[00;\substack{r^\tau=0\\q=0}\right]} \lambda^2_{\sigma\sigma\mathcal{O}} F^{\sigma\sigma\sigma\sigma}_{\Delta,-}(x) \tag{B.6}$$

$$0 = F^{\sigma\sigma\epsilon\epsilon}_{0,\mp}(x) + \sum_{\mathcal{O}\in\left[00;\substack{r^\tau=0\\q=0}\right]} \lambda_{\sigma\sigma\mathcal{O}}\lambda_{\epsilon\epsilon\mathcal{O}} F^{\sigma\sigma\epsilon\epsilon}_{\Delta,\mp}(x) \pm \sum_{\mathcal{O}\in\left[00;\substack{r^\tau=0,1\\q=1}\right]} |\lambda_{\epsilon\sigma\mathcal{O}}|^2 F^{\epsilon\sigma\sigma\epsilon}_{\Delta,\mp}(x) \tag{B.7}$$

$$0 = \sum_{\mathcal{O}\in\left[00;\substack{r^\tau=0,1\\q=1}\right]} (-1)^{r^\tau} |\lambda_{\epsilon\sigma\mathcal{O}}|^2 F^{\sigma\epsilon\sigma\epsilon}_{\Delta,-}(x) \tag{B.8}$$

$$0 = F^{\epsilon\epsilon\epsilon\epsilon}_{0,-}(x) + \sum_{\mathcal{O}\in\left[00;\substack{r^\tau=0\\q=0}\right]} \lambda^2_{\epsilon\epsilon\mathcal{O}} F^{\epsilon\epsilon\epsilon\epsilon}_{\Delta,-}(x). \tag{B.9}$$

The crossing equations lead to the following crossing vectors listed below. Note that for crossing vectors whose elements are non-trivial matrices, we use "0" to represent the zero

matrix of the appropriate dimension. Note that we also use ϕ to represent ϕ_0^{0+}.

$$\mathbf{V}_T(x) = \begin{pmatrix}
\begin{pmatrix} F_{3,-}^{\phi\phi\phi\phi} & 0 \\ 0 & 0 \end{pmatrix} \\
\begin{pmatrix} -F_{3,+}^{\phi\phi\phi\phi} & 0 \\ 0 & 0 \end{pmatrix} \\
\begin{pmatrix} F_{3,-}^{\phi\phi\phi\phi} & 0 \\ 0 & 0 \end{pmatrix} \\
\begin{pmatrix} -F_{3,+}^{\phi\phi\phi\phi} & 0 \\ 0 & 0 \end{pmatrix} \\
\begin{pmatrix} 0 & \frac{1}{2}F_{3,-}^{\sigma\sigma\phi\phi} \\ \frac{1}{2}F_{3,-}^{\sigma\sigma\phi\phi} & 0 \end{pmatrix} \\
\begin{pmatrix} 0 & -\frac{1}{2}F_{3,+}^{\sigma\sigma\phi\phi} \\ -\frac{1}{2}F_{3,+}^{\sigma\sigma\phi\phi} & 0 \end{pmatrix} \\
0 \\
0 \\
\begin{pmatrix} 0 & \frac{r_T}{2}F_{3,-}^{\epsilon\epsilon\phi\phi} \\ \frac{r_T}{2}F_{3,-}^{\epsilon\epsilon\phi\phi} & 0 \end{pmatrix} \\
\begin{pmatrix} 0 & -\frac{r_T}{2}F_{3,+}^{\epsilon\epsilon\phi\phi} \\ -\frac{r_T}{2}F_{3,+}^{\epsilon\epsilon\phi\phi} & 0 \end{pmatrix} \\
\begin{pmatrix} 0 & 0 \\ 0 & F_{3,-}^{\sigma\sigma\sigma\sigma} \end{pmatrix} \\
\begin{pmatrix} 0 & 0 \\ 0 & r_T F_{3,-}^{\sigma\sigma\epsilon\epsilon} \end{pmatrix} \\
\begin{pmatrix} 0 & 0 \\ 0 & r_T F_{3,+}^{\sigma\sigma\epsilon\epsilon} \end{pmatrix} \\
0 \\
\begin{pmatrix} 0 & 0 \\ 0 & r_T^2 F_{3,-}^{\epsilon\epsilon\epsilon\epsilon} \end{pmatrix}
\end{pmatrix}$$

$$\mathbf{V}_\Delta^{0,0}(x) = \begin{pmatrix}
\begin{pmatrix} F_{\Delta,-}^{\phi\phi\phi\phi} & 0 & 0 \\ 0 & 0 & 0 \\ 0 & 0 & 0 \end{pmatrix} \\
\begin{pmatrix} -F_{\Delta,+}^{\phi\phi\phi\phi} & 0 & 0 \\ 0 & 0 & 0 \\ 0 & 0 & 0 \end{pmatrix} \\
\begin{pmatrix} F_{\Delta,-}^{\phi\phi\phi\phi} & 0 & 0 \\ 0 & 0 & 0 \\ 0 & 0 & 0 \end{pmatrix} \\
\begin{pmatrix} -F_{\Delta,+}^{\phi\phi\phi\phi} & 0 & 0 \\ 0 & 0 & 0 \\ 0 & 0 & 0 \end{pmatrix} \\
\begin{pmatrix} 0 & \frac{1}{2}F_{\Delta,-}^{\sigma\sigma\phi\phi} & 0 \\ \frac{1}{2}F_{\Delta,-}^{\sigma\sigma\phi\phi} & 0 & 0 \\ 0 & 0 & 0 \end{pmatrix} \\
\begin{pmatrix} 0 & -\frac{1}{2}F_{\Delta,+}^{\sigma\sigma\phi\phi} & 0 \\ -\frac{1}{2}F_{\Delta,+}^{\sigma\sigma\phi\phi} & 0 & 0 \\ 0 & 0 & 0 \end{pmatrix} \\
0 \\
0 \\
\begin{pmatrix} 0 & 0 & \frac{1}{2}F_{\Delta,-}^{\epsilon\epsilon\phi\phi} \\ 0 & 0 & 0 \\ \frac{1}{2}F_{\Delta,-}^{\epsilon\epsilon\phi\phi} & 0 & 0 \end{pmatrix} \\
\begin{pmatrix} 0 & 0 & -\frac{1}{2}F_{\Delta,+}^{\epsilon\epsilon\phi\phi} \\ 0 & 0 & 0 \\ -\frac{1}{2}F_{\Delta,+}^{\epsilon\epsilon\phi\phi} & 0 & 0 \end{pmatrix} \\
\begin{pmatrix} 0 & 0 & 0 \\ 0 & F_{\Delta,-}^{\sigma\sigma\sigma\sigma} & 0 \\ 0 & 0 & 0 \end{pmatrix} \\
\begin{pmatrix} 0 & 0 & 0 \\ 0 & 0 & \frac{1}{2}F_{\Delta,-}^{\sigma\sigma\epsilon\epsilon} \\ 0 & \frac{1}{2}F_{\Delta,-}^{\sigma\sigma\epsilon\epsilon} & 0 \end{pmatrix} \\
\begin{pmatrix} 0 & 0 & 0 \\ 0 & 0 & \frac{1}{2}F_{\Delta,+}^{\sigma\sigma\epsilon\epsilon} \\ 0 & \frac{1}{2}F_{\Delta,+}^{\sigma\sigma\epsilon\epsilon} & 0 \end{pmatrix} \\
0 \\
\begin{pmatrix} 0 & 0 & 0 \\ 0 & 0 & 0 \\ 0 & 0 & F_{\Delta,-}^{\epsilon\epsilon\epsilon\epsilon} \end{pmatrix}
\end{pmatrix}$$

$$\mathbf{V}_{\Delta}^{1,0}(x) = \begin{pmatrix} \begin{pmatrix} F_{\Delta,-}^{\phi\phi\phi\phi} & 0 \\ 0 & 0 \end{pmatrix} \\ \begin{pmatrix} -F_{\Delta,+}^{\phi\phi\phi\phi} & 0 \\ 0 & 0 \end{pmatrix} \\ \begin{pmatrix} -F_{\Delta,-}^{\phi\phi\phi\phi} & 0 \\ 0 & 0 \end{pmatrix} \\ \begin{pmatrix} F_{\Delta,+}^{\phi\phi\phi\phi} & 0 \\ 0 & 0 \end{pmatrix} \\ 0 \\ 0 \\ \begin{pmatrix} 0 & \frac{1}{2}F_{\Delta,-}^{\sigma\epsilon\phi\phi} \\ \frac{1}{2}F_{\Delta,-}^{\sigma\epsilon\phi\phi} & 0 \end{pmatrix} \\ \begin{pmatrix} 0 & -\frac{1}{2}F_{\Delta,+}^{\sigma\epsilon\phi\phi} \\ -\frac{1}{2}F_{\Delta,+}^{\sigma\epsilon\phi\phi} & 0 \end{pmatrix} \\ 0 \\ 0 \\ 0 \\ \begin{pmatrix} 0 & 0 \\ 0 & F_{\Delta,-}^{\epsilon\sigma\sigma\epsilon} \end{pmatrix} \\ \begin{pmatrix} 0 & 0 \\ 0 & -F_{\Delta,+}^{\epsilon\sigma\sigma\epsilon} \end{pmatrix} \\ \begin{pmatrix} 0 & 0 \\ 0 & F_{\Delta,-}^{\epsilon\sigma\epsilon\sigma} \end{pmatrix} \\ 0 \end{pmatrix} \quad \mathbf{V}_{\Delta}^{1,1}(x) = \begin{pmatrix} 0 \\ 0 \\ 0 \\ 0 \\ 0 \\ 0 \\ 0 \\ 0 \\ 0 \\ 0 \\ F_{\Delta,-}^{\epsilon\sigma\sigma\epsilon} \\ -F_{\Delta,+}^{\epsilon\sigma\sigma\epsilon} \\ -F_{\Delta,-}^{\epsilon\sigma\epsilon\sigma} \\ 0 \end{pmatrix}$$

$$
\mathbf{V}_{\Delta}^{0,0,\mathrm{scal}} = \begin{pmatrix}
\begin{pmatrix} F^{\phi\phi\phi\phi}_{\Delta,-} & 0 & 0 & 0 \\ 0 & 0 & 0 & 0 \\ 0 & 0 & 0 & 0 \\ 0 & 0 & 0 & F^{\phi\phi\phi\phi}_{\Delta+2,-} \end{pmatrix} \\
\begin{pmatrix} -F^{\phi\phi\phi\phi}_{\Delta,+} & 0 & 0 & 0 \\ 0 & 0 & 0 & 0 \\ 0 & 0 & 0 & 0 \\ 0 & 0 & 0 & -F^{\phi\phi\phi\phi}_{\Delta+2,+} \end{pmatrix} \\
\begin{pmatrix} F^{\phi\phi\phi\phi}_{\Delta,-} & 0 & 0 & 0 \\ 0 & 0 & 0 & 0 \\ 0 & 0 & 0 & 0 \\ 0 & 0 & 0 & F^{\phi\phi\phi\phi}_{\Delta+2,-} \end{pmatrix} \\
\begin{pmatrix} -F^{\phi\phi\phi\phi}_{\Delta,+} & 0 & 0 & 0 \\ 0 & 0 & 0 & 0 \\ 0 & 0 & 0 & 0 \\ 0 & 0 & 0 & -F^{\phi\phi\phi\phi}_{\Delta+2,+} \end{pmatrix} \\
\begin{pmatrix} 0 & \frac{1}{2}F^{\sigma\sigma\phi\phi}_{\Delta,-} & 0 & 0 \\ \frac{1}{2}F^{\sigma\sigma\phi\phi}_{\Delta,-} & 0 & 0 & \frac{1}{2}\alpha^{(2)}_{\mathcal{O}\sigma\sigma}F^{\sigma\sigma\phi\phi}_{\Delta+2,-} \\ 0 & 0 & 0 & 0 \\ 0 & \frac{1}{2}\alpha^{(2)}_{\mathcal{O}\sigma\sigma}F^{\sigma\sigma\phi\phi}_{\Delta+2,-} & 0 & 0 \end{pmatrix} \\
\begin{pmatrix} 0 & -\frac{1}{2}F^{\sigma\sigma\phi\phi}_{\Delta,+} & 0 & 0 \\ -\frac{1}{2}F^{\sigma\sigma\phi\phi}_{\Delta,+} & 0 & 0 & -\frac{1}{2}\alpha^{(2)}_{\mathcal{O}\sigma\sigma}F^{\sigma\sigma\phi\phi}_{\Delta+2,+} \\ 0 & 0 & 0 & 0 \\ 0 & -\frac{1}{2}\alpha^{(2)}_{\mathcal{O}\sigma\sigma}F^{\sigma\sigma\phi\phi}_{\Delta+2,+} & 0 & 0 \end{pmatrix} \\
0 \\
0 \\
\begin{pmatrix} 0 & 0 & \frac{1}{2}F^{\varepsilon\varepsilon\phi\phi}_{\Delta,-} & 0 \\ 0 & 0 & 0 & 0 \\ \frac{1}{2}F^{\varepsilon\varepsilon\phi\phi}_{\Delta,-} & 0 & 0 & \frac{1}{2}\alpha^{(2)}_{\mathcal{O}\varepsilon\varepsilon}F^{\varepsilon\varepsilon\phi\phi}_{\Delta+2,-} \\ 0 & 0 & \frac{1}{2}\alpha^{(2)}_{\mathcal{O}\varepsilon\varepsilon}F^{\varepsilon\varepsilon\phi\phi}_{\Delta+2,-} & 0 \end{pmatrix} \\
\begin{pmatrix} 0 & 0 & -\frac{1}{2}F^{\varepsilon\varepsilon\phi\phi}_{\Delta,+} & 0 \\ 0 & 0 & 0 & 0 \\ -\frac{1}{2}F^{\varepsilon\varepsilon\phi\phi}_{\Delta,+} & 0 & 0 & -\frac{1}{2}\alpha^{(2)}_{\mathcal{O}\varepsilon\varepsilon}F^{\varepsilon\varepsilon\phi\phi}_{\Delta+2,+} \\ 0 & 0 & -\frac{1}{2}\alpha^{(2)}_{\mathcal{O}\varepsilon\varepsilon}F^{\varepsilon\varepsilon\phi\phi}_{\Delta+2,+} & 0 \end{pmatrix} \\
\begin{pmatrix} 0 & 0 & 0 & 0 \\ 0 & F^{\sigma\sigma\sigma\sigma}_{\Delta,-} + (\alpha^{(2)}_{\mathcal{O}\sigma\sigma})^2 F^{\sigma\sigma\sigma\sigma}_{\Delta+2,-} & 0 & 0 \\ 0 & 0 & 0 & 0 \\ 0 & 0 & 0 & 0 \end{pmatrix} \\
\begin{pmatrix} 0 & 0 & 0 & 0 \\ 0 & 0 & \frac{1}{2}F^{\sigma\sigma\varepsilon\varepsilon}_{\Delta,-} + \frac{1}{2}\alpha^{(2)}_{\mathcal{O}\varepsilon\varepsilon}\alpha^{(2)}_{\mathcal{O}\sigma\sigma}F^{\sigma\sigma\varepsilon\varepsilon}_{\Delta+2,-} & 0 \\ 0 & \frac{1}{2}F^{\sigma\sigma\varepsilon\varepsilon}_{\Delta,-} + \frac{1}{2}\alpha^{(2)}_{\mathcal{O}\varepsilon\varepsilon}\alpha^{(2)}_{\mathcal{O}\sigma\sigma}F^{\sigma\sigma\varepsilon\varepsilon}_{\Delta+2,-} & 0 & 0 \\ 0 & 0 & 0 & 0 \end{pmatrix} \\
\begin{pmatrix} 0 & 0 & 0 & 0 \\ 0 & 0 & \frac{1}{2}F^{\sigma\sigma\varepsilon\varepsilon}_{\Delta,+} + \frac{1}{2}\alpha^{(2)}_{\mathcal{O}\varepsilon\varepsilon}\alpha^{(2)}_{\mathcal{O}\sigma\sigma}F^{\sigma\sigma\varepsilon\varepsilon}_{\Delta+2,+} & 0 \\ 0 & \frac{1}{2}F^{\sigma\sigma\varepsilon\varepsilon}_{\Delta,+} + \frac{1}{2}\alpha^{(2)}_{\mathcal{O}\varepsilon\varepsilon}\alpha^{(2)}_{\mathcal{O}\sigma\sigma}F^{\sigma\sigma\varepsilon\varepsilon}_{\Delta+2,+} & 0 & 0 \\ 0 & 0 & 0 & 0 \end{pmatrix} \\
0 \\
\begin{pmatrix} 0 & 0 & 0 & 0 \\ 0 & 0 & 0 & 0 \\ 0 & 0 & F^{\varepsilon\varepsilon\varepsilon\varepsilon}_{\Delta,-} + (\alpha^{(2)}_{\mathcal{O}\varepsilon\varepsilon})^2 F^{\varepsilon\varepsilon\varepsilon\varepsilon}_{\Delta+2,-} & 0 \\ 0 & 0 & 0 & 0 \end{pmatrix} \\
0
\end{pmatrix}
$$

$$
\mathbf{V}_{\Delta}^{1,0,\mathrm{scal}}(x) = \begin{pmatrix}
\begin{pmatrix} F^{\phi\phi\phi\phi}_{\Delta,-} & 0 & 0 \\ 0 & 0 & 0 \\ 0 & 0 & F^{\phi\phi\phi\phi}_{\Delta+2,-} \end{pmatrix} \\
\begin{pmatrix} -F^{\phi\phi\phi\phi}_{\Delta,+} & 0 & 0 \\ 0 & 0 & 0 \\ 0 & 0 & -F^{\phi\phi\phi\phi}_{\Delta+2,+} \end{pmatrix} \\
\begin{pmatrix} -F^{\phi\phi\phi\phi}_{\Delta,-} & 0 & 0 \\ 0 & 0 & 0 \\ 0 & 0 & -F^{\phi\phi\phi\phi}_{\Delta+2,-} \end{pmatrix} \\
\begin{pmatrix} F^{\phi\phi\phi\phi}_{\Delta,+} & 0 & 0 \\ 0 & 0 & 0 \\ 0 & 0 & F^{\phi\phi\phi\phi}_{\Delta+2,+} \end{pmatrix} \\
0 \\
0 \\
\begin{pmatrix} 0 & \frac{1}{2}F^{\sigma\varepsilon\phi\phi}_{\Delta,-} & 0 \\ \frac{1}{2}F^{\sigma\varepsilon\phi\phi}_{\Delta,-} & 0 & \frac{1}{2}\alpha^{(2)}_{\mathcal{O}\sigma\varepsilon}F^{\sigma\varepsilon\phi\phi}_{\Delta+2,-} \\ 0 & \frac{1}{2}\alpha^{(2)}_{\mathcal{O}\sigma\varepsilon}F^{\sigma\varepsilon\phi\phi}_{\Delta+2,-} & 0 \end{pmatrix} \\
\begin{pmatrix} 0 & -\frac{1}{2}F^{\sigma\varepsilon\phi\phi}_{\Delta,+} & 0 \\ -\frac{1}{2}F^{\sigma\varepsilon\phi\phi}_{\Delta,+} & 0 & -\frac{1}{2}\alpha^{(2)}_{\mathcal{O}\sigma\varepsilon}F^{\sigma\varepsilon\phi\phi}_{\Delta+2,+} \\ 0 & -\frac{1}{2}\alpha^{(2)}_{\mathcal{O}\sigma\varepsilon}F^{\sigma\varepsilon\phi\phi}_{\Delta+2,+} & 0 \end{pmatrix} \\
0 \\
0 \\
0 \\
\begin{pmatrix} 0 & 0 & 0 \\ 0 & F^{\varepsilon\sigma\sigma\varepsilon}_{\Delta,-} + (\alpha^{(2)}_{\mathcal{O}\sigma\varepsilon})^2 F^{\varepsilon\sigma\sigma\varepsilon}_{\Delta+2,-} & 0 \\ 0 & 0 & 0 \end{pmatrix} \\
\begin{pmatrix} 0 & 0 & 0 \\ 0 & -F^{\varepsilon\sigma\sigma\varepsilon}_{\Delta,+} - (\alpha^{(2)}_{\mathcal{O}\sigma\varepsilon})^2 F^{\varepsilon\sigma\sigma\varepsilon}_{\Delta+2,+} & 0 \\ 0 & 0 & 0 \end{pmatrix} \\
\begin{pmatrix} 0 & 0 & 0 \\ 0 & F^{\sigma\varepsilon\sigma\varepsilon}_{\Delta,-} + (\alpha^{(2)}_{\mathcal{O}\sigma\varepsilon})^2 F^{\sigma\varepsilon\sigma\varepsilon}_{\Delta+2,-} & 0 \\ 0 & 0 & 0 \end{pmatrix} \\
0 \\
0
\end{pmatrix}
$$

$$\mathbf{V}_{\Delta}^{+-}(x) = \begin{pmatrix} F_{\Delta,-}^{\phi\phi\phi\phi} \\ F_{\Delta,+}^{\phi\phi\phi\phi} \\ 0 \\ 0 \\ 0 \\ 0 \\ 0 \\ 0 \\ 0 \\ 0 \\ 0 \\ 0 \\ 0 \\ 0 \\ 0 \\ 0 \end{pmatrix} \quad \mathbf{V}_{\Delta}^{+-}(x) = \begin{pmatrix} 0 \\ 0 \\ F_{\Delta,-}^{\phi\phi\phi\phi} \\ F_{\Delta,+}^{\phi\phi\phi\phi} \\ 0 \\ 0 \\ 0 \\ 0 \\ 0 \\ 0 \\ 0 \\ 0 \\ 0 \\ 0 \\ 0 \\ 0 \end{pmatrix} \quad \mathbf{V}_{\Delta}^{0+}(x) = \begin{pmatrix} 0 \\ 0 \\ 0 \\ 0 \\ \begin{pmatrix} F_{\Delta,-}^{\sigma\phi\phi\sigma} & 0 \\ 0 & 0 \end{pmatrix} \\ \begin{pmatrix} F_{\Delta,+}^{\sigma\phi\phi\sigma} & 0 \\ 0 & 0 \end{pmatrix} \\ \begin{pmatrix} 0 & \frac{1}{2}F_{\Delta,-}^{\epsilon\phi\phi\sigma} \\ \frac{1}{2}F_{\Delta,-}^{\epsilon\phi\phi\sigma} & 0 \end{pmatrix} \\ \begin{pmatrix} 0 & \frac{1}{2}F_{\Delta,+}^{\epsilon\phi\phi\sigma} \\ \frac{1}{2}F_{\Delta,+}^{\epsilon\phi\phi\sigma} & 0 \end{pmatrix} \\ \begin{pmatrix} 0 & 0 \\ 0 & F_{\Delta,-}^{\epsilon\phi\phi\epsilon} \end{pmatrix} \\ \begin{pmatrix} 0 & 0 \\ 0 & F_{\Delta,+}^{\epsilon\phi\phi\epsilon} \end{pmatrix} \\ 0 \\ 0 \\ 0 \\ 0 \\ 0 \end{pmatrix}$$

$$
\mathbf{V}_{\sigma\epsilon}(x) = \begin{pmatrix}
\begin{pmatrix} F^{\phi\phi\phi\phi}_{\Delta_\sigma,-} & 0 & 0 & 0 & 0 \\ 0 & F^{\phi\phi\phi\phi}_{\Delta_\varepsilon,-} & 0 & 0 & 0 \\ 0 & 0 & 0 & 0 & 0 \\ 0 & 0 & 0 & F^{\phi\phi\phi\phi}_{\Delta_\sigma+2,-} & 0 \\ 0 & 0 & 0 & 0 & F^{\phi\phi\phi\phi}_{\Delta_\varepsilon+2,-} \end{pmatrix} & & & & \\
& \begin{pmatrix} -F^{\phi\phi\phi\phi}_{\Delta_\sigma,+} & 0 & 0 & 0 & 0 \\ 0 & -F^{\phi\phi\phi\phi}_{\Delta_\varepsilon,+} & 0 & 0 & 0 \\ 0 & 0 & 0 & 0 & 0 \\ 0 & 0 & 0 & -F^{\phi\phi\phi\phi}_{\Delta_\sigma+2,+} & 0 \\ 0 & 0 & 0 & 0 & -F^{\phi\phi\phi\phi}_{\Delta_\varepsilon+2,+} \end{pmatrix} & & & \\
& & \begin{pmatrix} -F^{\phi\phi\phi\phi}_{\Delta_\sigma,-} & 0 & 0 & 0 & 0 \\ 0 & F^{\phi\phi\phi\phi}_{\Delta_\varepsilon,-} & 0 & 0 & 0 \\ 0 & 0 & 0 & 0 & 0 \\ 0 & 0 & 0 & -F^{\phi\phi\phi\phi}_{\Delta_\sigma+2,-} & 0 \\ 0 & 0 & 0 & 0 & F^{\phi\phi\phi\phi}_{\Delta_\varepsilon+2,-} \end{pmatrix} & & \\
& & & \begin{pmatrix} F^{\phi\phi\phi\phi}_{\Delta_\sigma,+} & 0 & 0 & 0 & 0 \\ 0 & -F^{\phi\phi\phi\phi}_{\Delta_\varepsilon,+} & 0 & 0 & 0 \\ 0 & 0 & 0 & 0 & 0 \\ 0 & 0 & 0 & F^{\phi\phi\phi\phi}_{\Delta_\sigma+2,+} & 0 \\ 0 & 0 & 0 & 0 & -F^{\phi\phi\phi\phi}_{\Delta_\varepsilon+2,+} \end{pmatrix} & \\
\begin{pmatrix} F^{\sigma\phi\phi\sigma}_{\Delta_0^{0+},-} & 0 & 0 & 0 & 0 \\ 0 & 0 & \frac{1}{2}F^{\sigma\sigma\phi\phi}_{\Delta_\varepsilon,-} & 0 & 0 \\ 0 & \frac{1}{2}F^{\sigma\sigma\phi\phi}_{\Delta_\varepsilon,-} & 0 & 0 & \frac{1}{2}\alpha^{(2)}_{\sigma\varepsilon\sigma}F^{\sigma\sigma\phi\phi}_{\Delta_\varepsilon+2,-} \\ 0 & 0 & 0 & 0 & 0 \\ 0 & 0 & \frac{1}{2}\alpha^{(2)}_{\sigma\varepsilon\sigma}F^{\sigma\sigma\phi\phi}_{\Delta_\varepsilon+2,-} & 0 & 0 \end{pmatrix} & & & & \\
& \begin{pmatrix} F^{\sigma\phi\phi\sigma}_{\Delta_0^{0+},+} & 0 & 0 & 0 & 0 \\ 0 & 0 & -\frac{1}{2}F^{\sigma\sigma\phi\phi}_{\Delta_\varepsilon,+} & 0 & 0 \\ 0 & -\frac{1}{2}F^{\sigma\sigma\phi\phi}_{\Delta_\varepsilon,+} & 0 & 0 & -\frac{1}{2}\alpha^{(2)}_{\sigma\varepsilon\sigma}F^{\sigma\sigma\phi\phi}_{\Delta_\varepsilon+2,+} \\ 0 & 0 & 0 & 0 & 0 \\ 0 & 0 & -\frac{1}{2}\alpha^{(2)}_{\sigma\varepsilon\sigma}F^{\sigma\sigma\phi\phi}_{\Delta_\varepsilon+2,+} & 0 & 0 \end{pmatrix} & & & \\
& & \begin{pmatrix} 0 & \frac{1}{2}F^{\varepsilon\phi\phi\sigma}_{\Delta_0^{0+},-} & \frac{1}{2}F^{\sigma\varepsilon\phi\phi}_{\Delta_\sigma,-} & 0 & 0 \\ \frac{1}{2}F^{\varepsilon\phi\phi\sigma}_{\Delta_0^{0+},-} & 0 & 0 & 0 & 0 \\ \frac{1}{2}F^{\sigma\varepsilon\phi\phi}_{\Delta_\sigma,-} & 0 & 0 & \frac{1}{2}\alpha^{(2)}_{\sigma\varepsilon\sigma}F^{\sigma\varepsilon\phi\phi}_{\Delta_\sigma+2,-} & 0 \\ 0 & 0 & \frac{1}{2}\alpha^{(2)}_{\sigma\varepsilon\sigma}F^{\sigma\varepsilon\phi\phi}_{\Delta_\sigma+2,-} & 0 & 0 \\ 0 & 0 & 0 & 0 & 0 \end{pmatrix} & & \\
& & & \begin{pmatrix} 0 & \frac{1}{2}F^{\varepsilon\phi\phi\sigma}_{\Delta_0^{0+},+} & -\frac{1}{2}F^{\sigma\varepsilon\phi\phi}_{\Delta_\sigma,+} & 0 & 0 \\ \frac{1}{2}F^{\varepsilon\phi\phi\sigma}_{\Delta_0^{0+},+} & 0 & 0 & 0 & 0 \\ -\frac{1}{2}F^{\sigma\varepsilon\phi\phi}_{\Delta_\sigma,+} & 0 & 0 & -\frac{1}{2}\alpha^{(2)}_{\sigma\varepsilon\sigma}F^{\sigma\varepsilon\phi\phi}_{\Delta_\sigma+2,+} & 0 \\ 0 & 0 & -\frac{1}{2}\alpha^{(2)}_{\sigma\varepsilon\sigma}F^{\sigma\varepsilon\phi\phi}_{\Delta_\sigma+2,+} & 0 & 0 \\ 0 & 0 & 0 & 0 & 0 \end{pmatrix} & \\
\begin{pmatrix} 0 & 0 & 0 & 0 & 0 \\ 0 & F^{\varepsilon,\phi,\phi,\varepsilon}_{\Delta_0^{0+},-} & \frac{1}{2}r_{\sigma\varepsilon}F^{\varepsilon,\varepsilon,\phi,\phi}_{\Delta_\varepsilon,-} & 0 & 0 \\ 0 & \frac{1}{2}r_{\sigma\varepsilon}F^{\varepsilon,\varepsilon,\phi,\phi}_{\Delta_\varepsilon,-} & 0 & 0 & \frac{1}{2}r_{\sigma\varepsilon}\alpha^{(2)}_{\varepsilon\varepsilon\varepsilon}F^{\varepsilon,\varepsilon,\phi,\phi}_{\Delta_\varepsilon+2,-} \\ 0 & 0 & 0 & 0 & 0 \\ 0 & 0 & \frac{1}{2}r_{\sigma\varepsilon}\alpha^{(2)}_{\varepsilon\varepsilon\varepsilon}F^{\varepsilon,\varepsilon,\phi,\phi}_{\Delta_\varepsilon+2,-} & 0 & 0 \end{pmatrix} & & & & \\
& \begin{pmatrix} 0 & 0 & 0 & 0 & 0 \\ 0 & F^{\varepsilon,\phi,\phi,\varepsilon}_{\Delta_0^{0+},+} & -\frac{1}{2}r_{\sigma\varepsilon}F^{\varepsilon,\varepsilon,\phi,\phi}_{\Delta_\varepsilon,+} & 0 & 0 \\ 0 & -\frac{1}{2}r_{\sigma\varepsilon}F^{\varepsilon,\varepsilon,\phi,\phi}_{\Delta_\varepsilon,+} & 0 & 0 & -\frac{1}{2}r_{\sigma\varepsilon}\alpha^{(2)}_{\varepsilon\varepsilon\varepsilon}F^{\varepsilon,\varepsilon,\phi,\phi}_{\Delta_\varepsilon+2,+} \\ 0 & 0 & 0 & 0 & 0 \\ 0 & 0 & -\frac{1}{2}r_{\sigma\varepsilon}\alpha^{(2)}_{\varepsilon\varepsilon\varepsilon}F^{\varepsilon,\varepsilon,\phi,\phi}_{\Delta_\varepsilon+2,+} & 0 & 0 \end{pmatrix} & & \\
& & \begin{pmatrix} 0 & 0 & 0 & 0 & 0 \\ 0 & 0 & 0 & 0 & 0 \\ 0 & 0 & F^{\sigma,\sigma,\sigma,\sigma}_{\Delta_\varepsilon,-} + (\alpha^{(2)}_{\sigma\varepsilon\sigma})^2 F^{\sigma,\sigma,\sigma,\sigma}_{\Delta_\varepsilon+2,-} & 0 & 0 \\ 0 & 0 & 0 & 0 & 0 \\ 0 & 0 & 0 & 0 & 0 \end{pmatrix} &
\end{pmatrix}
$$

$$\bigoplus \left(\begin{array}{c}
\begin{pmatrix} 0 & 0 & 0 & 0 & 0 \\ 0 & 0 & 0 & 0 & 0 \\ 0 & 0 & F^{\varepsilon,\sigma,\sigma,\varepsilon}_{\Delta_\sigma,-} + 2r_{\sigma\varepsilon}\left(\frac{1}{2}F^{\sigma,\sigma,\varepsilon,\varepsilon}_{\Delta_\varepsilon,-} + \frac{1}{2}\alpha^{(2)}_{\varepsilon\varepsilon\varepsilon}\alpha^{(2)}_{\sigma\varepsilon\sigma}F^{\sigma,\sigma,\varepsilon,\varepsilon}_{\Delta_\varepsilon+2,-}\right) + (\alpha^{(2)}_{\sigma\varepsilon\sigma})^2 F^{\varepsilon,\sigma,\sigma,\varepsilon}_{\Delta_\sigma+2,-} & 0 & 0 \\ 0 & 0 & 0 & 0 & 0 \\ 0 & 0 & 0 & 0 & 0 \end{pmatrix} \\
\begin{pmatrix} 0 & 0 & 0 & 0 & 0 \\ 0 & 0 & 0 & 0 & 0 \\ 0 & 0 & -F^{\varepsilon,\sigma,\sigma,\varepsilon}_{\Delta_\sigma,+} + 2r_{\sigma\varepsilon}\left(\frac{1}{2}F^{\sigma,\sigma,\varepsilon,\varepsilon}_{\Delta_\varepsilon,+} + \frac{1}{2}\alpha^{(2)}_{\varepsilon\varepsilon\varepsilon}\alpha^{(2)}_{\sigma\varepsilon\sigma}F^{\sigma,\sigma,\varepsilon,\varepsilon}_{\Delta_\varepsilon+2,+}\right) - (\alpha^{(2)}_{\sigma\varepsilon\sigma})^2 F^{\varepsilon,\sigma,\sigma,\varepsilon}_{\Delta_\sigma+2,+} & 0 & 0 \\ 0 & 0 & 0 & 0 & 0 \\ 0 & 0 & 0 & 0 & 0 \end{pmatrix} \\
\begin{pmatrix} 0 & 0 & 0 & 0 & 0 \\ 0 & 0 & 0 & 0 & 0 \\ 0 & 0 & F^{\sigma,\varepsilon,\sigma,\varepsilon}_{\Delta_\sigma,-} + (\alpha^{(2)}_{\sigma\varepsilon\sigma})^2 F^{\sigma,\varepsilon,\sigma,\varepsilon}_{\Delta_\sigma+2,-} & 0 & 0 \\ 0 & 0 & 0 & 0 & 0 \\ 0 & 0 & 0 & 0 & 0 \end{pmatrix} \\
\begin{pmatrix} 0 & 0 & 0 & 0 & 0 \\ 0 & 0 & 0 & 0 & 0 \\ 0 & 0 & r^2_{\sigma\varepsilon}\left(F^{\varepsilon,\varepsilon,\varepsilon,\varepsilon}_{\Delta_\varepsilon,-} + (\alpha^{(2)}_{\varepsilon\varepsilon\varepsilon})^2 F^{\varepsilon,\varepsilon,\varepsilon,\varepsilon}_{\Delta_\varepsilon+2,-}\right) & 0 & 0 \\ 0 & 0 & 0 & 0 & 0 \\ 0 & 0 & 0 & 0 & 0 \end{pmatrix} \\
\begin{pmatrix} 0 & 0 & 0 & 0 & 0 \\ 0 & 0 & 0 & 0 & 0 \\ 0 & 0 & 1 & 0 & 0 \\ 0 & 0 & 0 & 0 & 0 \\ 0 & 0 & 0 & 0 & 0 \end{pmatrix}
\end{array} \right)$$

Appendix C

CUTTING-CURVE ALGORITHM

Here we describe an algorithm to solve an optimization problem frequently encountered in this work. Throughout this section, we will assume all scaling dimensions of external operators are held fixed. Let $\mathbf{V}(x;\gamma)$ be a crossing vector that depends on some *internal* parameter γ that may take values within a finite interval $\gamma \in [\gamma_l, \gamma_h]$ (i.e. it does not represent the scaling dimension of an external operator—if it did, we expect the algorithm described in this section to be substantially less efficient than alternative approaches such as the navigator method.). We will either take γ to be the scaling dimension of an internal operator or a ratio of two OPE coefficients. Next, let $\mathbf{V}_{\Delta,i}(x)$ represent the remaining set of crossing vectors we will impose positivity on within some ranges S_i of the internal scaling dimension $\Delta \in S_i$, where S_i may be disconnected. Finally let $\mathcal{N}(x)$ be a normalization crossing vector.

We wish to numerically solve the problems

$$\begin{aligned}
&\text{(Maximize/Minimize) } \gamma \text{ subject to } \exists \alpha \text{ satisfying} \\
&\qquad\qquad \alpha[\mathcal{N}(x)] = 1 \\
&\qquad\qquad \alpha[\mathbf{V}(x;\gamma)] \succeq 0 \\
&\qquad\qquad \alpha[\mathbf{V}_{\Delta,i}(x)] \succeq 0 \qquad \Delta \in S_i
\end{aligned}$$

where α is defined as in the main text in (3.64). We will assume, for this implementation, that the set of allowed values of γ is connected—we have found no evidence to the contrary in the examples studied in this work. For the purpose of defining our algorithm, this means that when the scaling dimensions of all external operators are fixed, the allowed range of γ forms an interval. Note that we may not simply optimize γ using `SDPB` directly, since γ is not explicitly bounded by the value of a linear functional acting on some crossing vector, as

is the case when, say, optimizing the magnitude of OPE coefficients.

We require an algorithm that can efficiently do the following:

1. If there is actually no allowed $\gamma \in [\gamma_l, \gamma_h]$, rigorously rule out the entire range.

2. If there is an allowed $\gamma \in [\gamma_l, \gamma_h]$, find a single allowed point.

When there is at least one allowed point, the hardest part of the calculation is finding such an allowed point. Once an allowed point γ_* is found, since we assume the entire range of allowed values to be an interval we know $\gamma_l \leq \gamma_{\min} \leq \gamma_* \leq \gamma_{\max} \leq \gamma_h$, where $\gamma_{\min}, \gamma_{\max}$ represent the optimal lower/upper bounds. From there we may efficiently approximate $\gamma_{\min}, \gamma_{\max}$, to within some desired tolerance, by performing a standard binary search that tests for feasibility of different choices of γ, where we simply seek any α such that

$$\begin{aligned} \alpha[\mathcal{N}(x)] &= 1 \\ \alpha[\mathbf{V}(x;\gamma)] &\succeq 0 \\ \alpha[\mathbf{V}_{\Delta,i}(x)] &\succeq 0 \qquad \Delta \in S_i. \end{aligned}$$

If such an α is found, the semidefinite program is feasible (i.e. all of the constraints can be satisfied), which proves γ in the above is *disallowed* via the standard numerical bootstrap logic. Depending on whether we seek to approximate the lower or upper bounds, we then raise or lower γ and repeat.

To find the allowed point, we use the following strategy, which is essentially equivalent to the $m = 2$ case of the "cutting-surface" algorithm described in [40], although there is a very minor technical difference in our problem which is that $\alpha[\mathbf{V}(x;\gamma)]$ will not be a quadratic form in γ[1]. Define $\mathcal{A}_0 = [\gamma_l, \gamma_h]$, the set of initially allowed γ, and let $\gamma_0 = (\gamma_h - \gamma_l)/2$ be the initial value of γ to check. The trick noticed in [40] is that any time some linear functional α rules out a point γ, it will also rule out points in some neighborhood of γ. We define this

[1]When we are computing OPE ratios with this method we will let the OPE ratio equal e.g. $\cot\gamma, \tan\gamma$, which compactifies the possible values that must be scanned over. When γ is an internal scaling dimension $\alpha[\mathbf{V}(x;\gamma)]$ will be a higher-degree polynomial.

neighborhood by computing the nearest roots below and above γ of $\det \alpha[\mathbf{V}(x;\gamma)]$, defining some interval $\mathcal{I}_0$ that is totally ruled out since the eigenvalues of $\alpha[\mathbf{V}(x;\gamma)]$ are necessarily positive at points continuously connected to γ_0 without encountering a root of $\det \alpha[\mathbf{V}(x;\gamma)]$, which is a smooth function of γ (this is actually a weaker condition than could possibly be imposed, but we find it sufficient.). The set of allowed points then becomes $\mathcal{A}_1 = \mathcal{A}_0 \backslash \mathcal{I}_0$. To proceed in the algorithm, each $\mathcal{A}_i$ representing the allowed region after checking γ_i will be expressible as a union of intervals $\mathcal{A}_i = \bigcup_n J_n^i$. There are different ways to choose γ_{i+1}, but we found in practice that choosing γ_{i+1} to be the midpoint of the widest $\mathcal{J}_n^i$ the most efficient for finding an allowed point. Once we find an allowed γ, we enter the binary search phase described previously.

Sometimes the aforementioned choice of γ_{i+1} struggles to fully exclude all values of γ when there should be no allowed value, but we consider a point ruled out if it does not find an allowed value within 75 iterations. This seems to happen due to the fact that we use "hot-starting," i.e. for each call to `SDPB` we recycle α from the previous run since it will necessarily be positive when evaluated on all the fixed constraints $\alpha[\mathbf{V}_{\Delta,i}(x)] \succeq 0$. As the algorithm proceeds, $\mathcal{I}_i$ typically shrinks in width[2], whereas $\mathcal{I}_0$ usually is sufficiently wide such that $\mathcal{A}_1$ is still connected. We experimented with letting `SDPB` run longer for each check of γ by saving a checkpoint at termination only after every few runs, but it is unclear the ultimate effect this choice has on the overall efficiency. There are also other choices of γ_{i+1} that seem to perform somewhat better at ruling out the full range of γ when applicable, but we find choosing a method optimized for disallowed points less desirable since another way to judge when there should be no allowed γ is the point, as a function of the external dimension, at which the upper and lower bounds on γ agree, although this is arguably not fully rigorous. However, in our problem the external dimension is Δ_0^{0+}, and all evidence suggests that there are two connected components of the allowed values of Δ_0^{0+} which we confirmed at small Λ, so we find the approach described here satisfactory.

[2]Strangely, this seems to be the opposite behavior to what is described in [40], where the functional near the boundary of the allowed region apparently rules out roughly half of the search space at each step.

BIBLIOGRAPHY

[1] Ian Affleck and Elliott H. Lieb. A proof of part of haldane's conjecture on spin chains. *Letters in Mathematical Physics*, 12(1):57–69, 1986.

[2] Ian Affleck and Andreas W. W. Ludwig. Universal noninteger 'ground state degeneracy' in critical quantum systems. *Phys. Rev. Lett.*, 67:161–164, 1991.

[3] Nima Afkhami-Jeddi, Henry Cohn, Thomas Hartman, and Amirhossein Tajdini. Free partition functions and an averaged holographic duality. *Journal of High Energy Physics*, 2021(1), jan 2021.

[4] Yahya Alavirad and Maissam Barkeshli. Anomalies and unusual stability of multicomponent luttinger liquids in $\mathbb{Z}_n \times \mathbb{Z}_n$ spin chains. *Phys. Rev. B*, 104:045151, Jul 2021.

[5] Soner Albayrak, Rajeev S. Erramilli, Zhijin Li, David Poland, and Yuan Xin. Bootstrapping N_f=4 conformal QED_3. *Phys. Rev. D*, 105(8):085008, 2022.

[6] Andrea Allais. Magnetic defect line in a critical ising bath, 2014.

[7] Andrea Allais and Subir Sachdev. Spectral function of a localized fermion coupled to the wilson-fisher conformal field theory. *Phys. Rev. B*, 90:035131, Jul 2014.

[8] P. W. Anderson. More Is Different. *Science*, 177(4047):393–396, 1972.

[9] N. Andrei. Diagonalization of the Kondo Hamiltonian. *Phys. Rev. Lett.*, 45:379, 1980.

[10] Nikolaos Angelinos, Debarghya Chakraborty, and Anatoly Dymarsky. Optimal narain cfts from codes, 2022.

[11] Tarek Anous, Raghu Mahajan, and Edgar Shaghoulian. Parity and the modular bootstrap. *SciPost Physics*, 5(3), sep 2018.

[12] Thomas Bartsch, Mathew Bullimore, and Andrea Grigoletto. Higher representations for extended operators, 4 2023.

[13] A.A. Belavin, A.M. Polyakov, and A.B. Zamolodchikov. Infinite conformal symmetry in two-dimensional quantum field theory. *Nuclear Physics B*, 241(2):333–380, 1984.

[14] Alexandre Belin, Jan de Boer, and Jorrit Kruthoff. Comments on a state-operator correspondence for the torus. *SciPost Physics*, 5(6), dec 2018.

[15] Francesco Benini, Clay Córdova, and Po-Shen Hsin. On 2-group global symmetries and their anomalies. *Journal of High Energy Physics*, 2019(3), mar 2019.

[16] Nathan Benjamin, Scott Collier, A. Liam Fitzpatrick, Alexander Maloney, and Eric Perlmutter. Harmonic analysis of 2d CFT partition functions. *Journal of High Energy Physics*, 2021(9), sep 2021.

[17] Nathan Benjamin and Ying-Hsuan Lin. Lessons from the ramond sector. *SciPost Physics Proceedings*, 9(5), 11 2020.

[18] Lakshya Bhardwaj, Lea Bottini, Sakura Schafer-Nameki, and Apoorv Tiwari. Non-invertible higher-categorical symmetries, 2022.

[19] Lakshya Bhardwaj and Sakura Schafer-Nameki. Generalized charges, part I: Invertible symmetries and higher representations. *SciPost Phys.*, 16(4):093, 2024.

[20] Lakshya Bhardwaj and Yuji Tachikawa. On finite symmetries and their gauging in two dimensions. *Journal of High Energy Physics*, 2018(3):189, 2018.

[21] Marco Billò, Vasco Gonçalves, Edoardo Lauria, and Marco Meineri. Defects in conformal field theory. *Journal of High Energy Physics*, 2016(4):91, apr 2016.

[22] M. Billó, M. Caselle, D. Gaiotto, F. Gliozzi, M. Meineri, and R. Pellegrini. Line defects in the 3d ising model, 2013.

[23] Jacob C. Bridgeman and Dominic J. Williamson. Anomalies and entanglement renormalization. *Phys. Rev. B*, 96(12):125104, 2017.

[24] Nick Bultinck. Uv perspective on mixed anomalies at critical points between bosonic symmetry-protected phases. *Phys. Rev. B*, 100:165132, Oct 2019.

[25] John Cardy. *Scaling and Renormalization in Statistical Physics*. Cambridge Lecture Notes in Physics. Cambridge University Press, 1996.

[26] John L. Cardy. Boundary Conditions, Fusion Rules and the Verlinde Formula. *Nucl. Phys. B*, 324:581–596, 1989.

[27] John L. Cardy and David C. Lewellen. Bulk and boundary operators in conformal field theory. *Phys. Lett. B*, 259:274–278, 1991.

[28] Horacio Casini, Ignacio Salazar Landea, and Gonzalo Torroba. The g-theorem and quantum information theory. *JHEP*, 10:140, 2016.

[29] Chi-Ming Chang and Ying-Hsuan Lin. Lorentzian dynamics and factorization beyond rationality. *Journal of High Energy Physics*, 2021(10), oct 2021.

[30] Chi-Ming Chang, Ying-Hsuan Lin, Shu-Heng Shao, Yifan Wang, and Xi Yin. Topological defect lines and renormalization group flows in two dimensions. *Journal of High Energy Physics*, 2019(1):26, 2019.

[31] Xie Chen, Zheng-Cheng Gu, Zheng-Xin Liu, and Xiao-Gang Wen. Symmetry protected topological orders and the group cohomology of their symmetry group. *Physical Review B*, 87(15), apr 2013.

[32] Xie Chen, Zheng-Cheng Gu, and Xiao-Gang Wen. Local unitary transformation, long-range quantum entanglement, wave function renormalization, and topological order. *Physical Review B*, 82(15), oct 2010.

[33] Xie Chen, Zheng-Cheng Gu, and Xiao-Gang Wen. Classification of gapped symmetric phases in one-dimensional spin systems. *Phys. Rev. B*, 83:035107, Jan 2011.

[34] Xie Chen and Xiao-Gang Wen. Chiral symmetry on the edge of 2D symmetry protected topological phases. *Phys. Rev. B*, 86:235135, 2012.

[35] Meng Cheng. Fermionic lieb-schultz-mattis theorems and weak symmetry-protected phases. *Phys. Rev. B*, 99:075143, Feb 2019.

[36] Meng Cheng and Nathan Seiberg. Lieb-Schultz-Mattis, Luttinger, and 't Hooft – anomaly matching in lattice systems, 11 2022.

[37] Meng Cheng and Dominic J. Williamson. Relative anomaly in $(1 + 1)$d rational conformal field theory. *Phys. Rev. Research*, 2:043044, Oct 2020.

[38] Meng Cheng, Michael Zaletel, Maissam Barkeshli, Ashvin Vishwanath, and Parsa Bonderson. Translational symmetry and microscopic constraints on symmetry-enriched topological phases: A view from the surface. *Physical Review X*, 6(4), dec 2016.

[39] Shai M. Chester. Weizmann lectures on the numerical conformal bootstrap, 2019.

[40] Shai M. Chester, Walter Landry, Junyu Liu, David Poland, David Simmons-Duffin, Ning Su, and Alessandro Vichi. Carving out OPE space and precise $O(2)$ model critical exponents. *JHEP*, 06:142, 2020.

[41] Shai M. Chester and Silviu S. Pufu. Towards bootstrapping qed3. *Journal of High Energy Physics*, 2016(8), August 2016.

[42] Gil Young Cho, Chang-Tse Hsieh, and Shinsei Ryu. Anomaly manifestation of lieb-schultz-mattis theorem and topological phases. *Phys. Rev. B*, 96:195105, Nov 2017.

[43] Yichul Choi, Brandon C. Rayhaun, Yaman Sanghavi, and Shu-Heng Shao. Remarks on boundaries, anomalies, and noninvertible symmetries. *Phys. Rev. D*, 108(12):125005, 2023.

[44] Scott Collier, Ying-Hsuan Lin, and Xi Yin. Modular bootstrap revisited. *Journal of High Energy Physics*, 2018(9):61, 2018.

[45] Scott Collier, Dalimil Mazac, and Yifan Wang. Bootstrapping boundaries and branes. *JHEP*, 02:019, 2023.

[46] Clay Córdova, Thomas T. Dumitrescu, and Kenneth Intriligator. Exploring 2-group global symmetries. *Journal of High Energy Physics*, 2019(2), feb 2019.

[47] Clay Córdova and Kantaro Ohmori. Anomaly obstructions to symmetry preserving gapped phases, 2019.

[48] Clay Córdova and Kantaro Ohmori. Anomaly constraints on gapped phases with discrete chiral symmetry. *Phys. Rev. D*, 102:025011, Jul 2020.

[49] Gabriel Cuomo, Zohar Komargodski, and Márk Mezei. Localized magnetic field in the o(n) model. *Journal of High Energy Physics*, 2022(2), feb 2022.

[50] Gabriel Cuomo, Zohar Komargodski, Márk Mezei, and Avia Raviv-Moshe. Spin impurities, wilson lines and semiclassics. *Journal of High Energy Physics*, 2022(6), jun 2022.

[51] Gabriel Cuomo, Zohar Komargodski, and Avia Raviv-Moshe. Renormalization Group Flows on Line Defects. *Phys. Rev. Lett.*, 128(2):021603, 2022.

[52] Philippe Di Francesco, Pierre Mathieu, and David Sénéchal. *Conformal field theory*. Graduate texts in contemporary physics. Springer, New York, NY, 1997.

[53] Robbert Dijkgraaf and Edward Witten. Topological Gauge Theories and Group Cohomology. *Commun. Math. Phys.*, 129:393, 1990.

[54] Nadav Drukker and David J. Gross. An Exact prediction of N=4 SUSYM theory for string theory. *J. Math. Phys.*, 42:2896–2914, 2001.

[55] Anatoly Dymarsky, Filip Kos, Petr Kravchuk, David Poland, and David Simmons-Duffin. The 3d stress-tensor bootstrap. *Journal of High Energy Physics*, 2018(2):164, 2018.

[56] Anatoly Dymarsky, Joao Penedones, Emilio Trevisani, and Alessandro Vichi. Charting the space of 3d cfts with a continuous global symmetry. *Journal of High Energy Physics*, 2019(5):98, 2019.

[57] Anatoly Dymarsky and Alfred Shapere. Quantum stabilizer codes, lattices, and CFTs. *Journal of High Energy Physics*, 2021(3), mar 2021.

[58] Freeman J. Dyson. Existence of a phase transition in a one-dimensional Ising ferromagnet. *Commun. Math. Phys.*, 12:91–107, 1969.

[59] Sheer El-Showk and Miguel F. Paulos. Bootstrapping Conformal Field Theories with the Extremal Functional Method. *Phys. Rev. Lett.*, 111(24):241601, 2013.

[60] Sheer El-Showk, Miguel F. Paulos, David Poland, Slava Rychkov, David Simmons-Duffin, and Alessandro Vichi. Solving the 3d ising model with the conformal bootstrap. *Physical Review D*, 86(2), jul 2012.

[61] Sheer El-Showk, Miguel F. Paulos, David Poland, Slava Rychkov, David Simmons-Duffin, and Alessandro Vichi. Solving the 3d ising model with the conformal bootstrap II. $$c$$ c -minimization and precise critical exponents. *Journal of Statistical Physics*, 157(4-5):869–914, jun 2014.

[62] Dominic V. Else and Chetan Nayak. Classifying symmetry-protected topological phases through the anomalous action of the symmetry on the edge. *Phys. Rev. B*, 90:235137, Dec 2014.

[63] Dominic V. Else and Ryan Thorngren. Topological theory of lieb-schultz-mattis theorems in quantum spin systems. *Phys. Rev. B*, 101:224437, Jun 2020.

[64] J. K. Erickson, G. W. Semenoff, and K. Zarembo. Wilson loops in N=4 supersymmetric Yang-Mills theory. *Nucl. Phys. B*, 582:155–175, 2000.

[65] Pavel Etingof, Shlomo Gelaki, Dmitri Nikshych, and Victor Ostrik. *Tensor Categories*. American Mathematical Society, 2015.

[66] Pavel Etingof, Dmitri Nikshych, and Viktor Ostrik. On fusion categories, 3 2002.

[67] Daniel Friedan and Anatoly Konechny. On the boundary entropy of one-dimensional quantum systems at low temperature. *Phys. Rev. Lett.*, 93:030402, 2004.

[68] Daniel Friedan, Zongan Qiu, and Stephen Shenker. Conformal invariance, unitarity, and critical exponents in two dimensions. *Phys. Rev. Lett.*, 52:1575–1578, Apr 1984.

[69] Jurg Frohlich, Jurgen Fuchs, Ingo Runkel, and Christoph Schweigert. Kramers-Wannier duality from conformal defects. *Phys. Rev. Lett.*, 93:070601, 2004.

[70] Jurg Frohlich, Jurgen Fuchs, Ingo Runkel, and Christoph Schweigert. Duality and defects in rational conformal field theory. *Nucl. Phys. B*, 763:354–430, 2007.

[71] Shunsuke C. Furuya and Masaki Oshikawa. Symmetry Protection of Critical Phases and a Global Anomaly in $1 + 1$ Dimensions. *Phys. Rev. Lett.*, 118(2):021601, 2017.

[72] Davide Gaiotto, Anton Kapustin, Zohar Komargodski, and Nathan Seiberg. Theta, time reversal and temperature. *Journal of High Energy Physics*, 2017(5):91, 2017.

[73] Davide Gaiotto, Anton Kapustin, Nathan Seiberg, and Brian Willett. Generalized global symmetries. *Journal of High Energy Physics*, 2015(2), feb 2015.

[74] Davide Gaiotto, Dalimil Mazac, and Miguel F. Paulos. Bootstrapping the 3d ising twist defect. *Journal of High Energy Physics*, 2014(3), mar 2014.

[75] The GAP Group. *GAP – Groups, Algorithms, and Programming, Version 4.11.1*, 2021.

[76] Aleix Gimenez-Grau, Edoardo Lauria, Pedro Liendo, and Philine van Vliet. Bootstrapping line defects with O(2) global symmetry. *JHEP*, 11:018, 2022.

[77] Aleix Gimenez-Grau and Pedro Liendo. Bootstrapping line defects in

$$\mathcal{N}$$

$= 2$ theories. *Journal of High Energy Physics*, 2020(3), March 2020.

[78] Mocho Go and Yuji Tachikawa. autoboot: a generator of bootstrap equations with global symmetry. *Journal of High Energy Physics*, 2019(6):84, 2019.

[79] Andrea Grigoletto. Anomalies of fermionic cfts via cobordism and bootstrap, 2021.

[80] Andrea Grigoletto and Pavel Putrov. Spin-cobordisms, surgeries and fermionic modular bootstrap, 2021.

[81] F. D. M. Haldane. Nonlinear field theory of large-spin heisenberg antiferromagnets: Semiclassically quantized solitons of the one-dimensional easy-axis néel state. *Phys. Rev. Lett.*, 50:1153–1156, Apr 1983.

[82] M. B. Hastings. Lieb-schultz-mattis in higher dimensions. *Phys. Rev. B*, 69:104431, Mar 2004.

[83] Yin-Chen He, Junchen Rong, and Ning Su. A roadmap for bootstrapping critical gauge theories: decoupling operators of conformal field theories in $d > 2$ dimensions. *SciPost Phys.*, 11:111, 2021.

[84] Yin-Chen He, Junchen Rong, and Ning Su. Conformal bootstrap bounds for the $u(1)$ dirac spin liquid and $n = 7$ stiefel liquid, 2021.

[85] Simeon Hellerman. A universal inequality for cft and quantum gravity. *Journal of High Energy Physics*, 2011(8):130, 2011.

[86] G.'t Hooft. *Naturalness, Chiral Symmetry, and Spontaneous Chiral Symmetry Breaking*, pages 135–157. Springer US, Boston, MA, 1980.

[87] Liangdong Hu, Yin-Chen He, and W. Zhu. Solving conformal defects in 3d conformal field theory using fuzzy sphere regularization, 2023.

[88] Sheng-Jie Huang, Hao Song, Yi-Ping Huang, and Michael Hermele. Building crystalline topological phases from lower-dimensional states. *Phys. Rev. B*, 96:205106, Nov 2017.

[89] Tzu-Chen Huang, Ying-Hsuan Lin, and Sahand Seifnashri. Construction of two-dimensional topological field theories with non-invertible symmetries. *Journal of High Energy Physics*, 2021(12):028, dec 2021.

[90] Alexei Kitaev. Anyons in an exactly solved model and beyond. *Annals Phys.*, 321(1):2–111, 2006.

[91] Alexei Kitaev and Liang Kong. Models for Gapped Boundaries and Domain Walls. *Commun. Math. Phys.*, 313(2):351–373, 2012.

[92] Ryohei Kobayashi, Ken Shiozaki, Yuta Kikuchi, and Shinsei Ryu. Lieb-schultz-mattis type theorem with higher-form symmetry and the quantum dimer models. *Physical Review B*, 99(1), jan 2019.

[93] J. Kondo. Resistance Minimum in Dilute Magnetic Alloys. *Prog. Theor. Phys.*, 32(1):37–49, 1964.

[94] Filip Kos, David Poland, David Simmons-Duffin, and Alessandro Vichi. Precision islands in the Ising and O(N) models. *JHEP*, 08:036, 2016.

[95] David C. Lewellen. Sewing constraints for conformal field theories on surfaces with boundaries. *Nucl. Phys. B*, 372:654–682, 1992.

[96] Elliott H. Lieb, Theodore Schultz, and Daniel Mattis. Two soluble models of an antiferromagnetic chain. *Annals Phys.*, 16:407–466, 1961.

[97] Pedro Liendo, Carlo Meneghelli, and Vladimir Mitev. Bootstrapping the half-bps line defect. *Journal of High Energy Physics*, 2018(10), October 2018.

[98] Ying-Hsuan Lin, David Meltzer, Shu-Heng Shao, and Andreas Stergiou. Bounds on triangle anomalies in (3+1)d. *Physical Review D*, 101(12), jun 2020.

[99] Ying-Hsuan Lin and Shu-Heng Shao. Anomalies and bounds on charged operators. *Phys. Rev. D*, 100:025013, Jul 2019.

[100] Ying-Hsuan Lin and Shu-Heng Shao. $\mathbb{Z}_N$ symmetries, anomalies, and the modular bootstrap. *Phys. Rev. D*, 103:125001, Jun 2021.

[101] Ying-Hsuan Lin and Shu-Heng Shao. Bootstrapping Non-invertible Symmetries. 2 2023.

[102] Aike Liu, David Simmons-Duffin, Ning Su, and Balt C. van Rees. Skydiving to Bootstrap Islands. 7 2023.

[103] Shang Liu, Hassan Shapourian, Ashvin Vishwanath, and Max A. Metlitski. Magnetic impurities at quantum critical points: Large-n expansion and connections to symmetry-protected topological states. *Phys. Rev. B*, 104:104201, Sep 2021.

[104] Yuan-Ming Lu. Lieb-schultz-mattis theorems for symmetry protected topological phases, 2017.

[105] Simão Meneses, João Penedones, Slava Rychkov, J. M. Viana Parente Lopes, and Pierre Yvernay. A structural test for the conformal invariance of the critical 3d Ising model. *JHEP*, 04:115, 2019.

[106] Max Metlitski and Ryan Thorngren. Intrinsic and emergent anomalies at deconfined critical points. *Physical Review B*, 98, 07 2017.

[107] Gregory Moore and Nathan Seiberg. Classical and quantum conformal field theory. *Communications in Mathematical Physics*, 123(2):177–254, 1989.

[108] Yu Nakayama. Scale invariance vs conformal invariance, 2013.

[109] Yoshiko Ogata, Yuji Tachikawa, and Hal Tasaki. General lieb–schultz–mattis type theorems for quantum spin chains. *Communications in Mathematical Physics*, 385(1):79–99, jun 2021.

[110] Yoshiko Ogata and Hal Tasaki. Lieb–schultz–mattis type theorems for quantum spin chains without continuous symmetry. *Communications in Mathematical Physics*, 372(3):951–962, 2019.

[111] H. Osborn. Conformal blocks for arbitrary spins in two dimensions. *Physics Letters B*, 718(1):169–172, nov 2012.

[112] Masaki Oshikawa. Commensurability, excitation gap, and topology in quantum many-particle systems on a periodic lattice. *Phys. Rev. Lett.*, 84:1535–1538, Feb 2000.

[113] Masaki Oshikawa and Ian Affleck. Defect lines in the Ising model and boundary states on orbifolds. *Phys. Rev. Lett.*, 77:2604–2607, 1996.

[114] Masaki Oshikawa and Ian Affleck. Boundary conformal field theory approach to the critical two-dimensional Ising model with a defect line. *Nucl. Phys. B*, 495(3):533–582, jun 1997.

[115] Siddharth A. Parameswaran, Ari M. Turner, Daniel P. Arovas, and Ashvin Vishwanath. Topological order and absence of band insulators at integer filling in non-symmorphic crystals. *Nature Physics*, 9(5):299–303, 2013.

[116] Francesco Parisen Toldin, Fakher F. Assaad, and Stefan Wessel. Critical behavior in the presence of an order-parameter pinning field. *Physical Review B*, 95(1), January 2017.

[117] V. B. Petkova and J. B. Zuber. Generalized twisted partition functions. *Phys. Lett. B*, 504:157–164, 2001.

[118] David Poland, Slava Rychkov, and Alessandro Vichi. The conformal bootstrap: Theory, numerical techniques, and applications. *Rev. Mod. Phys.*, 91:015002, Jan 2019.

[119] David Poland, David Simmons-Duffin, and Alessandro Vichi. Carving Out the Space of 4D CFTs. *JHEP*, 05:110, 2012.

[120] Joseph Polchinski. Scale and conformal invariance in quantum field theory. *Nuclear Physics B*, 303(2):226–236, 1988.

[121] Abhishodh Prakash. An elementary proof of 1d lsm theorems, 2020.

[122] Mark de Wild Propitius. Topological interactions in broken gauge theories, 1995.

[123] Thomas Quella, Ingo Runkel, and Gerard M. T. Watts. Reflection and transmission for conformal defects. *JHEP*, 04:095, 2007.

[124] Riccardo Rattazzi, Vyacheslav S Rychkov, Erik Tonni, and Alessandro Vichi. Bounding scalar operator dimensions in 4d CFT. *Journal of High Energy Physics*, 2008(12):031–031, dec 2008.

[125] Marten Reehorst. Rigorous bounds on irrelevant operators in the 3d Ising model CFT. *JHEP*, 09:177, 2022.

[126] Marten Reehorst, Slava Rychkov, David Simmons-Duffin, Benoit Sirois, Ning Su, and Balt van Rees. Navigator Function for the Conformal Bootstrap. *SciPost Phys.*, 11:072, 2021.

[127] Daniel Robbins and Thomas Vandermeulen. Orbifolds from Modular Orbits. *Phys. Rev. D*, 101(10):106021, 2020.

[128] P. Ruelle and O. Verhoeven. Discrete symmetries of unitary minimal conformal theories. *Nuclear Physics B*, 535(3):650–680, dec 1998.

[129] Ingo Runkel. *Boundary problems in conformal field theory.* PhD thesis, King's College London, 2000.

[130] Luiz H. Santos and Juven Wang. Symmetry-protected many-body Aharonov-Bohm effect. *Phys. Rev. B*, 89(19):195122, 2014.

[131] David Simmons-Duffin. A semidefinite program solver for the conformal bootstrap. *Journal of High Energy Physics*, 2015(6):174, 2015.

[132] David Simmons-Duffin. The lightcone bootstrap and the spectrum of the 3d ising CFT. *Journal of High Energy Physics*, 2017(3):086, mar 2017.

[133] Alexander Söderberg. Fusion of conformal defects in four dimensions. *Journal of High Energy Physics*, 2021(4):87, 2021.

[134] Ning Su. The Hybrid Bootstrap. 2 2022.

[135] Yuji Tachikawa. On gauging finite subgroups. *SciPost Phys.*, 8(1):015, 2020.

[136] Nathanan Tantivasadakarn, Ryan Thorngren, Ashvin Vishwanath, and Ruben Verresen. Building models of topological quantum criticality from pivot hamiltonians, 2021.

[137] Nathanan Tantivasadakarn, Ryan Thorngren, Ashvin Vishwanath, and Ruben Verresen. Pivot hamiltonians as generators of symmetry and entanglement, 2021.

[138] Ryan Thorngren and Dominic V. Else. Gauging Spatial Symmetries and the Classification of Topological Crystalline Phases. *Phys. Rev. X*, 8(1):011040, 2018.

[139] Ryan Thorngren and Yifan Wang. Fusion category symmetry i: Anomaly in-flow and gapped phases, 2019.

[140] Apoorv Tiwari, Xiao Chen, Ken Shiozaki, and Shinsei Ryu. Bosonic topological phases of matter: Bulk-boundary correspondence, symmetry protected topological invariants, and gauging. *Phys. Rev. B*, 97(24):245133, 2018.

[141] Lokman Tsui, Yen-Ta Huang, Hong-Chen Jiang, and Dung-Hai Lee. The phase transitions between z×z bosonic topological phases in 1+1d, and a constraint on the central charge for the critical points between bosonic symmetry protected topological phases. *Nuclear Physics B*, 919:470–503, jun 2017.

[142] Lokman Tsui, Yen-Ta Huang, and Dung-Hai Lee. A holographic theory for the phase transitions between fermionic symmetry-protected topological states. *Nuclear Physics B*, 949:114799, dec 2019.

[143] Lokman Tsui, Hong-Chen Jiang, Yuan-Ming Lu, and Dung-Hai Lee. Quantum phase transitions between a class of symmetry protected topological states. *Nuclear Physics B*, 896:330–359, jul 2015.

[144] Cumrun Vafa. Modular Invariance and Discrete Torsion on Orbifolds. *Nucl. Phys. B*, 273:592–606, 1986.

[145] Cumrun Vafa and Edward Witten. On orbifolds with discrete torsion. *J. Geom. Phys.*, 15:189–214, 1995.

[146] Ruben Verresen, Roderich Moessner, and Frank Pollmann. One-dimensional symmetry protected topological phases and their transitions. *Physical Review B*, 96(16), oct 2017.

[147] Ruben Verresen, Ryan Thorngren, Nick G. Jones, and Frank Pollmann. Gapless topological phases and symmetry-enriched quantum criticality. *Phys. Rev. X*, 11:041059, Dec 2021.

[148] Ruben Verresen, Ryan Thorngren, Nick G. Jones, and Frank Pollmann. Gapless topological phases and symmetry-enriched quantum criticality. *Phys. Rev. X*, 11:041059, Dec 2021.

[149] Alessandro Vichi. A new method to explore conformal field theories in any dimension. *EPFL*, page 181, 2011.

[150] Matthias Vojta, Chiranjeeb Buragohain, and Subir Sachdev. Quantum impurity dynamics in two-dimensional antiferromagnets and superconductors. *Physical Review B*, 61(22):15152–15184, June 2000.

[151] Chenjie Wang and Michael Levin. Topological invariants for gauge theories and symmetry-protected topological phases. *Phys. Rev. B*, 91(16):165119, 2015.

[152] Juven Wang, Luiz H. Santos, and Xiao-Gang Wen. Bosonic Anomalies, Induced Fractional Quantum Numbers and Degenerate Zero Modes: the anomalous edge physics of Symmetry-Protected Topological States. *Phys. Rev. B*, 91(19):195134, 2015.

[153] Yan-Cheng Wang, Meng Cheng, and Zi Yang Meng. Scaling of the disorder operator at $(2+1)d$ u(1) quantum criticality. *Phys. Rev. B*, 104:L081109, Aug 2021.

[154] Yan-Cheng Wang, Nvsen Ma, Meng Cheng, and Zi Yang Meng. Scaling of disorder operator at deconfined quantum criticality, 2021.

[155] Haruki Watanabe, Hoi Chun Po, Ashvin Vishwanath, and Michael Zaletel. Filling constraints for spin-orbit coupled insulators in symmorphic and nonsymmorphic crystals. *Proceedings of the National Academy of Sciences*, 112(47):14551–14556, 2015.

[156] Kenneth G. Wilson. The Renormalization Group: Critical Phenomena and the Kondo Problem. *Rev. Mod. Phys.*, 47:773, 1975.

[157] Kenneth G. Wilson and Michael E. Fisher. Critical exponents in 3.99 dimensions. *Phys. Rev. Lett.*, 28:240–243, Jan 1972.

[158] Xu Yang, Shenghan Jiang, Ashvin Vishwanath, and Ying Ran. Dyonic lieb-schultz-mattis theorem and symmetry protected topological phases in decorated dimer models. *Phys. Rev. B*, 98:125120, Sep 2018.

[159] Weicheng Ye, Meng Guo, Yin-Chen He, Chong Wang, and Liujun Zou. Topological characterization of Lieb-Schultz-Mattis constraints and applications to symmetry-enriched quantum criticality. *SciPost Phys.*, 13(3):066, 2022.

[160] Alexander B. Zamolodchikov. Irreversibility of the flux of the renormalization group in a 2d field theory. *Journal of Experimental and Theoretical Physics Letters*, 43(12):565, June 1986.

[161] Zheng Zhou, Davide Gaiotto, Yin-Chen He, and Yijian Zou. The g-function and Defect Changing Operators from Wavefunction Overlap on a Fuzzy Sphere. 12 2023.

[162] Zheng Zhou, Davide Gaiotto, Yin-Chen He, and Yijian Zou. The g-function and defect changing operators from wavefunction overlap on a fuzzy sphere, 2024.

[163] Wei Zhu, Chao Han, Emilie Huffman, Johannes S. Hofmann, and Yin-Chen He. Uncovering Conformal Symmetry in the 3D Ising Transition: State-Operator Correspondence from a Quantum Fuzzy Sphere Regularization. *Phys. Rev. X*, 13(2):021009, 2023.

[164] Liujun Zou, Yin-Chen He, and Chong Wang. Stiefel liquids: Possible non-lagrangian quantum criticality from intertwined orders. *Phys. Rev. X*, 11:031043, Aug 2021.